

9-26-2018 1:30 PM

# The Brain-Heart Connection: Establishment of a Novel Rodent Model of Focal Insular Ischemic Stroke to Examine the Pathophysiology of Stroke-Induced Heart Injury

Victoria Thorburn, *The University of Western Ontario*

Supervisor: Whitehead, Shawn N., *The University of Western Ontario*

Co-Supervisor: Sposato, Luciano A., *The University of Western Ontario*

A thesis submitted in partial fulfillment of the requirements for the Master of Science degree in Anatomy and Cell Biology

© Victoria Thorburn 2018

Follow this and additional works at: <https://ir.lib.uwo.ca/etd>



Part of the [Nervous System Diseases Commons](#)

---

## Recommended Citation

Thorburn, Victoria, "The Brain-Heart Connection: Establishment of a Novel Rodent Model of Focal Insular Ischemic Stroke to Examine the Pathophysiology of Stroke-Induced Heart Injury" (2018). *Electronic Thesis and Dissertation Repository*. 5738.

<https://ir.lib.uwo.ca/etd/5738>

This Dissertation/Thesis is brought to you for free and open access by Scholarship@Western. It has been accepted for inclusion in Electronic Thesis and Dissertation Repository by an authorized administrator of Scholarship@Western. For more information, please contact [wlsadmin@uwo.ca](mailto:wlsadmin@uwo.ca).

## Abstract

The neurological influence of ischemic stroke in the initiation and perpetuation of stroke-induced heart injury (SIHI) has been acknowledged for several years. However, an underlying pathophysiological mechanism remains uncertain. Clinically, it is hypothesized that stroke involving the insular cortex (IC) initiates SIHI; since the IC controls autonomic regulation of cardiovascular function. Yet, given the high prevalence of shared risk factors between ischemic stroke and cardiovascular disorders, mechanistic conclusions from clinical studies are largely speculative. We therefore sought to establish a novel rodent model of focal insular ischemic stroke, used to evaluate potential behavioural and pathological outcomes of SIHI. Focal ischemic stroke was induced into the right or left IC of 6-month-old male Wistar rats, through stereotaxic injection of endothelin-1 (ET-1). Control groups received an injection of ibotenic acid (IA), phosphate-buffered saline (PBS) or no injection (NI). Before euthanasia, rats were assessed for autonomic deficits in sensorimotor gating. At 28 days post-injection, rats with left IC damage displayed an overall trend of deficiencies in sensorimotor gating; compared to rats with right IC damage and PBS/NI control groups. Pathologically, all injured groups (IA/ET-1) exhibited a chronic increase in microglia activation, present at the IC and remote white/grey matter regions. Furthermore, these groups expressed cardiac fibrosis within the left atrium. When correlated, a positive association between microglia activation and cardiac fibrosis was observed. With this novel model, we have successfully identified several downstream consequences of IC stroke within the brain and heart, affirming the focal contribution of IC damage to SIHI. Taken together, these preliminary results provide important insight into potential mechanisms of post-stroke cardiac damage, serving as future therapeutic targets for SIHI.

**Keywords:** ischemic stroke, stroke-induced heart injury, insular cortex, autonomic dysfunction, neuroinflammation

## Acknowledgements

As I sit here finishing the final edits of my thesis, I'm in disbelief that my time with the Vulnerable Brain Lab is already nearing an end. I cannot help but think how fortunate I am to have had such an enjoyable and fulfilling graduate experience, all thanks to the incredible mentors, classmates and lab members I have had the pleasure of meeting.

To my supervisors, Dr. Shawn Whitehead and Dr. Luciano Sposato, thank you for allowing me this opportunity to pursue a graduate degree with your research group. Thank you for creating a supportive, yet challenging environment, that maximized my growth as a young researcher. Because of you both, I have accomplished things I never thought I could.

A big thank you to Dr. Susanne Schmid for offering the generous use of her behaviour equipment, and to Cleusa De Oliveira for her assistance with training. I must also thank Dr. Raj Rajakumar and Dr. Paul Walton for serving on my advisory committee these past two years. Your guidance, feedback and collaboration have been greatly appreciated.

Thank you to current (Dr. Seung Hun Oh, Alex Levit, Dr. Nadia Ivanova, Mona Alshaikh, Dr. Asmahan Elsariti, Jessica Garabon, Austyn Roseborough, Aaron Harris, Victoria Jaremek, Fan Liu) and past (Dr. Brittany Balint, Dr. Sarah Caughlin, Aaron Regis) Vulnerable Brain Lab members for your valued friendship and moral support these last two years! You all are incredible individuals, and I am so grateful for the memories we have created together.

Many thanks to Matthew Zhou, for his dedicated assistance with tissue imaging and quantification. A very special thank you must also go to Dr. Lynn Wang, for her immeasurable amount of technical support. I think it is fair to say that I would currently not be writing my thesis, if it weren't for both of you!

Finally, thank you to my family for your unconditional love, support and encouragement. Nick, thank you for your humor. You always manage to cheer me up, even during times of stress or disappointment. Mom and Dad, thank you for being such selfless, hardworking role models (and my loudest cheerleaders!). I am who I am because of you.

## Table of Contents

<b>Abstract.....</b>	<b>ii</b>
<b>Acknowledgements .....</b>	<b>iii</b>
<b>Table of Contents .....</b>	<b>iv</b>
<b>List of Tables .....</b>	<b>vii</b>
<b>List of Figures.....</b>	<b>viii</b>
<b>List of Abbreviations .....</b>	<b>x</b>
<b>Section 1: INTRODUCTION.....</b>	<b>1</b>
1.1 <i>The Brain-Heart Connection.....</i>	2
1.2 <i>Stroke .....</i>	2
1.2.1 Stroke epidemiology and societal implications	2
1.2.2 Stroke subtypes	2
1.2.3 Ischemic stroke interventions	3
1.2.4 Pathophysiology of ischemic stroke	3
1.2.5 Rodent models of ischemic stroke	4
1.3 <i>Ischemic Stroke and Neuroinflammation .....</i>	5
1.4 <i>Secondary Consequences of Ischemic Stroke .....</i>	6
1.4.1 Ischemic stroke and white matter injury	6
1.4.2 Ischemic stroke and neurodegeneration	7
1.4.3 Ischemic stroke and heart injury	8
1.5 <i>Mechanisms of Stroke-Induced Heart Injury .....</i>	9
1.5.1 The autonomic nervous system	9
1.5.2 Neural control of cardiovascular function	10
1.5.3 Increased sympathetic activity and stroke-induced heart injury	12
1.5.4 Inflammation and stroke-induced heart injury	12
1.6 <i>The Insular Cortex and Stroke-Induced Heart Injury.....</i>	13
1.6.1 Insular cortex structure and function	13
1.6.2 Clinical evidence of insular ischemic stroke-induced heart injury	13
1.6.3 Lateralization of insular autonomic function	14
1.6.4 Rodent models of insular ischemic stroke	14
1.7 <i>The Acoustic Startle Response .....</i>	15
1.7.1 Circuitry of the acoustic startle response	15
1.7.2 Prepulse inhibition of the acoustic startle response	17
1.7.3 Rodent models of the acoustic startle response	17

1.8 <i>Rationale, Objective and Hypothesis</i> .....	19
<b>Section 2: METHODS</b> .....	<b>22</b>
2.1 <i>Animals</i> .....	23
2.2 <i>Rat Models</i> .....	23
2.2.1 Endothelin-1 ischemic model	23
2.2.2 Ibotenic acid neurotoxic model	23
2.2.3 Surgical procedures	24
2.3 <i>Behaviour Testing</i> .....	26
2.3.1 Prepulse inhibition of the acoustic startle response	26
2.4 <i>Euthanasia</i> .....	29
2.5 <i>Brain Histology and Immunohistochemistry</i> .....	29
2.5.1 Tissue sectioning	29
2.5.2 Thionine histochemistry	29
2.5.3 Immunohistochemistry	29
2.6 <i>Heart Histology</i> .....	30
2.6.1 Tissue sectioning	32
2.6.2 Masson's trichrome histochemistry	32
2.7 <i>Tissue Analysis</i> .....	32
2.7.1 Imaging and quantification	32
2.7.2 Statistical analysis	36
<b>Section 3: RESULTS</b> .....	<b>37</b>
3.1 <i>Qualitative Confirmation of Targeted Insular Damage</i> .....	38
3.2 <i>Behavioural Assessment</i> .....	38
3.2.1 Left insular damage corresponds with an observed trend of reduced prepulse inhibition	38
3.3 <i>Analysis of Brain Immunohistochemistry</i> .....	40
3.3.1 Insular damage enhances white matter microgliosis, but not astrogliosis, in the corpus callosum	40
3.3.2 Insular damage does not enhance white matter microgliosis or astrogliosis in the forceps minor	42
3.3.3 Insular damage enhances white matter microgliosis, but not astrogliosis, in the ipsilateral internal capsule	45
3.3.4 Insular damage enhances grey matter microgliosis, but not astrogliosis, in the ipsilateral ventroposterior thalamus	51
3.3.5 Insular damage does not generate secondary neuronal loss in remote forebrain regions	53

3.4 <i>Analysis of Heart Histology</i> .....	55
3.4.1 Left atrial fibrosis of the heart is observed 28 days following insular injury .....	55
3.5 <i>Correlative Analysis of Microglia Activation and Cardiac Fibrosis</i> .....	61
3.5.1 Increased white and grey matter microglia activation positively correlates with left atrial cardiac fibrosis .....	61
<b>Section 4: DISCUSSION</b> .....	<b>65</b>
4.1 <i>Summary of Key Findings</i> .....	66
4.2 <i>Endothelin-1 vs. Ibotenic Acid</i> .....	66
4.3 <i>Behavioural Assessment: Prepulse Inhibition of the Acoustic Startle Response</i> ...	67
4.4 <i>Insular Ischemic Stroke and Secondary Neuroinflammation</i> .....	68
4.4.1 White matter inflammation and axonal degeneration .....	68
4.4.2 Additional causes of microglia activation .....	70
4.4.3 Pathological absence of lateralization .....	70
4.4.4 Insular ischemic stroke and astrogliosis .....	71
4.5 <i>Insular Ischemic Stroke and Remote Neurodegeneration</i> .....	71
4.6 <i>Insular Ischemic Stroke and Stroke-Induced Heart Injury</i> .....	73
4.7 <i>Inflammation and Stroke-Induced Heart Injury</i> .....	75
4.8 <i>Limitations and Future Directions</i> .....	76
<b>Section 5: CONCLUSION</b> .....	<b>80</b>
<b>References</b> .....	<b>83</b>
<b>Appendix</b> .....	<b>100</b>
<b>Curriculum Vitae</b> .....	<b>101</b>

## List of Tables

<b>Table 1.</b> Prepulse and startle stimuli parameters used during Block II of the PPI behaviour test .....	28
<b>Table 2.</b> Product summary of primary antibodies used for the immunohistochemical staining of brain tissue .....	31

## List of Figures

<b>Figure 1.</b> Neural control of cardiovascular function .....	11
<b>Figure 2.</b> Neural circuitry of the acoustic startle response.....	16
<b>Figure 3.</b> Schematic overview of PPI and associated neural circuitry.....	18
<b>Figure 4.</b> Schematic representation of targeted insular cortex brain region .....	25
<b>Figure 5.</b> Experimental timeline.....	27
<b>Figure 6.</b> Schematic representation of brain ROIs selected for OX-6 and GFAP analysis .....	34
<b>Figure 7.</b> Schematic representation of brain ROIs selected for NeuN analysis.....	35
<b>Figure 8.</b> Qualitative confirmation of insular damage .....	39
<b>Figure 9.</b> Left insular damage corresponds with an observed trend of reduced prepulse inhibition .....	41
<b>Figure 10.</b> Insular damage significantly increases white matter microgliosis within the corpus callosum .....	43
<b>Figure 11.</b> Insular damage does not enhance white matter astrogliosis within the corpus callosum .....	44
<b>Figure 12.</b> Insular damage does not enhance white matter microgliosis within the forceps minor .....	46
<b>Figure 13.</b> Insular damage does not enhance white matter astrogliosis within the forceps minor .....	47
<b>Figure 14.</b> Insular damage significantly increases white matter microgliosis within the ipsilateral internal capsule.....	49
<b>Figure 15.</b> Insular damage does not enhance white matter astrogliosis within the internal capsule .....	50
<b>Figure 16.</b> Insular damage significantly increases grey matter microgliosis within the ipsilateral ventroposterior thalamus.....	52
<b>Figure 17.</b> Insular damage does not enhance grey matter astrogliosis within the ventroposterior thalamus.....	54
<b>Figure 18.</b> Insular damage does not generate secondary neuronal loss within the prefrontal cortex.....	56



<b>Figure 19.</b> Insular damage does not generate secondary neuronal loss within the anterior cingulate cortex .....	57
<b>Figure 20.</b> Insular damage does not generate secondary neuronal loss within the amygdala .....	58
<b>Figure 21.</b> Insular damage does not generate secondary neuronal loss within the hypothalamus .....	59
<b>Figure 22.</b> Insular damage does not generate secondary neuronal loss within the ventroposterior thalamus.....	60
<b>Figure 23.</b> Left atrial fibrosis of the heart significantly increases following injury to the insular cortex.....	62
<b>Figure 24.</b> Increased white and grey matter microglia activation positively correlates with left atrial cardiac fibrosis .....	64
<b>Figure 25.</b> Schematic summary outlining the proposed pathophysiological cascade of stroke-induced heart injury .....	79

## List of Abbreviations

<b>ABC</b>	Avidin-Biotin Complex
<b>AC</b>	Adenylyl Cyclase
<b>ACC</b>	Anterior Cingulate Cortex
<b>ACh</b>	Acetylcholine
<b>AF</b>	Atrial Fibrillation
<b>AMPA</b>	$\alpha$ -amino-3-hydroxy-5-methyl-4-propionate
<b>ANOVA</b>	Analysis of Variance
<b>ANS</b>	Autonomic Nervous System
<b>AP</b>	Anterior/Posterior
<b>ASR</b>	Acoustic Startle Response
<b>ATP</b>	Adenine Triphosphate
<b>BBB</b>	Blood-Brain Barrier
<b>Ca<sup>2+</sup></b>	Calcium Ion
<b>CN</b>	Cochlear Nucleus
<b>CNS</b>	Central Nervous System
<b>CRN</b>	Cochlear Root Neuron
<b>CRP</b>	C-Reactive Protein
<b>cTnT</b>	Cardiac Troponin T
<b>DAB</b>	3,3'-diaminobenzidine tetrahydrochloride
<b>dH<sub>2</sub>O</b>	Distilled Water
<b>DMV</b>	Dorsal Motor Nucleus of the Vagus
<b>DV</b>	Dorsal/Ventral
<b>ECG</b>	Electrocardiogram

<b>ET-1</b>	Endothelin-1
<b>GABA</b>	Gamma-Aminobutyric Acid
<b>GFAP</b>	Glial Fibrillary Acidic Protein
<b>H<sub>2</sub>O</b>	Water
<b>H<sub>2</sub>O<sub>2</sub></b>	Hydrogen Peroxide
<b>HRV</b>	Heart Rate Variability
<b>IA</b>	Ibotenic Acid
<b>IC</b>	Insular Cortex
<b>IFC</b>	Inferior Colliculus
<b>IL-1<math>\beta</math></b>	Interleukin-1 Beta
<b>ISI</b>	Interstimulus Interval
<b>K<sup>+</sup></b>	Potassium Ion
<b>L</b>	Left
<b>LA</b>	Left Atrium
<b>MCA</b>	Middle Cerebral Artery
<b>MCAO</b>	Middle Cerebral Artery Occlusion
<b>MHC II</b>	Major Histocompatibility Complex II
<b>ML</b>	Medial/Lateral
<b>MMP</b>	Matrix Metalloproteinase
<b>NA</b>	Nucleus Ambiguus
<b>Na<sup>+</sup></b>	Sodium Ion
<b>NE</b>	Norepinephrine
<b>NeuN</b>	Neuronal Nuclei
<b>NI</b>	No Injection

<b>NMDA</b>	N-methyl-D-aspartate
<b>NO</b>	Nitric Oxide
<b>NTS</b>	Nucleus of the Solitary Tract
<b>PbN</b>	Parabrachial Nucleus
<b>PBS</b>	Phosphate-Buffered Saline
<b>PFA</b>	Paraformaldehyde
<b>PFC</b>	Prefrontal Cortex
<b>PnC</b>	Caudal Pontine Reticular Nucleus
<b>PNS</b>	Peripheral Nervous System
<b>PPI</b>	Prepulse Inhibition
<b>PPTg</b>	Pedunculopontine Tegmental Nucleus
<b>PSNS</b>	Parasympathetic Nervous System
<b>PV</b>	Pulmonary Vein
<b>R</b>	Right
<b>ROI</b>	Region of Interest
<b>ROS</b>	Reactive Oxygen Species
<b>rtPA</b>	Recombinant Tissue Plasminogen Activator
<b>RVLM</b>	Rostral Ventrolateral Medulla
<b>SEM</b>	Standard Error of the Mean
<b>SIHI</b>	Stroke-Induced Heart Injury
<b>SNS</b>	Sympathetic Nervous System
<b>SPC</b>	Superior Colliculus
<b>TGFβ</b>	Transforming Growth Factor Beta-1
<b>TIA</b>	Transient Ischemic Attack

<b>TNF<math>\alpha</math></b>	Tumour Necrosis Factor Alpha
<b>VP</b>	Ventroposterior
<b>VPT</b>	Ventroposterior Thalamus
<b>WMI</b>	White Matter Inflammation

## Section 1: INTRODUCTION

## 1.1 The Brain-Heart Connection

Acknowledgement and identification of the brain-heart connection was first reported in 1942 by Walter B. Cannon, in his paper entitled “Voodoo Death.” Here, Cannon recounted early incidents of sudden death from fright, hypothesizing the innate capability of the nervous system to injure the heart <sup>1</sup>. Since then, numerous neurological disorders have been associated with adverse cardiovascular events <sup>2</sup>. Among these, stroke stands out; contributing to a high-frequency of neurocardiac arrhythmias and lesions <sup>3-6</sup>. While it has been speculated that insular cortex damage, and arising autonomic dysfunction, contribute to this observed brain-heart phenomenon <sup>7</sup>, little is known about the underlying pathophysiology; making this intricate relationship between the brain and heart a clinically relevant topic of interest.

## 1.2 Stroke

### 1.2.1 Stroke epidemiology and societal implications

Stroke is a global burden, negatively impacting the health and wellbeing of individuals worldwide <sup>8</sup>. In industrialized countries like Canada, stroke is the most common cause of morbidity and a prominent source of mortality; only second to heart disease <sup>9</sup>. As such, numerous research efforts have been dedicated to the investigation of stroke occurrence and prevention; resulting in the identification of key risk factors. In particular, high blood pressure, diabetes, smoking, heart disease and age have all been recognized as major contributors of stroke <sup>10-15</sup>. While increased knowledge and public awareness of these risk factors have produced a recent North American decline in stroke occurrence <sup>16</sup>, age remains a dominant and uncontrollable risk factor. With the current ageing population, stroke incidence among the elderly is expected to rise, significantly increasing stroke-related socioeconomic and healthcare demands <sup>9,17</sup>.

### 1.2.2 Stroke subtypes

Traditionally, stroke has been generalized into two basic categories: hemorrhagic and ischemic. Hemorrhagic strokes are the less frequent subtype, accounting for approximately 10-15% of all strokes <sup>18</sup>. Manifestation of these strokes occur following the rupture of a cranial blood vessel, an associated outcome of chronic hypertension <sup>19-21</sup>. Consequently, this bleeding within the brain increases intracranial pressure, further causing reduced blood flow to surrounding tissue; ultimately expanding the region of hemorrhagic brain damage <sup>22</sup>.

Ischemic strokes are typically less severe than hemorrhagic strokes, but much more common – accounting for approximately 85-90% of all strokes<sup>18</sup>. Due to this greater incidence of ischemic strokes, our research will specifically study ischemic-induced cardiovascular changes, despite a similar prevalence in both subgroups<sup>6</sup>.

Mechanistically, ischemic strokes occur following the occlusion of a cranial blood vessel, which inhibits local blood flow<sup>23</sup>. Numerous factors can contribute to this physical blockade, including narrowing of the vessel wall (as observed in atherosclerosis) or the presence of a blood clot<sup>23</sup>. In some circumstances, a temporary blockage of short duration can occur, generating a transient ischemic attack (TIA)<sup>24</sup>. While the accompanying symptoms and damage associated with TIAs are minimal, the occurrence of these “mini-strokes” are known to increase the risk of a future ischemic episode<sup>24-26</sup>.

### *1.2.3 Ischemic stroke interventions*

Presently, intravenous administration of recombinant tissue plasminogen activator (rtPA) serves as the only viable treatment for acute ischemic stroke<sup>27,28</sup>. This protein acts to dissolve the intraluminal clotted material, restoring blood flow to the ischemic region<sup>28</sup>. However, the therapeutic window for this drug is limited, requiring administration within 4.5 hours of occlusion onset<sup>28,29</sup>. According to epidemiological reports, less than 10% of the eligible stroke population receives rtPA<sup>30-32</sup>; indicating a strong need for alternative stroke therapies.

### *1.2.4 Pathophysiology of ischemic stroke*

The pathophysiological response that occurs following ischemic stroke is a complex process. Upon vessel occlusion, nutrient transport is obstructed; depleting local brain tissue of key metabolites, such as glucose<sup>33-37</sup>. Consequently, cells are incapable of producing adenine triphosphate (ATP), an energy storage molecule crucial for tissue cell survival<sup>38</sup>. In this absence of ATP, an ischemic cascade is activated, initiating the response of several cellular mechanisms<sup>33-37</sup>.

An initial loss of blood perfusion, and subsequent energy reduction, impairs cellular ionic homeostasis<sup>33-37</sup>. In a normal functioning neuron, the influx of potassium (K<sup>+</sup>) ions and efflux of sodium (Na<sup>+</sup>) and/or calcium (Ca<sup>2+</sup>) ions across the cell membrane is tightly regulated, due to a neuron’s vital role in impulse transmission<sup>39</sup>. However, in the absence of ATP, this



regulation is inhibited; allowing for the uncontrolled build-up of intracellular  $\text{Na}^+$  and  $\text{Ca}^{2+}$  <sup>33-37</sup>. Compensation for this increase in cellular  $\text{Na}^+$  stimulates the movement of water ( $\text{H}_2\text{O}$ ) into the cell, causing cytotoxic edema <sup>40,41</sup>. This further restricts cerebral blood flow in surrounding areas, enlarging the infarct region <sup>40</sup>.

In response to the overaccumulation of cellular  $\text{Ca}^{2+}$ , excess glutamate neurotransmitters are released at the neuronal synapse and bind to nearby glutamate receptors: N-methyl-D-aspartate (NMDA) or  $\alpha$ -amino-3-hydroxy-5-methyl-4-propionate (AMPA) <sup>42,43</sup>. This further disrupts the ionic balance of neighbouring cells, initiating an excitotoxic cascade <sup>44</sup>. Additionally, this increased presence of cellular  $\text{Ca}^{2+}$  activates degradative enzymes and reactive oxygen species (ROS) production; damaging key cellular components, like mitochondria <sup>33-37</sup>. Consequently, injured mitochondria release apoptotic factors <sup>45</sup>, further contributing to ischemic cell death.

Irreversible cell death is the end-product of ischemic stroke, beginning to occur within minutes of occlusion <sup>33-37</sup>. At the site of blockage, blood levels are reduced to approximately 10% of basal levels, causing severe brain tissue necrosis <sup>46</sup>. Over time, this region becomes void of glial cells and neurons, resulting in an undesirable loss of brain function <sup>33-37</sup>.

Adjacent to this core region exists a viable brain area comprised of vulnerable, but potentially salvageable tissue; referred to as the ischemic penumbra <sup>33</sup>. Collateralization of vessel circuitry provides alternative sources of blood supply to this ischemic region, recovering blood flow to approximately 20-60% of basal levels <sup>46</sup>. Due to the redeeming potential of this region, the penumbra serves as an optimal target for future stroke interventions.

### *1.2.5 Rodent models of ischemic stroke*

Currently, numerous animal models and techniques are available for the experimental study of stroke <sup>47-53</sup>. However, selection of the appropriate model should be reflective of the clinical research question, as origin, location and size can all change outcomes of human ischemic stroke <sup>53,54</sup>. Rodents particularly function as an advantageous stroke model, due to extensive knowledge of their neuroanatomy <sup>55</sup> and similarities with human cranial circulation <sup>52</sup>.

Traditionally, middle cerebral artery occlusion (MCAO) has served as a popular technique for the induction of ischemic injury. In this method, an endovascular monofilament is inserted into the cerebral vasculature of the rat, blocking the middle cerebral artery (MCA)

bifurcation <sup>56</sup>. This ultimately impairs cerebral blood flow, generating rapid ischemia within the cortex and subcortical brain regions <sup>56</sup>.

While implementation of MCAO produces a consistent infarct region, resulting damage is widespread and severe <sup>56</sup>. Alternatively, intracranial injection of the vasoconstrictor endothelin-1 (ET-1) has been used to produce a more targeted area of focal ischemia <sup>57-59</sup>. Following administration, ET-1 binds to endothelin receptors present on the endothelial cells of blood vessels, inducing vasoconstriction <sup>58</sup>. Based upon previous MRI perfusion studies, resulting ischemia lasts for approximately 1 h before reperfusion <sup>57</sup>. Unlike MCAO, use of ET-1 provides versatility of infarct size and location <sup>54,57</sup>. However, it is important to note that application of this method causes invasive damage unrelated to ischemic stroke. Intracranial insertion of the cannula disrupts the skull, blood-brain barrier (BBB) and secondary brain regions <sup>47,53,54</sup>; which must be taken into account when analyzing results. In the present study, neurocardiac influences associated with insular injury will be examined, requiring the production of focal damage. For this reason, the ET-1 ischemic stroke model will be used for experiments outlined in this thesis.

### 1.3 Ischemic Stroke and Neuroinflammation

Inflammation is a vital mechanism of ischemic injury, largely modulated by microglia and astrocytes – immune cells of the central nervous system (CNS) <sup>35-37,53</sup>. During ischemia, these cells work to retain neuron health and homeostasis, through active participation in tissue repair and regeneration. However, not all forms of cerebral inflammation appear to produce beneficial effects. Recent literature has identified a co-existing and contradictory influence of neuroinflammation, capable of enhancing peri-infarct damage <sup>60</sup>.

In response to toxic stimuli released by injured neurons during the ischemic cascade, resting astrocytes become activated; referred to as astrogliosis <sup>61</sup>. During acute recovery, astrocytes function to encapsulate the infarcted region within a glial scar (comprised of astrocytes and microglia) in an effort to contain and repair the damaged area <sup>61,62</sup>. Recent reports suggest that astrocytes may also amplify the ischemic inflammatory response through the release of pro-inflammatory cytokines, such as tumour necrosis factor alpha (TNF $\alpha$ ) and interleukin-1 beta (IL-1 $\beta$ ) <sup>63</sup>, but exact mechanisms remain unclear.

Similar to astrocytes, microglia become activated in response to noxious stimuli; termed microgliosis <sup>35-37,53</sup>. Upon activation, microglia undergo morphological changes,

transitioning from a ramified to amoeboid appearance<sup>64</sup>. Interestingly, activated microglia can exhibit phenotypic and functional variance depending on the nature, strength and duration of presenting stimuli<sup>60,64</sup>. Currently, two activated microglia subtypes have been identified: M1 and M2<sup>60</sup>. M2 microglia are characteristically involved with anti-inflammatory efforts; phagocytosing toxic debris, releasing anti-inflammatory cytokines, such as transforming growth factor beta-1 (TGFβ), and promoting neurogenesis<sup>60,65</sup>. Often deemed “helpful” microglia, this M2 subtype works to minimize ischemic damage<sup>60</sup>. Contrarily, M1 microglia, frequently referred to as the “harmful” subtype, display an enhanced pro-inflammatory response<sup>60</sup>. Activation of these microglia results in the release of numerous pro-inflammatory compounds, including TNFα, IL-1β, matrix metalloproteinases (MMPs), ROS and nitric oxide (NO)<sup>60,65</sup>. The particular presence of MMPs results in disruption of the BBB, allowing for the infiltration of peripheral leukocytes<sup>64</sup>. This ultimately exacerbates local damage, while inducing systemic inflammation; contributing to further stimulation of the immune response. Occurrence of this systemic response is evident in a stroke patient’s blood sample, displaying increased levels of white blood cells and the inflammatory marker, C-reactive protein (CRP)<sup>37,66</sup>.

In a recent study by Hu and colleagues, expression profiles of M1/M2 polarization post-ischemic stroke were outlined. Intriguingly, ischemic microglia activation displayed a differential shift in subtype expression<sup>67</sup>. Soon after ischemic injury, an increased presence of M2 microglia was observed<sup>67</sup>. However, this M2 appearance remained transient, gradually transitioning to M1 phenotypic-dominance at 7 days post-stroke; suggesting a causative role of chronic inflammation in ischemic injury expansion<sup>67</sup>.

## **1.4 Secondary Consequences of Ischemic Stroke**

### *1.4.1 Ischemic stroke and white matter injury*

Damaging effects of ischemia on local grey matter remains a primary focus of stroke research. Yet, recent clinical imaging studies have reported persistent white matter inflammation (WMI) in major fibre tracts following ischemic stroke; with continued presence several months into the recovery period<sup>68-71</sup>. Alarmingly, this clinical manifestation of white matter pathology has been functionally implicated in post-stroke prognosis; associated with worse outcomes of prolonged recovery<sup>68,72,73</sup>. As such, secondary presentation of ischemic WMI should not be ignored.

In the healthy brain, white matter fibre tracts serve as an internal communication network, transferring information between remote grey matter regions <sup>66</sup>. Macroscopically, white matter consists of bundled axons, oligodendrocytes and astrocytes <sup>66</sup>. Axons serve as the central mechanism for action potential conduction, while also playing an important role in nutrient/mediator transport between cell soma and synapse <sup>66</sup>. Oligodendrocytes are myelin-producing cells responsible for axonal myelination <sup>66,74</sup>; enhancing the accuracy and speed of signal conduction <sup>74</sup>. Astrocytes act to support oligodendrocyte and axonal health, influencing myelination and maintaining homeostatic equilibrium <sup>74</sup>. Together, this white matter unit functions to orchestrate rapid neuron-neuron communication <sup>66,74</sup>. Damage to any component will perturb impulse signalling, causing detrimental sensory, motor and/or cognitive disruption <sup>66,75</sup>.

Similar to grey matter, white matter is critically dependent on a continuous supply of oxygen and nutrients <sup>66</sup>. However, unlike grey matter, white matter has a small blood supply with limited collateral circulation; making it extremely susceptible to the toxic effects caused by post-stroke ischemia <sup>66</sup>. Additionally, white matter becomes increasingly susceptible to ischemia with age <sup>76,77</sup>, further stressing the powerful contribution of white matter injury to overall ischemic damage. The pathophysiological cascade of white matter injury following ischemic stroke is similar to that observed in grey matter. Depletion of local nutrients inhibits oligodendrocyte and astrocyte cellular energy production, causing ionic dyshomeostasis <sup>76</sup>. This increases extracellular glutamate and ATP, leading to excitotoxicity, oxidative stress and initiation of the inflammatory response <sup>76</sup>. Necrotic death of local oligodendrocytes ultimately induces axonal demyelination and damage, impairing signal transduction <sup>34</sup>. It is important to note that the efficient conduction of an action potential through white matter circuitry requires the persistent supply of energy along the entire length of the axon <sup>66</sup>. Consequently, local reduction of blood flow at the occluded site can destroy the electrophysiological properties of an entire axon, initiating delayed anterograde and/or retrograde secondary axonal degeneration <sup>66,71</sup>.

#### *1.4.2 Ischemic stroke and neurodegeneration*

Acute grey matter damage at the occlusion site, and within peri-infarct regions, is a known consequence of ischemic stroke and an intense focus of pre-clinical neuroprotective therapies <sup>78,79</sup>. However, recent clinical research has described a delayed occurrence of

secondary damage in remote brain regions <sup>80-85</sup> at chronic post-stroke timepoints <sup>68,85</sup>; suggesting the existence of an ongoing or prolonged ischemic pathology. Neurologically, the unfavourable manifestation of this remote injury has corresponded with adverse functional deficits in ischemic stroke patients <sup>68,72,73</sup>, commonly referred to as “diaschisis” <sup>86</sup>.

Experimentally, several animal studies have observed a similar appearance of remote neuronal loss post-ischemic stroke <sup>87-91</sup>. In particular, chronic pathology after MCAO in the rat has consistently displayed secondary thalamic damage <sup>87-90</sup>. More recently, Weishaupt and colleagues reported ischemic neurodegeneration and neuronal loss within the retrosplenial cortex of the rat, at 28 days following bilateral injection of ET-1 into the prefrontal cortex <sup>91</sup>; further supporting the aforementioned clinical findings.

Exact mechanisms of this delayed secondary pathology remain largely unknown and may vary depending on the affected structures <sup>91</sup>. Yet, an intriguing commonality exists between all observations of remote neuronal damage: location of the secondary degeneration is dependent on anatomical connectivity to the primary infarct <sup>87-91</sup>, suggesting a causative role of the previously described white matter injury and axonal degeneration <sup>92</sup>. Presently, it is hypothesized that following ischemic stroke, axonal degeneration of local inhibitory GABAergic neurons prompts a loss of disinhibition to distant brain regions <sup>90,92</sup>. Inevitably, this fosters an excitotoxic response, evoking neuronal cell death in these secondary areas <sup>90,92</sup>. A corresponding activation of local inflammatory mechanisms, in particular M1 microglia, further enhances necrotic damage, contributing to ongoing chronic neurodegeneration <sup>90,92</sup>.

While the exacerbated presence of secondary inflammation and neurodegeneration is not ideal, the delayed nature of its pathology may widen the therapeutic window for stroke intervention <sup>91</sup>. As such, future use of anti-inflammatory agents post-ischemic stroke could serve to minimize associated functional deficits of secondary damage, ultimately improving recovery time.

#### *1.4.3 Ischemic stroke and heart injury*

Adverse consequences of stroke are not limited to the brain. In fact, extensive clinical and experimental research has demonstrated that damage incurred by stroke can extend to the heart, causing structural and functional impairments <sup>93-102</sup>; referred to as stroke-induced heart injury (SIHI). Initial reports of SIHI date back to the early 1950s, when Burch and colleagues first identified electrocardiogram (ECG) abnormalities in hemorrhagic stroke patients <sup>101</sup>. Soon

after, Koskelo and colleagues reported post-mortem presentation of subendocardial hemorrhages in patients previously displaying stroke-induced ECG changes <sup>100</sup>. Further supporting these clinical results, Burch and colleagues were first to confirm the histological presence of stroke-induced myocardial lesions in a mouse model of hemorrhagic stroke <sup>98</sup>. Since then, several animal models of hemorrhagic stroke have reproduced similar arrhythmias and/or myocardial lesions <sup>95,96,97,99</sup>.

While early research efforts largely concentrated on hemorrhagic SIHI, similar cardiac outcomes have been observed in ischemic stroke patients <sup>102-104</sup>. As mentioned previously, ischemic stroke accounts for roughly 85-90% of all strokes <sup>18</sup>, making this specific neurocardiac relationship a great concern. Of particular attention, is the observed contribution of ischemic stroke to the development of atrial fibrillation (AF) <sup>102</sup>. AF is a form of cardiac arrhythmia known to increase the risk of stroke 5-fold <sup>15</sup>. Currently, approximately 25% of ischemic stroke patients display post-stroke cardiac episodes of AF <sup>102</sup>; and yet, pathological underpinnings remain unknown <sup>105</sup>. Furthermore, 20-60% of ischemic stroke patients exhibit elevated serum cardiac troponin T (cTnT) levels post-stroke, a known biomarker of myocardial injury <sup>104</sup>. In a recent report by Wrigley and colleagues, this increased presence of cTnT appeared to enhance the long-term risk for death after ischemic stroke <sup>104</sup>; implying a capable manifestation of acute SIHI into chronic, deadly outcomes.

## **1.5 Mechanisms of Stroke-Induced Heart Injury**

### *1.5.1 The autonomic nervous system*

To date, precise mechanisms of SIHI remain unclear, however, longstanding evidence suggests a significant role of autonomic dysfunction <sup>93,97</sup>. The autonomic nervous system (ANS) is a critical component of the peripheral nervous system (PNS), responsible for the maintenance of internal homeostasis <sup>106,107</sup>. Traditionally, the ANS has been separated into two antagonistic divisions: the sympathetic nervous system (SNS) and the parasympathetic nervous system (PSNS) <sup>106,107</sup>. Together, these two autonomic branches act to unconsciously regulate visceral organ function, including cardiac activity <sup>106,107</sup>. A dysfunction in one system often leads to adverse changes in the other, resulting in undesirable physiological consequences <sup>2</sup>.

### 1.5.2 Neural control of cardiovascular function

Predominant modulation of autonomic cardiovascular function occurs through an expansive network of cortical and subcortical brain regions<sup>2,108-111</sup>. Together, these areas alter sympathetic and parasympathetic outflow, initiating a change in cardiac activity<sup>2</sup>. Physiologically, the successful mediation of this neural control requires efficient afferent and efferent communication between the brain and heart<sup>108</sup>.

Afferent cardiac signal transduction depends on the internal surveillance of cardiovascular mechanical and chemical receptors<sup>106,107,112</sup>. Upon activation, these sensory receptors will excite intrinsic cardiac neurons, initiating signal propagation<sup>106,107,112</sup>. Within this autonomic circuitry, the brainstem acts as a vital communication link, relaying sensory information from the periphery to upper forebrain regions<sup>2,108</sup>. As such, the nucleus of the solitary tract (NTS), located within the medulla, serves as the first neural synaptic site of afferent cardiac signals (Figure 1A)<sup>2,108-110</sup>. From here, the signal is relayed to the parabrachial nucleus (PbN) of the pons, prior to reaching the forebrain. Afferent projections from the PbN directly synapse at the hypothalamus, amygdala, anterior cingulate cortex (ACC) and prefrontal cortex (PFC)<sup>108,109</sup>; while the ventroposterior thalamus (VPT) serves as an additional relay centre between the PbN and insular cortex (Figure 1A)<sup>108</sup>. These cortical and subcortical regions act as critical integration sites for autonomic cardiovascular function, modulating cardiac activity in response to internal conditions<sup>2,106,107,112</sup>.

Efferent alteration of heart function is directly mediated through sympathetic and parasympathetic changes<sup>2</sup>. Upon receipt of afferent cardiac information, the aforementioned forebrain regions will alter efferent autonomic activity<sup>108-110</sup>, evoking an increase or decrease in cardiovascular function (Figure 1B)<sup>106,107,112</sup>. Increased cardiac activity requires enhanced sympathetic output from cardiac nerves, initiated through the excitation of presympathetic efferent neurons in the rostral ventrolateral medulla (RVLM)<sup>2</sup>. Axons of the RVLM synapse with preganglionic cholinergic sympathetic neurons in the spinal cord, which in turn, synapse with postganglionic noradrenergic sympathetic neurons of cardiac stellate ganglia (Figure 1B)<sup>2</sup>. Excitation of these noradrenergic sympathetic neurons promotes the release of norepinephrine (NE), a neurotransmitter capable of interacting with cardiac adrenergic receptors; ultimately increasing heart function<sup>106,107,112</sup>.

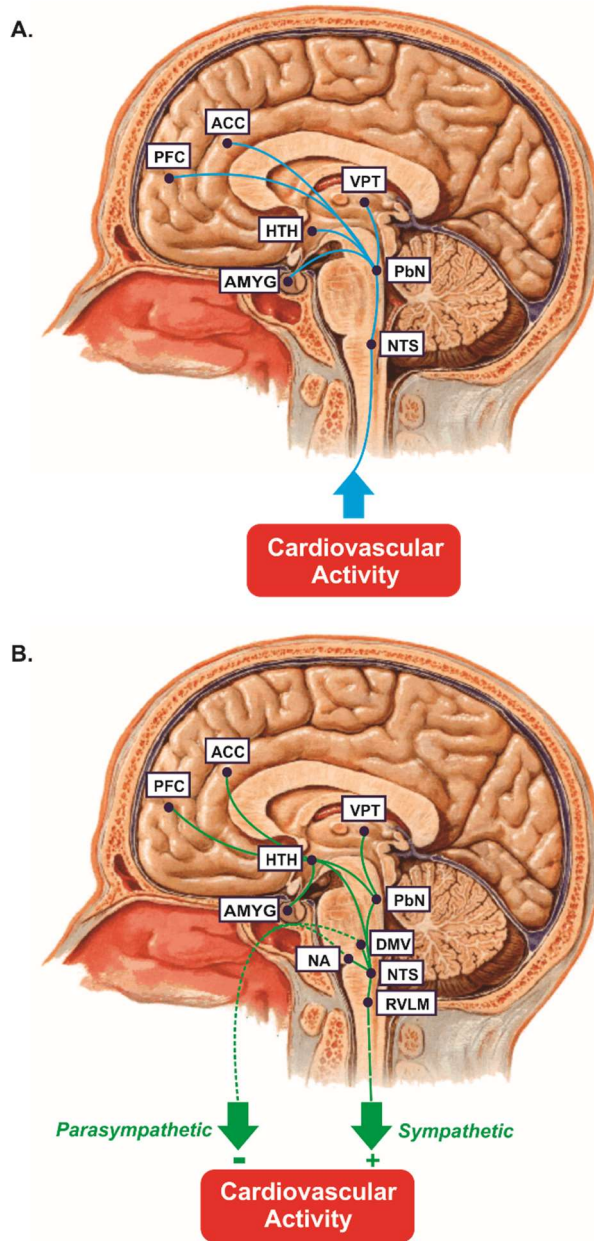


**Figure 1. Neural control of cardiovascular function. (A)** Afferent pathway of autonomic cardiovascular regulation. Brainstem cardiovascular sites (NTS/PbN) act as a vital relay centre for the transmission of peripheral cardiac sensory information to regulatory forebrain regions (PFC/ACC/HTH/AMYG/IC). The VPT serves as an additional autonomic relay centre between the PbN and IC (region not shown). **(B)** Efferent pathway of autonomic cardiovascular regulation. Autonomic modulation by PFC/ACC/HTH/AMYG/IC forebrain regions alters sympathetic (RVLM) or parasympathetic (DMV/NA) output, generating an overall increase (sympathetic) or decrease (parasympathetic) in heart rhythm. ACC = anterior cingulate cortex, PFC = prefrontal cortex, VPT = ventroposterior thalamus, IC = insular cortex, HTH = hypothalamus, AMYG = amygdala, PbN = parabrachial nucleus, DMV = dorsal motor nucleus of the vagus, NA = nucleus ambiguus, NTS = nucleus of the solitary tract, RVLM = rostral ventrolateral medulla. Adapted from Tahsili-Fahadan and Geocadin (2017) <sup>2</sup>.



Not surprisingly, decreased cardiac activity requires enhanced parasympathetic output, initiated through the vagus nerve <sup>2</sup>. Upon excitation, preganglionic cholinergic parasympathetic neurons at the dorsal motor nucleus of the vagus (DMV) and/or nucleus ambiguus (NA), both located within the medulla, will synapse with postganglionic cholinergic parasympathetic neurons of efferent cardiac ganglia <sup>2</sup>; releasing acetylcholine (ACh) (Figure 1B) <sup>106,107,112</sup>. In turn, this parasympathetic neurotransmitter binds to cardiac muscarinic receptors, decreasing heart rate <sup>106,107,112</sup>.

### *1.5.3 Increased sympathetic activity and stroke-induced heart injury*

Early reports of SIHI have identified an accompanying increase in post-stroke sympathetic activity <sup>93-97</sup>. Yet, it remains unclear whether this enhanced sympathetic tone is a direct effect of sympathetic upregulation, or indirect result of parasympathetic downregulation <sup>104</sup>. Regardless, this sympathetic hyperactivation increases NE release <sup>106,107,112</sup>, insinuating a potential role of NE toxicity in the development of SIHI <sup>2,93</sup>.

Mechanistically, NE stimulates the synthesis of adenylyl cyclase (AC), an important regulator of myocardial Ca<sup>2+</sup> channels <sup>113</sup>. In the presence of AC, Ca<sup>2+</sup> channels will open, initiating an influx of Ca<sup>2+</sup> into local myocytes <sup>113</sup>. These elevated levels of Ca<sup>2+</sup> enable actin and myosin filaments to interact; an action necessary for cardiac muscle contraction <sup>93,113</sup>. Pathologically, prolonged exposure to NE will sustain channel opening and Ca<sup>2+</sup> availability, permitting an unnatural period of continuous contraction <sup>93,113</sup>. Consequently, myocytes will die, leading to irreversible structural cardiac damage and a corresponding alteration in cardiac rhythm <sup>2,93</sup>. Furthermore, the increased presence of cellular Ca<sup>2+</sup> activates degradative enzymes capable of injuring the subendocardial conductive network <sup>2</sup>. This ultimately impedes proper signal transduction, further disrupting normal heart rate and function <sup>2,93</sup>.

### *1.5.4 Inflammation and stroke-induced heart injury*

Recently, Olshansky hypothesized a regulatory role of the ANS in myocardial cytokine production; similar to that observed in the spleen, liver and intestines <sup>114</sup>. Referred to as the “inflammatory reflex” or “cholinergic anti-inflammatory pathway,” this neural regulation of visceral inflammation is controlled by the vagus nerve <sup>115</sup>. In short, the presence of peripheral cytokines (TNF $\alpha$ , IL-1 $\beta$ ) during an immune response will activate parasympathetic nerve fibers, stimulating postganglionic release of ACh from visceral organs <sup>106,107,112,114</sup>. This ACh

can then enter immune cells through the  $\alpha7nAChR$  nicotinic receptor, directly inhibiting further transcription of proinflammatory cytokines; attenuating the inflammatory response<sup>116,117</sup>. As mentioned previously, sympathetic hyperactivation is a known outcome of stroke<sup>93-97</sup>. Consequently, an associated decrease in parasympathetic tone could abolish beneficial effects of the “inflammatory reflex,” perpetuating SIHI through enhanced cardiac and/or systemic inflammation<sup>105</sup>.

## **1.6 The Insular Cortex and Stroke-Induced Heart Injury**

### *1.6.1 Insular cortex structure and function*

The insular cortex (IC) is a highly-conserved, multimodal brain region, responsible for a variety of cognitive functions<sup>118-121</sup>. In humans, the IC lies deep within the lateral sulcus, beneath the frontal, parietal and temporal lobes<sup>118</sup>. Traditionally, the IC has anatomically been divided into an anterior and posterior region; with each extremity substantially differing in connectivity to other brain structures<sup>122</sup>. As such, the IC remains heavily connected to an expansive network of cortical and subcortical regions, serving as a vital sensorimotor integration hub<sup>118-120,122</sup>. To date, the IC has been implicated in an assortment of higher-order functional tasks: ranging from sensory processing to representing feelings and emotions, autonomic and motor control, risk prediction and decision-making, as well as complex social functions – like empathy<sup>118-123</sup>.

Recently, the pathophysiological relationship between IC damage and SIHI has gained increased interest. As mentioned previously, the IC exerts autonomic control over cardiovascular function, serving as an important forebrain site for the integration and alteration of cardiac activity<sup>2,108,109</sup>. It is therefore hypothesized that SIHI is a specific consequence of insular ischemic stroke, with damage to the IC disrupting autonomic function; resulting in the dysregulation of normal cardiac activity<sup>123</sup>.

### *1.6.2 Clinical evidence of insular ischemic stroke-induced heart injury*

Supporting this hypothesis, various clinical and epidemiological studies have discerned an association between IC damage and SIHI<sup>7,124-127</sup>. Most recently, Gonzalez Toledo and colleagues identified IC damage in 30.4% of ischemic stroke patients exhibiting atypical post-stroke ECGs; compared to a 7.3% prevalence in patients with normal post-stroke cardiac function<sup>7</sup>. While these results suggest an increased risk of cardiac dysfunction following

insular ischemic stroke <sup>7</sup>, it is important to note that preliminary mechanistic conclusions from these clinical studies are largely speculative <sup>105</sup>. Given the high prevalence of shared risk factors between ischemic stroke and cardiovascular disorders, it is clinically challenging in these studies to confidently establish the neurological injury as the cause (or consequence) of SIHI <sup>2</sup>. Moreover, IC proximity to the MCA further complicates the pathophysiological interpretation of current clinical findings. In the past, clinical studies of SIHI predominantly recruited MCAO patients, due to the high incidence of this ischemic event. However, resulting damage in this stroke region extends beyond the IC <sup>56,120</sup>; minimizing the specificity of observed results. As such, experimental establishment of a focal insular ischemic stroke animal model is critical for the elimination of these clinically-inevitable confounding variables.

### *1.6.3 Lateralization of insular autonomic function*

Lateralization of insular autonomic function remains a current topic of discussion, bound by contradicting clinical results <sup>127-132</sup>. While early researchers identified right IC control over sympathetic activity <sup>127,131,132</sup>, present studies have produced opposing observations <sup>128-130</sup>. Most recently, Krause and colleagues were able to temporally localize autonomic lateralization to the anatomical subdivisions of the IC; discerning a right-sided parasympathetic (and left-sided sympathetic) predominance in the posterior IC <sup>130</sup>.

Intriguingly, current clinical reports have correlated right insular ischemic stroke to worsened outcomes <sup>125,133,134</sup>. As such, it is theorized that ischemic damage to the right IC inhibits parasympathetic control, shifting cardiovascular balance towards an increased sympathetic tone <sup>105,130</sup>; ultimately causing more severe outcomes of SIHI.

### *1.6.4 Rodent models of insular ischemic stroke*

In 1989, Cechetto and colleagues were first to examine stroke-induced autonomic and myocardial changes using a rodent model of MCAO; identifying an increase in blood pressure, NE and myocardial damage 3 h after ischemic stroke <sup>55</sup>. Based upon these results, Cechetto and colleagues concluded that their acute stroke model successfully mimicked clinical observations of post-stroke autonomic dysfunction <sup>55</sup>, further using it to examine lateralization of IC autonomic control <sup>135</sup>. Interestingly, this subsequent study identified the presentation of severe sympathetic consequences following right MCAO <sup>135</sup>, implying a right-sided

parasympathetic dominance of IC lateralization in the rat. Yet, to our knowledge, additional experimental studies have not been performed to validate this finding.

As mentioned previously, MCAO (within humans and rodents) creates a large infarct region, extending beyond the IC<sup>55,56,120</sup>. As such, the isolated association of ischemic IC damage with SIHI has yet to be confirmed. In 1995, Butcher and Cechetto reproduced similar autonomic changes to those observed in their MCAO stroke model, following injection of the excitotoxin D,L-homocysteic acid into the rat IC<sup>136</sup>. However, while this method produced focal IC damage, the injury was not ischemic; limiting translational potential. With recent advances in experimental stroke techniques<sup>57-59</sup>, ET-1 can be used to establish a more focal, and thus applicable, rodent model of insular ischemic stroke; confirming the mechanistic role of IC damage in SIHI.

## 1.7 The Acoustic Startle Response

### 1.7.1 Circuitry of the acoustic startle response

In animals, including humans, the startle response is an autonomic reflex that serves to protect the body<sup>137-139</sup>. Following a sudden and intense stimulus, excitation of the startle reflex will initiate rapid activation of cranial, facial and skeletal motor neurons; in preparation for facilitation of a fight-or-flight reaction<sup>138,139</sup>. Initiation of the startle response can be evoked through a variety of sensory signals; including acoustic, tactile, visual and vestibular stimuli<sup>140</sup> – of which the acoustic startle response (ASR) remains the most studied<sup>139</sup>. In humans, behavioural observations of this ASR are predominantly measured through the eye-blink reflex<sup>141,142</sup>.

Mediation of the ASR occurs through a simple neural circuit in the lower brainstem<sup>139,143,144</sup>, consisting of three main synaptic sites: cochlear root neurons (CRNs), the caudal pontine reticular nucleus (PnC) and facial motor neurons (Figure 2)<sup>145,146</sup>. In response to a loud auditory stimulus, spiral ganglion cells of the cochlea will directly stimulate neighbouring hair cells, transferring the sensory signal to CRNs of the auditory nerve<sup>145</sup>. From here, axons of CRNs extend to the brainstem, synapsing with the cochlear nucleus (CN), which in turn, synapses with the PnC<sup>146,147</sup>. The PnC serves as the indispensable sensorimotor interface of the ASR<sup>148-152</sup>. Upon receiving direct acoustic input from CN axons, giant neurons of the PnC will project onto cranial, facial and skeletal neurons<sup>152,153</sup> to initiate a reflexive motor response (Figure 2).

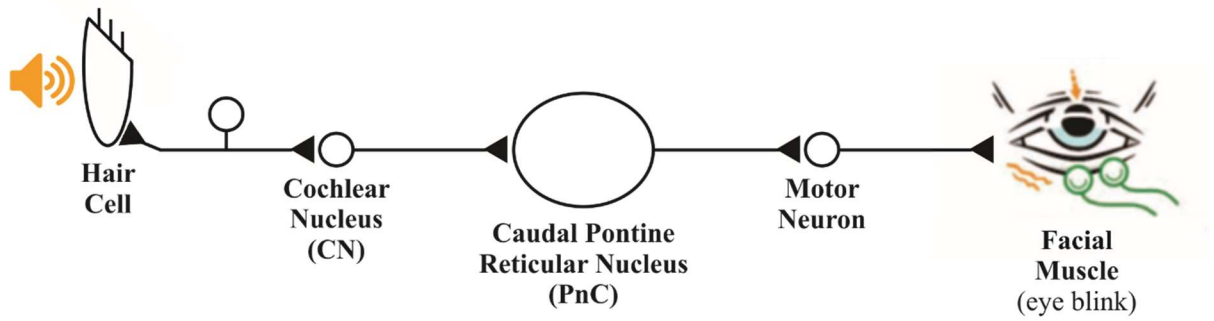


**Figure 2. Neural circuitry of the acoustic startle response.** In response to a loud auditory stimulus, spiral ganglion cells of the cochlea will stimulate cochlear hair cells; transferring the sensory signal along the auditory nerve to the cochlear nucleus (CN) of the lower brainstem. CN axons provide direct acoustic input to giant neurons of the caudal pontine reticular nucleus (PnC). In turn, these giant neurons of the PnC directly synapse onto cranial, facial and skeletal motor neurons, to initiate a rapid reflexive response. Adapted from Koch (1999) <sup>139</sup>.

### 1.7.2 Prepulse inhibition of the acoustic startle response

Enhancement or attenuation of the ASR can be modulated through a variety of influences, including habituation<sup>144,154,155</sup>, sensitization<sup>144,156,157</sup> and prepulse inhibition (PPI)<sup>158,159</sup>. In recent years, PPI of the ASR has received growing attention; serving as a reliable measure of sensorimotor gating<sup>139,160,161</sup>. Sensory gating is an autonomic process responsible for the filtration of unnecessary or redundant external stimuli<sup>160-162</sup>. Proper function of this gating system is imperative for efficient cognitive processing, minimizing overstimulation of higher cortical brain regions<sup>160,161</sup>.

PPI is the neurological phenomenon in which a weak prestimulus (prepulse) inhibits the reaction to a subsequent strong, startling stimulus; attenuating normal ASR amplitude (Figure 3A)<sup>145,159</sup>. Exact modulatory mechanisms of PPI on the ASR remain unknown<sup>139,145,163</sup>, however, present evidence suggests a direct inhibition of the PnC (Figure 3B)<sup>148,152,164,165</sup>. In response to an acoustic prepulse stimulus, CN axons will directly innervate the inferior colliculus (IFC); a midbrain structure vital for acoustic PPI propagation<sup>166-169</sup>. From here, the sensory signal is relayed to the superior colliculus (SPC)<sup>170</sup>, which in turn, synapses with the pedunculopontine tegmental nucleus (PPTg)<sup>171-173</sup>. Anatomically, the PPTg contains a descending cholinergic projection, directly extending to the PnC of the ASR pathway<sup>174-176</sup>. As such, stimulation of the PPTg initiates the release of ACh, inhibiting PnC excitation (Figure 3B)<sup>174-176</sup>. Interestingly, ACh acts on the PnC through slow-responding muscarinic receptors, eliciting a prolonged inhibitory effect<sup>163,167</sup>. Consequently, this long-lasting inhibition will attenuate any subsequent startle responses occurring within 30-500 ms after prepulse administration<sup>163</sup>.

Currently, recognition of autonomic dysfunction within the rat is predominantly classified through measurements of heart rate variability (HRV) or nerve discharge, requiring the use of invasive experimental procedures<sup>135,136</sup>. However, Saitoh and colleagues have reported a noradrenergic influence on PPI; observing deficits in sensorimotor gating following blockage of this sympathetically-controlled hormonal system<sup>177</sup>. As such, PPI of the ASR was implemented in this thesis, to serve as an alternate (and less intrusive) behavioural measurement of autonomic impairment.

### 1.7.3 Rodent models of the acoustic startle response

Recognition of the ASR in rats was first reported by Prosser and Hunter in 1936,

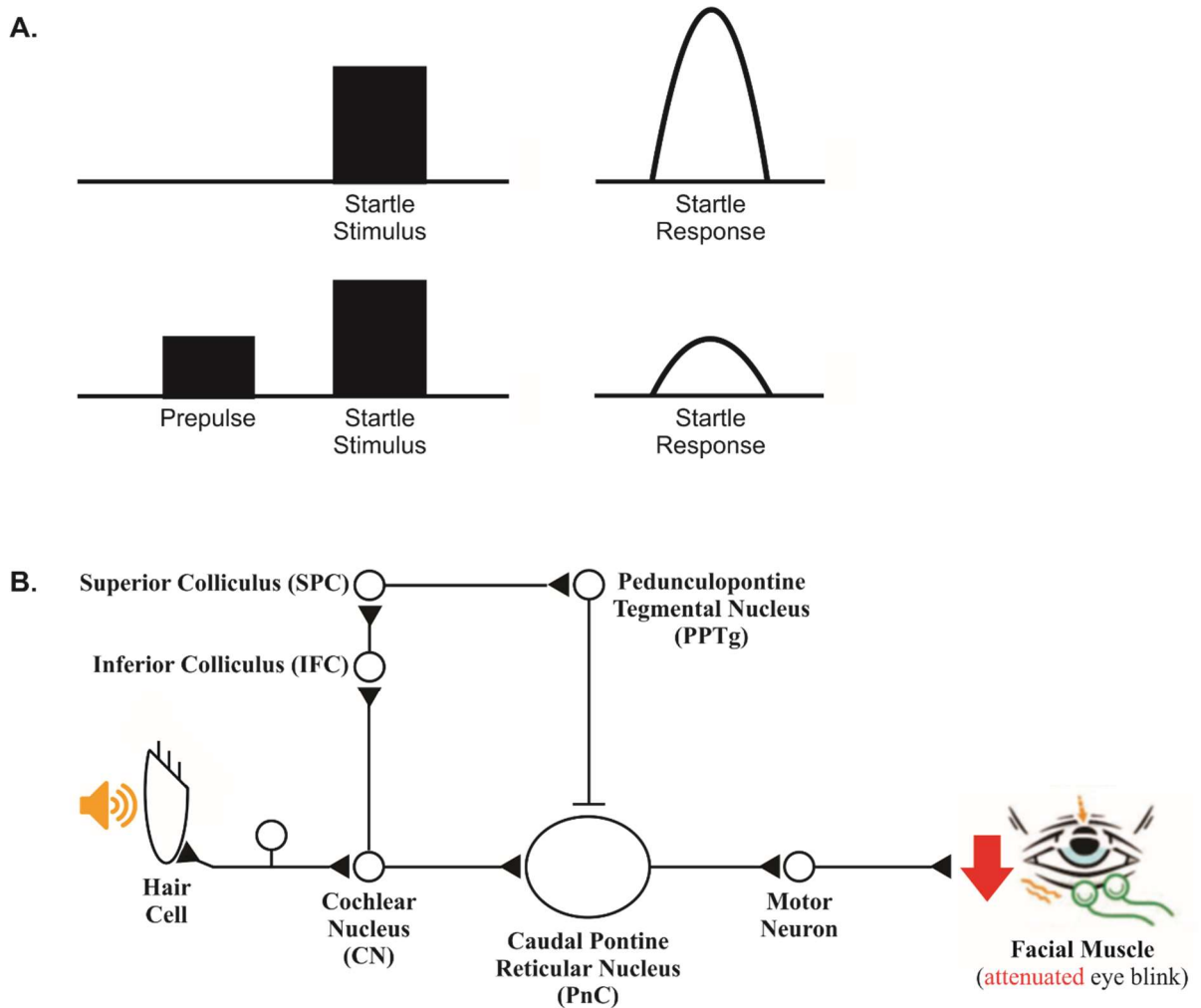


**Figure 3. Schematic overview of PPI and associated neural circuitry. (A)** Schematic representation of PPI. Administration of a weak prestimulus (prepulse) inhibits the reaction to a subsequent strong, startling stimulus; attenuating normal ASR amplitude. Adapted from Koch and Schnitzler (1997)<sup>145</sup>. **(B)** Neural circuitry of PPI. In response to an acoustic prepulse stimulus, cochlear nucleus (CN) axons will directly innervate the inferior colliculus (IFC). The sensory signal is then relayed to the superior colliculus (SPC), which in turn, synapses with the pedunclopontine tegmental nucleus (PPTg). Stimulation of the PPTg initiates the release of acetylcholine, ultimately inhibiting PnC excitation and attenuating the ASR. Adapted from Fendt, Li and Yeomans (2001)<sup>163</sup>.

confirming identical elicitation and ASR patterns in both humans and rats <sup>139,178</sup>. Since then, the rodent ASR has been extensively studied, in an attempt to better understand human mechanisms of sensorimotor integration <sup>139</sup>. In small animals, like the rat, measurements of the ASR are recorded from a “whole body” reflex; analogous to the “eye-blink” reflex in humans <sup>141,142,178</sup>. The ASR becomes functional immediately after the onset of hearing, at approximately postnatal day 12 in rats <sup>179,180</sup>. Differences in strain, and individual variability, can alter the magnitude of the ASR <sup>181,182</sup>. However, this does not change the quality, or pattern, of the reflex; simply causing an enhancement or attenuation of startle magnitude <sup>145</sup>. As such, the ASR in rodents serves as a reliable and robust measurement of sensorimotor integration <sup>145</sup>.

Similar to the ASR, identical mechanisms of PPI have been observed in humans and rats <sup>158,161,183</sup>. In both species, the amplitude of PPI remains dependent on the intensity of the prepulse stimulus, as well as the time interval between presentation of the prepulse and subsequent startle stimulus, referred to as the interstimulus interval (ISI) <sup>163,184,185</sup>. It is important to note that due to the neural complexity of PPI mediation and modulation, certain physiological manipulations may only affect PPI outcomes at a specific prepulse intensity or ISI <sup>184</sup>. As such, administration of assorted prepulse trials, varying in intensity (75 dB and 85 dB) and ISI (30 ms and 100 ms), is encouraged when assessing PPI of sensorimotor gating <sup>184</sup>.

## 1.8 Rationale, Objective and Hypothesis

The neurological influence of ischemic stroke in the generation of SIHI has been acknowledged for several years <sup>2,93</sup>. Yet, despite decades of research, the underlying pathophysiology of this intricate brain-heart connection remains unknown. Past studies have inferred a causative role of autonomic dysfunction in the manifestation of SIHI <sup>93-97</sup>. Supporting this, recent clinical data has identified an enhanced prevalence of SIHI in patients with damage to the IC <sup>7,124-127</sup>, a cortical site vital for the autonomic regulation of cardiovascular function <sup>2,108,109</sup>. Intriguingly, these clinical studies have discerned worse prognostic outcomes with *right* IC damage <sup>125,133,134</sup>; implying a lateralization of IC autonomic function. However, it is important to note that preliminary mechanistic conclusions from these clinical studies are largely speculative <sup>105</sup>, given the high prevalence of shared risk factors between ischemic stroke and cardiovascular disorders. As such, the establishment of a novel focal insular ischemic stroke animal model is crucial to eliminate these clinically-inevitable



confounding variables, and affirm current pathophysiological predictions. Furthermore, development of this novel rodent model will allow for the implementation of an accompanying, non-invasive behaviour test; aimed to evaluate functional post-insular stroke autonomic deficits. Successful application of this behavioural test could vitally improve current knowledge of IC autonomic lateralization.

In 1989, Cechetto and colleagues successfully reproduced clinical outcomes of stroke-induced autonomic and myocardial damage, using a rat model of MCAO<sup>55</sup>. However, use of this technique creates a large infarct region, extending beyond the IC<sup>55,56,120</sup>. Consequently, the isolated association of ischemic IC damage with SIHI has yet to be confirmed. Additionally, due to the invasiveness and severity of the procedure<sup>186</sup>, this experimental study only assessed acute timepoints<sup>55</sup>. Therefore, to date, little is known about the long-term prognosis and chronic effects of SIHI. Development of a focal insular stroke rodent model will confine primary ischemic damage to the IC, and allow for the extended observation of chronic pathology.

Recently, the contribution of inflammation, both cerebral and systemic, to SIHI has gained increased interest<sup>105,187,188</sup>. Pathologically, remote regions of neuroinflammation post-ischemic stroke have negatively corresponded to worse functional outcomes<sup>68,72,73,86</sup>. As described previously, the IC belongs to an intricate network of cortical and subcortical structures, responsible for the regulation of autonomic cardiovascular function<sup>2,108,109,189</sup>. As such, histological identification of secondary neuroinflammation, in any of these forebrain regions, could provide crucial insight into the neural manifestation of SIHI. Systemically, the neuroinflammatory activation of M1 microglia has been known to disrupt the BBB, initiating a peripheral immune response<sup>64</sup>. Intriguingly, Olshansky has hypothesized a parasympathetic role in the downregulation of myocardial inflammation<sup>114</sup>. A decrease in parasympathetic tone following IC damage could abolish beneficial effects of this PSNS regulation; enhancing systemic influence on cardiac inflammation, and resulting SIHI<sup>105</sup>; a mechanistic pathway yet to be examined.

The brain-heart connection remains a relevant and fascinating area of research. While past clinical, epidemiological and experimental studies have led to the identification and classification of this complex phenomenon, questions of mechanistic contribution remain unanswered. Successful establishment of a novel focal insular ischemic stroke rodent model

will allow for the extensive investigation of downstream behavioural and pathological outcomes; enhancing current pathophysiological knowledge of SIHI.

**Hypothesis:** SIHI is the consequence of autonomic dysfunction and inflammation, specific to insular ischemic stroke.

**Objective:** To establish a novel rodent model of focal insular ischemic stroke that can be used to evaluate chronic downstream behavioural and pathological outcomes of the brain and heart; improving mechanistic knowledge of SIHI.

## Section 2: METHODS

## 2.1 Animals

Experimental animal procedures were performed in accordance with the Canadian Council on Animal Care guidelines and approved by the Western University Animal Care Committee (Protocol 2016-027; Appendix). Upon arrival, 54 six-month old male Wistar rats (Charles River Laboratories, Montreal, QC), weighing 550-750 g, were individually housed at Western University's Animal Care and Veterinary Services on a 12:12 hour light/dark cycle alternating at 1 AM/PM. Room temperature was maintained at 22-24°C, and all rats accessed food and water *ad libitum*. Prior to surgical procedures, rats were randomly assigned to experimental groups.

## 2.2 Rat Models

### 2.2.1 Endothelin-1 ischemic model

ET-1 is a potent vasoconstrictor frequently used in animal models to produce ischemic strokes, similar to those observed in humans<sup>57-59,190-192</sup>. Focal injection of ET-1 inhibits cerebral blood flow to the targeted brain region for approximately 1 h, prior to reperfusion<sup>57</sup>. To mimic ischemic stroke in our rodent model, human ET-1 (Lot E7764; Sigma-Aldrich, Oakville, ON) was dissolved in sterile saline to achieve a final concentration of 20 pmol/μL. Aliquots of 10 μL were stored at -80°C until required.

### 2.2.2 Ibotenic acid neurotoxic model

Although ET-1 is most representative of focal human ischemic stroke<sup>191</sup>, associated ischemia can damage all structures located at the injection site; including intersecting white matter fibers<sup>190,193</sup>. This makes it difficult to conclude whether observed behavioural and pathological outcomes are a direct effect of targeted damage, or an indirect effect of unspecific white matter injury. To overcome this confounding dilemma, administration of the neurotoxin ibotenic acid (IA) was used as a positive control in this study; causing selective neuronal damage within the IC<sup>193,194</sup>. For this thesis, IA (Lot ab120041; Abcam Inc., Toronto, ON) was dissolved in 0.1 M sterile phosphate-buffered saline (PBS) to achieve a final concentration of 5 μg/μL. Aliquots of 10 μL were stored at -80°C until required. An additional group of saline control animals received administration of 0.1 M sterile PBS.

### 2.2.3 Surgical procedures

Rats were placed in a Harvard anesthesia box (Harvard Apparatus, Holliston, MA) and anesthetized with 4% isoflurane (Baxter Corporation, Mississauga, ON) mixed with 2.0 L/min of oxygen. Once fully anesthetized, the head of the rat was shaved to expose the scalp. Rats were then transferred to a Kopf stereotaxic frame (David Kopf Instruments, Tujunga, CA) to secure head position. While under anesthesia, rat body temperature was maintained at 37°C by heating pad. Anesthesia was maintained at 2.5% isoflurane for the duration of surgery.

Prior to incision, the rat's scalp was sanitized with soap, followed by 70% ethanol and iodine; to minimize risk of infection. A skin incision was then made along the scalp, exposing the rat skull and bregma. Pre-determined stereotaxic coordinates<sup>195</sup> (in reference to bregma) were used to locate the targeted IC brain region (anterior/posterior (AP): -1.00 mm, medial/lateral (ML):  $\pm 6.50$  mm, dorsal/ventral (DV): -7.00 mm) (Figure 4). Upon identification, a single burr hole was drilled into the skull to allow for the 1  $\mu$ L unilateral injection of ET-1, IA or PBS into the right (R) or left (L) IC (n=8/experimental group). Injections were performed at a rate of 0.2  $\mu$ L/min using a 32-gauge Hamilton syringe (Hamilton Company, Reno, NV), followed by an *in situ* period of 5 min to prevent solution backflow. Post-injection, the burr hole was covered with bone wax (Ethicon LLC, Puerto Rico, TX) prior to suturing of the incision site. Rats were then administered a 1 mL/kg subcutaneous injection of buprenorphine analgesic (Champion Alstoe Inc., Whitby, ON) and a 0.03 mL intramuscular injection of Baytril antibiotic (Bayer Inc., Toronto, ON). Following surgery, rats were returned to their individual cage and monitored closely until sternal recumbency was regained. Rats were then left freely until behaviour testing and euthanasia 28 d post-surgery. Experimental groups were balanced during each surgical day to avoid the introduction of day-specific confounding variables.

In addition to the aforementioned groups, an additional control group of no injection (NI) animals (n=6) were included in this study. Aside from not receiving a burr hole within the skull, or intracranial injection, these rats underwent identical surgical procedures, remaining under anesthesia for an equivalent amount of time as injection groups. A post-surgery mortality rate of 3.8% was observed in PBS-injected control animals (n=2), with a 0% mortality rate observed in all other experimental groups.

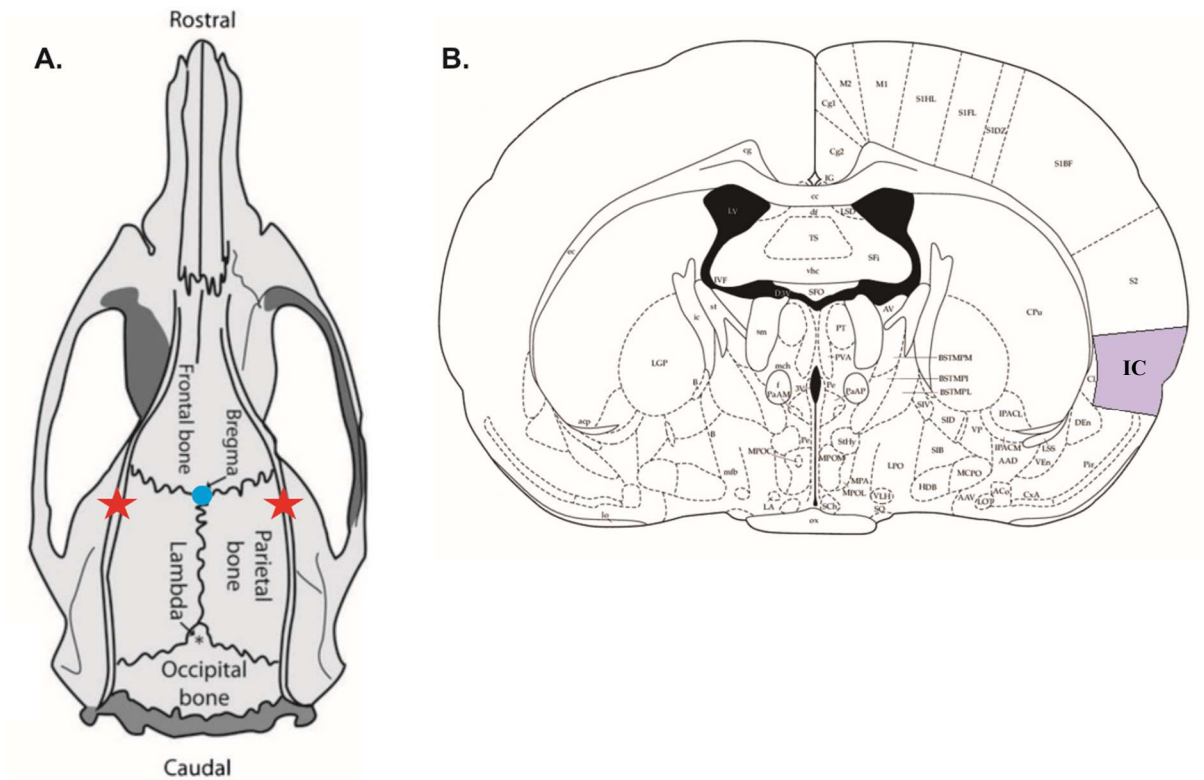


**Figure 4.** Schematic representation of targeted insular cortex brain region. (A) Pre-determined stereotaxic coordinates were used to locate the IC (red star), in reference to bregma (blue dot). Upon identification, a single burr hole was drilled into the rat's skull to allow for the 1  $\mu$ L unilateral injection of ET-1, IA or PBS into (B) the right or left IC (purple region). IC = insular cortex

## 2.3 Behaviour Testing

### 2.3.1 Prepulse inhibition of the acoustic startle response

Twenty-eight days post-surgery, rats were subjected to behaviour testing. PPI of the ASR was used to assess deficits in sensorimotor gating following IC injury<sup>139,160,161,184</sup>. Experimental groups were balanced throughout behavioural testing to avoid the introduction of day-specific confounding variables.

Two days prior to PPI measurement (day 26), rats were randomly assigned to 1 of 4 startle boxes (Med Associates Inc., St. Albans, VT) and subjected to four acclimation periods (2/day) (Figure 5). Rats were placed into the same startle chamber for the duration of their behavioural testing to avoid the introduction of instrument-specific confounding variables.

All rats were held inside the startle chambers using plastic holders. These holders were then attached to transducer platforms, which were used to measure motor output; a reliable indicator of the ASR<sup>184</sup>. During the first three acclimation periods, rats were exposed to 65 dB of white background noise for 5 min. For the final acclimation period, rats were subjected to 65 dB of white background noise for 5 min, followed by 12 acoustic startle stimuli increasing in volume by 5 dB intervals (65-120 dB). This measured and accounted for differences in individual startle responses between rats, as some naturally startled more or less than others. Sensitivity of the transducer platform was then adjusted, based off natural ASR to these 12 stimuli.

Following acclimation, rats underwent PPI testing (day 28) comprised of three phases: an acclimation phase, habituation phase (Block I) and PPI phase (Block II). During the acclimation phase, rats were exposed to 65 dB of white background noise for 5 min. This was immediately followed by Block I, in which rats were subjected to 50 identical trials containing an acoustic startle stimulus of 120 dB, administered every 20 s for a duration of 20 ms. Throughout Block II, rats were exposed to 50 randomized trials of varying prepulse stimuli, occurring every 20 s (Table 1).

Startle response data was collected and analyzed using Startle Reflex 5.95 software (Med Associates Inc., St. Albans, VT). PPI was calculated for each rat as a comparison to their individual startle response, using the following formula:

$$\% \text{ PPI} = [1 - (\text{PPI-pulse trial amplitude} / \text{pulse alone trial amplitude})] * 100$$

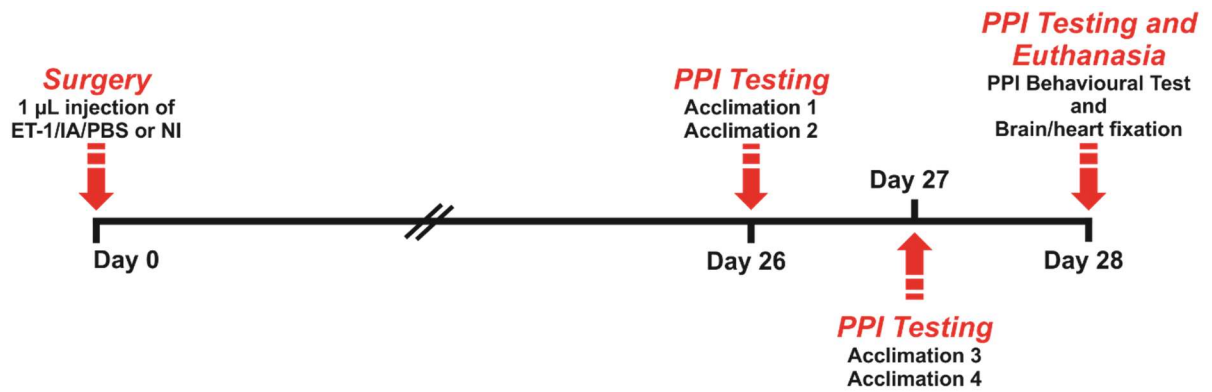


**Figure 5. Experimental timeline.** Six-month old male Wistar rats underwent stereotaxic surgery to receive a 1  $\mu\text{L}$  unilateral intracranial injection of ET-1 (20 pmol/ $\mu\text{L}$ ), IA (5  $\mu\text{g}/\mu\text{L}$ ) or PBS (0.1 M) into the right or left IC. An additional control group of NI rats received identical surgical procedures, without reagent injection. At 26 and 27 d post-surgery, rats were subjected to four acclimation periods (2/day), in preparation for the PPI behaviour test. At 28 d post-surgery, rats underwent PPI behaviour testing prior to euthanasia.



**Table 1. Prepulse and startle stimuli parameters used during Block II of the PPI behaviour test.** Rats were exposed to 50 randomized trials of varying prepulse intensity and interstimulus intervals (ISIs) to examine changes in sensorimotor gating following IC injury.

	Number of Trials	Prepulse Intensity	Prepulse Duration	Startle Intensity	Startle Duration	Interstimulus Interval
<b>Trial A</b>	10	-	-	120 dB	20 ms	-
<b>Trial B</b>	10	75 dB	4 ms	120 dB	20 ms	30 ms
<b>Trial C</b>	10	75 dB	4 ms	120 dB	20 ms	100 ms
<b>Trial D</b>	10	85 dB	4 ms	120 dB	20 ms	30 ms
<b>Trial E</b>	10	85 dB	4 ms	120 dB	20 ms	100 ms

## 2.4 Euthanasia

Immediately following behaviour testing (day 28), rats were euthanized via 2.5 mL intraperitoneal injection of pentobarbital (48 mg/mL; Bimeda-MTC, Cambridge, ON). Rats were transcardially perfused with 200 mL of 0.01 M PBS (pH 7.35), followed by 300 mL of 4% paraformaldehyde (PFA). After perfusion, brain and heart tissue were extracted and temporarily stored in 4% PFA at 4°C for an additional 24 and 48 h, respectively. Tissue was then transferred to 30% sucrose and stored at 4°C until sectioned.

## 2.5 Brain Histology and Immunohistochemistry

### 2.5.1 Tissue sectioning

Brain tissue was flash frozen in Tissue-Tek® O.C.T. Compound (Sakura Finetek USA Inc., Torrance, CA) and sectioned into 35 µm coronal sections using the CryoStar NX50 cryostat (Thermo Fisher Scientific, Waltham, MA). Free-floating sections were divided into 6 series (210 µm serial sections) and stored in cryoprotectant solution at -20°C until stained.

### 2.5.2 Thionine histochemistry

Brain tissue was histologically stained with thionine to visualize cellular Nissl substance and identify local cell death following IC injury<sup>196</sup>. Prior to staining, tissue sections were washed in 0.01 M PBS (pH 7.35) for 1 h at room temperature to remove residual cryoprotectant. Sections were then pre-mounted on VWR VistaVision™ microscope slides (VWR International, Radnor, PA) with 0.3% gelatin (Sigma-Aldrich, Oakville, ON) and left to air-dry overnight. The next day, mounted sections were rehydrated by immersion into descending concentrations of ethanol (100%, 95%, 70%, 50%), followed by immersion into distilled water (dH<sub>2</sub>O). Sections were then submerged into 0.5% thionin solution for 35 s, prior to dehydration. During dehydration, sections were exposed to a series of ascending ethanol concentrations (50%, 70%, 95%, 100%) before cleared in xylene (Caledon Laboratories Ltd., Georgetown, ON). Slides were then coverslipped using DePex mounting medium (VWR International, Radnor, PA) and stored at room temperature.

### 2.5.3 Immunohistochemistry

Brain tissue was immunohistochemically stained for either (i) activated M1 subtype microglia, (ii) astrocytes or (iii) neurons, to assess neuroinflammation (microglia/astrocyte

activation)<sup>197-200</sup> and secondary neuronal damage (loss of neurons)<sup>201,202</sup> post-insular injury. Activated microglia were identified through detection of the major histocompatibility complex II (MHC II) molecule, using an OX-6 primary antibody (Lot 554926; BD Biosciences, Mississauga, ON). Reactive astrocytes were identified through detection of the glial fibrillary acidic protein (GFAP), using a GFAP primary antibody (Lot G3893; Sigma-Aldrich, Oakville, ON). Neurons were identified through detection of the DNA-binding neuronal nuclei (NeuN) protein, using a NeuN primary antibody (Lot MAB377; Sigma-Aldrich, Oakville, ON).

For all three stains, tissue sections were washed in 0.01 M PBS (pH 7.35) for 1 h at room temperature to remove residual cryoprotectant. Free-floating sections were then incubated in 1% hydrogen peroxide (H<sub>2</sub>O<sub>2</sub>) for 10 min prior to blocking in 2% horse serum (Lot H0146, Sigma-Aldrich, Oakville, ON) for 1 h at room temperature. Sections were then incubated in diluted primary antibody solution (OX-6, GFAP or NeuN) overnight at 4°C (Table 2). The next day, sections were briefly washed with 0.01 M PBS (pH 7.35) for 15 min prior to incubation in diluted (1:500) biotinylated anti-mouse IgG secondary antibody solution (Lot 31806; Thermo Fisher Scientific, Waltham, MA). Tissue remained in secondary antibody solution for 1 h at room temperature. Sections were then incubated in 2% Avidin-Biotin Complex (ABC) reagent (Lot PI32020; Thermo Fisher Scientific, Waltham, MA) for 1 h. Sections were then stained with 0.05% 3,3'-diaminobenzidine tetrahydrochloride (DAB; Sigma-Aldrich, Oakville, ON) diluted in 1% H<sub>2</sub>O<sub>2</sub> for 5 min (OX-6) or 30 s (GFAP; NeuN). Sections were mounted onto VWR VistaVision™ microscope slides with 0.3% gelatin and left to air-dry overnight. The following day, sections were dehydrated via exposure to ascending ethanol concentrations (50%, 70%, 95%, 100%) and cleared in xylene. Slides were then coverslipped using DePex mounting medium and stored at room temperature. Each staining cohort included tissue representation from all experimental groups to eliminate day-specific confounding factors associated with natural variance in staining procedures.

## 2.6 Heart Histology

Heart tissue preparation and analysis was completed with assistance from Dr. Brittany Balint (Vulnerable Brain Lab, Schulich School of Medicine & Dentistry, Western University) and Caroline O'Neil (Molecular Pathology Facility, Robarts Research Institute, Western University).

**Table 2. Product summary of primary antibodies used for the immunohistochemical staining of brain tissue.**

Antibody	Host Species	Dilution Ratio	Cellular Target
OX-6	Mouse - monoclonal	1:1000	Activated microglia
GFAP	Mouse - monoclonal	1:2000	Reactive astrocytes
NeuN	Mouse - monoclonal	1:1000	Neurons

### 2.6.1 Tissue sectioning

Excess connective tissue was removed from rat hearts, prior to placement into tissue cassettes (Thermo Fisher Scientific, Waltham, MA) and dehydration via immersion into ascending ethanol concentrations (70%, 95%, 100%). Heart tissue was then cleared in xylene, before embedded in 65°C paraffin wax. Hearts were embedded to cassette blocks in their anterior anatomical position.

Prior to sectioning, heart tissue was rehydrated in an ice bath for 15 min. Tissue was then sliced into 5 µm coronal sections using the Leica CM350 microtome (Leica Biosystems Inc., Concord, ON). Ribbons of 5-6 tissue sections were then placed into a warm water bath to allow for flattening and separation of tissue. Individual sections were then mounted to SuperFrost Plus microscope slides (VWR International, Radnor, PA) and incubated overnight at 42°C for optimal adhesion. Slides were stored at -20°C until stained.

### 2.6.2 Masson's trichrome histochemistry

Heart tissue was histologically stained with Masson's trichrome to identify regions of collagen deposition post-insular injury, indicating cardiac fibrosis<sup>203,204</sup>. Prior to staining, pre-mounted tissue sections were deparaffinized in xylene for 15 min. Sections were then rehydrated by immersion into descending concentrations of ethanol (100%, 95%, 70%), followed by immersion into dH<sub>2</sub>O. Tissue sections were then placed into Bouin's fixative at 56°C for 1 h, prior to treatment with Weigert's hematoxylin for 10 min. Sections were then stained with Biebrich scarlet-acid fuchsin solution for 2 min and rinsed using 1% phosphotungstic acid. Tissue was then transferred to an Aniline blue dye for 5 min and rinsed using 1% acetic acid, prior to dehydration. During dehydration, sections were rapidly exposed to a series of ascending ethanol concentrations (95%, 100%) before cleared in xylene. Slides were then coverslipped using DePex mounting medium. Heart tissue was stained red, blue and purple; representing cardiomyocytes, collagen fibers and nuclei, respectively.

## 2.7 Tissue Analysis

### 2.7.1 Imaging and quantification

All stained tissue sections were visualized and imaged using a Nikon Eclipse Ni-E upright microscope with Nikon DS Fi2 colour camera and NIS Elements imaging software (Version 4.30.02; Nikon Instruments Inc., Melville, NY). The experimenter remained blinded

to all group identities throughout quantification to eliminate bias observations. Brain tissue stained with thionine confirmed injury location within the IC and was used to select a staining cohort (n=6) for each experimental group, dependent on precision of injury location. One NI animal was excluded as an outlier during quantification, due to abnormal amounts of neuroinflammation (activated microglia).

To analyze OX-6 and GFAP-stained brain tissue, four stitched photomicrographs (per animal; 10X magnification) of 35 µm coronal sections were imaged for each stain (AP: +2.70 mm, +1.20 mm, -0.40 mm and -3.30 mm, in reference to bregma). Using ImageJ software (Version 1.45; National Institute of Health, Bethesda, MD), % area coverage densitometry measurements of OX-6 and GFAP immunoreactivity were quantified for four regions of interest (ROI): forceps minor, corpus callosum, internal capsule and ventroposterior (VP) thalamus (Figure 6). For forceps minor (AP: +2.70 mm), internal capsule (AP: -3.30 mm) and VP thalamus assessment (AP: -3.30 mm), analysis was performed using a single coronal section. Furthermore, OX-6 and GFAP immunoreactivity was quantified in both hemispheres; comparing regions contralateral and ipsilateral to the injection site. To quantify OX-6 and GFAP immunoreactivity within the corpus callosum, % area coverage measurements were calculated and averaged for three coronal sections (AP: +1.20 mm, -0.40 mm and -3.30 mm, in reference to bregma).

To analyze NeuN-stained brain tissue, four stitched photomicrographs (per animal; 10X magnification) of 35 µm coronal sections were imaged (AP: +2.70 mm, +1.60 mm, -2.12 mm and -3.30 mm, in reference to bregma). Using NIS Elements imaging software, automated cell count measurements of NeuN immunoreactivity were performed for five ROIs: PFC (AP: +2.70 mm), ACC (AP: +1.60 mm), amygdala (AP: -2.12 mm), hypothalamus (AP: -2.12 mm) and VP thalamus (AP: -3.30 mm) (Figure 7). For all five ROIs, NeuN immunoreactivity was quantified in both hemispheres of a single coronal section, comparing regions contralateral and ipsilateral to the injection site.

To analyze Masson's Trichrome-stained heart tissue, eight stitched photomicrographs (per animal; 10X magnification) of 5 µm coronal sections were imaged from the left atrium (LA). Using ImageJ software, colour deconvolution was performed to isolate blue-stained tissue (collagen fibers). Percent area coverage of LA cardiac fibrosis was identified as the averaged total fraction of blue-stained tissue present within the eight imaged tissue regions.

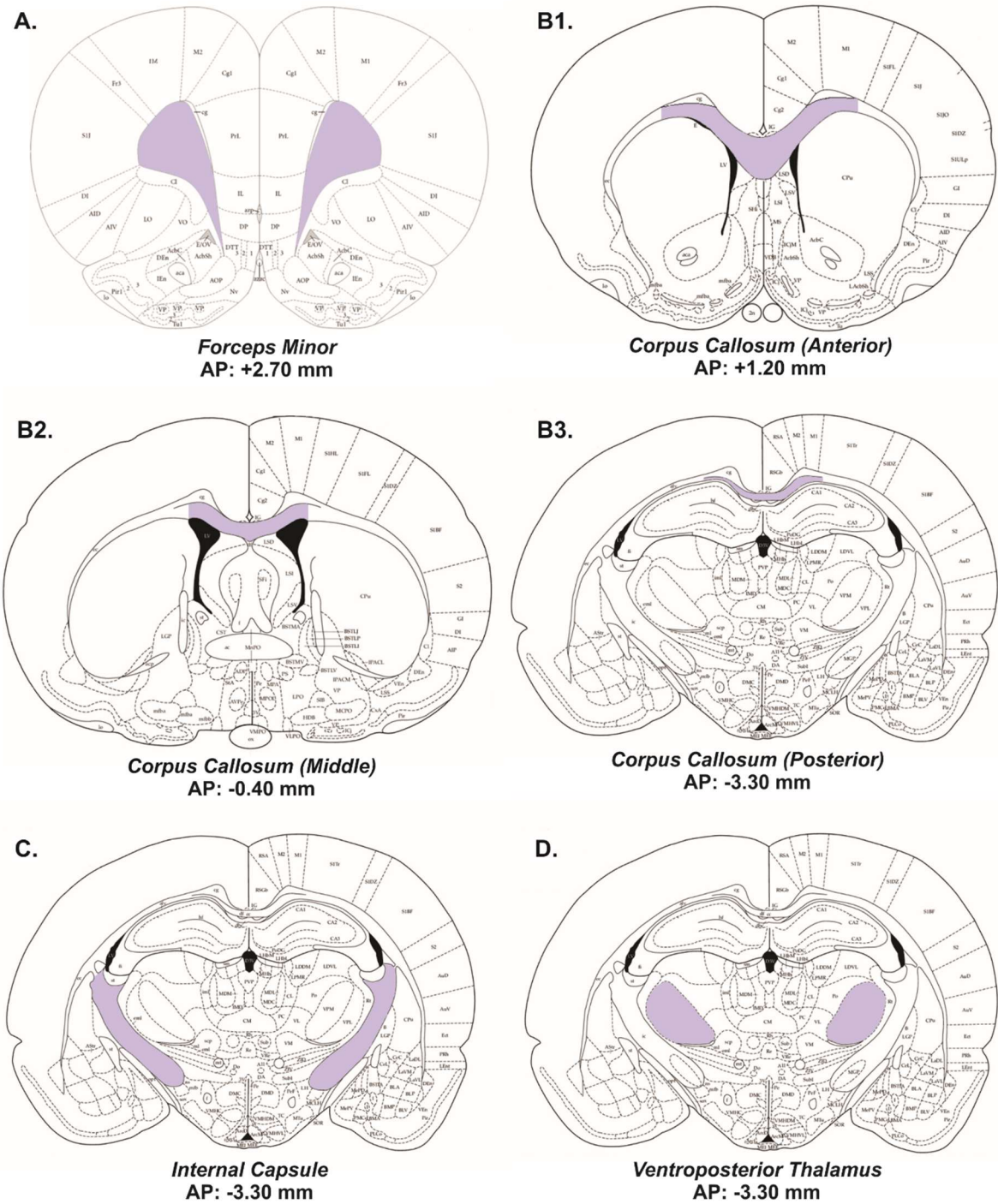


**Figure 6.** Schematic representation of brain ROIs selected for OX-6 and GFAP analysis. To investigate the presence of neuroinflammation, densitometry measurements of OX-6 or GFAP immunoreactivity were performed within the (A) forceps minor, (B1-B3) corpus callosum, (C) internal capsule and (D) ventroposterior thalamus. Purple regions represent areas of interest. AP = anterior/posterior stereotaxic coordinate (in reference to bregma).

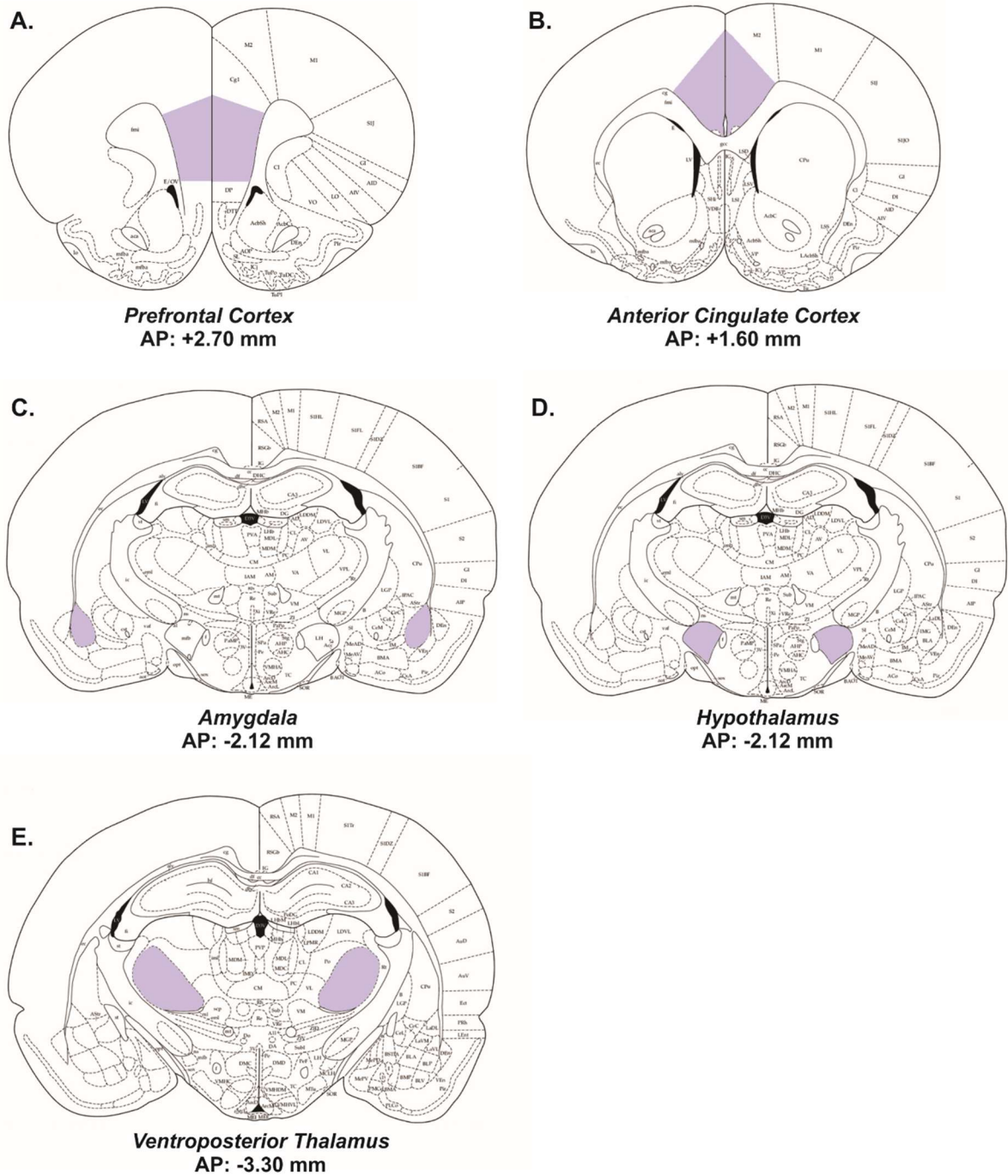


**Figure 7.** Schematic representation of brain ROIs selected for NeuN analysis. To investigate the presence of neuronal loss, automated cell count measurements of NeuN immunoreactivity were performed within the (A) prefrontal cortex, (B) anterior cingulate cortex, (C) amygdala, (D) hypothalamus and (E) ventroposterior thalamus. Purple regions represent areas of interest. AP = anterior/posterior stereotaxic coordinate (in reference to bregma).



### 2.7.2 Statistical analysis

Statistical analyses were conducted using GraphPad Prism software (Version 7.0; GraphPad Software Inc., La Jolla, CA). Statistical significance of dependent variables was assessed through two-way analysis of variance (ANOVA) followed by Tukey's multiple comparison test. Data are presented as mean  $\pm$  standard error of the mean (SEM), with a statistical alpha of 0.05.

### Section 3: RESULTS

### 3.1 Qualitative Confirmation of Targeted Insular Damage

Initial qualitative analysis of injury location was performed to confirm IC damage. Brain tissue was histologically stained with thionine to identify Nissl bodies (Figure 8A,B), indicating the presence of healthy cell populations. Due to the rapid recovery rate of ischemic injury (induced by ET-1), infarct scars were often difficult to clearly visualize at low magnification (2X objective lens). However, use of a 20X objective lens revealed a loss of neurons and increased presence of supporting glial cells within the IC of injured groups (IA/ET-1), compared to uninjured groups (PBS/NI; Figure 8A,B). Additionally, brain tissue was immunohistochemically stained with NeuN (Figure 8C,D) and OX-6 (Figure 8E,F) for secondary confirmation of targeted IC damage. Staining of tissue with NeuN was used to identify neurons and confirmed neuronal loss within the IC of injured groups (IA/ET-1; Figure 8C). Tissue stained with OX-6 identified substantial amounts of activated microglia present within the IC of injured groups (IA/ET-1; Figure 1E), further confirming local damage.

### 3.2 Behavioural Assessment

#### 3.2.1 Left insular damage corresponds with an observed trend of reduced prepulse inhibition

In developing this rodent model of focal insular ischemic stroke, it was crucial to establish an accompanying behaviour test, capable of identifying autonomic deficits post-insular injury. More importantly, successful implementation of this test could provide valuable insight into the lateralization of IC autonomic function. To identify and evaluate autonomic dysfunction, PPI of the ASR was measured 28 d following insular injury; indicating functional changes in sensorimotor gating. In the past, blockage of the sympathetically-controlled noradrenergic system has corresponded with impaired sensorimotor gating<sup>177</sup>. As such, rats subjected to IC injury, causing decreased sympathetic outflow, were expected to display a reduction in PPI; with damage to the IC disrupting sympathetic control of the noradrenergic system, inhibiting normal sensorimotor gating processes.

Administration of the ASR subjected rats to 40 randomized trials of varying prepulse stimuli, changing in stimulus intensity (75 dB or 85 dB) and ISI (30 ms or 100 ms). An additional 10 trials presented startle stimuli only, to attain baseline startle responses of each rat. Percent PPI was calculated as the startle reduction of this averaged baseline measurement, with a higher % PPI representing a greater reduction in startle response.

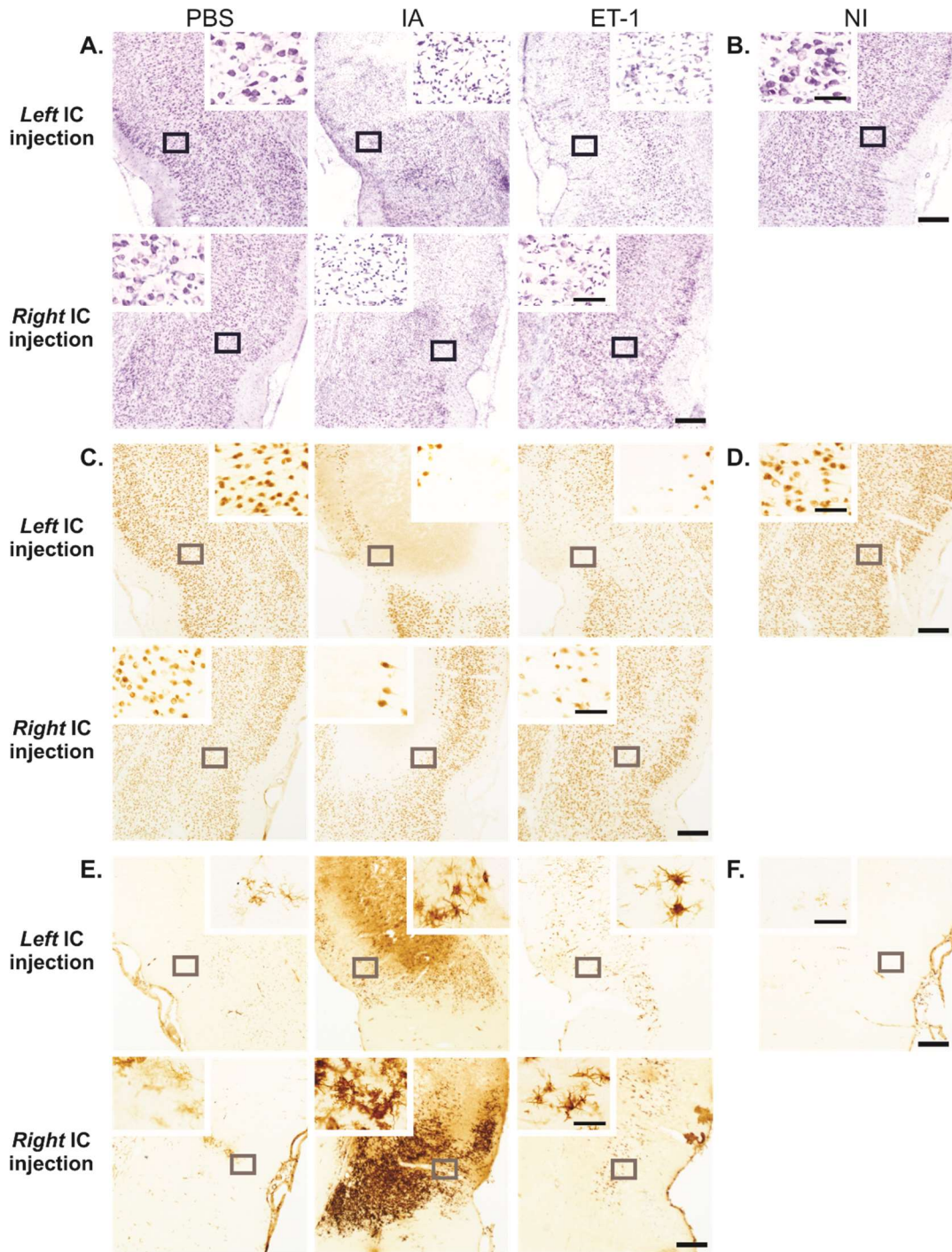


**Figure 8. Qualitative confirmation of insular damage.** Representative 2X photomicrographs of coronal rat brain tissue histologically stained with (A,B) thionine, or immunohistochemically stained with (C,D) NeuN or (E,F) OX-6, 28 d following intracranial injection of PBS (n=7), IA (n=8), ET-1 (n=8) or NI (n=6) into the right or left insular cortex. Outlined areas represent higher-magnified regions (20X) of the insular cortex. At 28 d post-injection, injured rats displayed neuronal loss (A,C: IA/ET-1) and enhanced microgliosis (A,E: IA/ET-1) compared to uninjured groups (A,C,E: PBS; B,D,F: NI), confirming insular damage. Scale bar = 500  $\mu$ m (2X) or 50  $\mu$ m (20X). IC = insular cortex, PBS = phosphate-buffered saline, IA = ibotenic acid, ET-1 = endothelin-1, NI = no injection

At 28 d post-insular injury, rats subjected to left IC damage (IA/ET-1) displayed an observed trend of deficient sensorimotor gating. Administration of a 75 dB prepulse, with 30 ms ISI, caused a notable decrease in % PPI of IA-L (60.69% ± 14.05%) and ET1-L (59.58% ± 10.89%) groups, compared to (i) IA-R (96.24% ± 12.93%) and ET1-R (88.51% ± 13.78%) injury groups and (ii) PBS-L (102.31% ± 12.65%) and NI (100.00% ± 6.00%) control groups (Figure 9A). However, completion of a two-way ANOVA identified no significant effect of injury ( $F_{(3,50)} = 2.42$ ,  $p = 0.08$ ) and/or insular damage lateralization ( $F_{(1,50)} = 2.38$ ,  $p = 0.13$ ). Additional trials consisting of (i) 75 dB prepulse with 100 ms ISI (Figure 9B), (ii) 85 dB prepulse with 30 ms ISI (Figure 9C) and (iii) 85 dB prepulse with 100 ms ISI (Figure 9D) displayed similar results, demonstrating a minor decrease in % PPI of left injury groups (IA/ET-1). However, these observed reductions were not as substantial as the trending deficits observed after administration of a 75 dB prepulse with 30 ms ISI (Figure 9A).

### 3.3 Analysis of Brain Immunohistochemistry

#### 3.3.1 *Insular damage enhances white matter microgliosis, but not astrogliosis, in the corpus callosum*

Neuroinflammation is a known consequence of ischemic stroke, vital for post-ischemic tissue repair<sup>35-37,53</sup>. However, not all neuroinflammation has been associated with beneficial effects. In particular, post-stroke chronic inflammation, of remote grey and white matter regions, has been shown to perpetuate secondary neurodegeneration in brain regions anatomically connected to the primary ischemic infarct<sup>87-91</sup>; worsening prognostic outcomes and recovery time<sup>68,72,73</sup>. We therefore used our established rodent model of focal insular ischemic stroke to identify remote regions of secondary cerebral inflammation that may contribute to the functional autonomic deficits observed, both clinically and experimentally, post-insular injury.

Initial analysis of white matter neuroinflammation was performed in the corpus callosum; the largest commissural fibre of the brain. Brain tissue was immunohistochemically stained with OX-6 or GFAP to identify activated microglia or reactive astrocytes, respectively, as both microgliosis and astrogliosis are known mechanisms of neuroinflammation<sup>35-37,53,61</sup>. Densitometry measurements of % area coverage were quantified as the averaged total fraction of OX-6 or GFAP immunolabelled cells present within the corpus callosum of three coronal tissue sections.

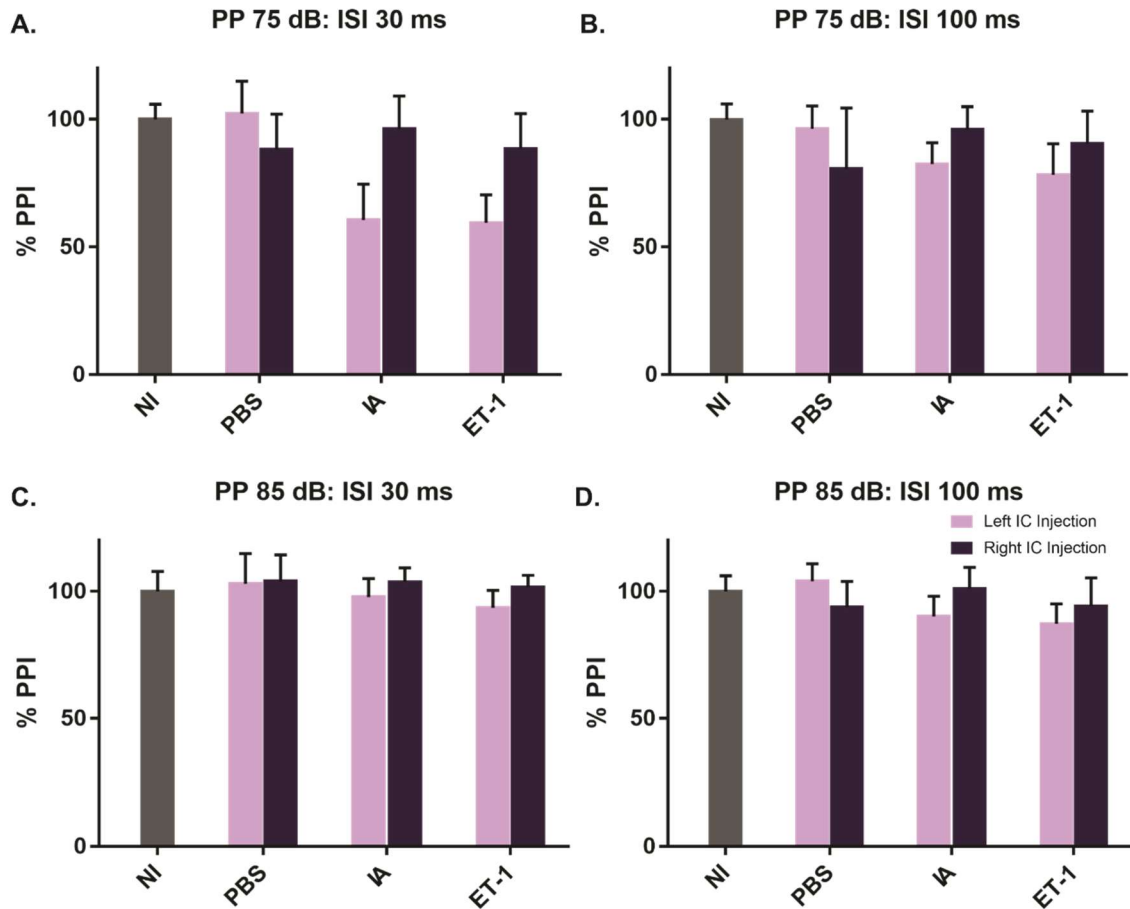


**Figure 9. Left insular damage corresponds with an observed trend of reduced prepulse inhibition.** Percent PPI of the ASR was measured 28 d following intracranial injection of PBS (n=7), IA (n=8), ET-1 (n=8) or NI (n=6) into the right or left insular cortex. Rats were subjected to randomized trials of varying prepulse stimuli administered at (A) 75 dB, 30 ms before startle stimulus, (B) 75 dB, 100 ms before startle stimulus, (C) 85 dB, 30 ms before startle stimulus or (D) 85 dB, 100 ms before startle stimulus. Damage to the left insular cortex notably reduced % PPI, particularly during administration of a (A) 75 dB prepulse, 30 ms prior to startle stimulus. Data is presented as mean  $\pm$  SEM and normalized to the NI group. IC = insular cortex, PPI = prepulse inhibition, PP = prepulse, ISI = interstimulus interval, NI = no injection, PBS = phosphate-buffered saline, IA = ibotenic acid, ET-1 = endothelin-1

At 28 d post-insular injury, OX-6 staining for activated microglia presented a significant effect of injury ( $F_{(3,38)} = 12.59$ ,  $p < 0.01$ , two-way ANOVA). Left IC damage resulted in enhanced corpus callosum microgliosis in rats injected with IA ( $9.82\% \pm 2.06\%$ ) or ET-1 ( $8.15\% \pm 2.24\%$ ), compared to PBS ( $3.32\% \pm 0.54\%$ ) and NI ( $1.41\% \pm 0.31\%$ ) rats (Figure 10A-C). Increased corpus callosum microgliosis was also observed following injection of IA ( $9.60\% \pm 1.71\%$ ) or ET-1 ( $5.71\% \pm 1.78\%$ ) into the right IC (Figure 10A,C), indicating no significant effect of insular damage lateralization ( $F_{(1,38)} = 0.56$ ,  $p = 0.46$ , two-way ANOVA). Rats subjected to injection of PBS into the right IC also displayed minimal microgliosis ( $2.84\% \pm 0.47\%$ ), similar to the PBS-L group (Figure 10A,C). Upon completion of Tukey's multiple comparison test, a significant difference in corpus callosum microgliosis between NI/IA-L ( $p = 0.01$ ), NI/IA-R ( $p = 0.01$ ) and PBS-R/IA-R ( $p = 0.04$ ) groups was confirmed (Figure 10C). A significant difference between injured groups (IA/ET-1;  $p = 0.26$ ) or uninjured groups (NI/PBS;  $p = 0.83$ ) was not observed (Figure 10C). GFAP staining for reactive astrocytes indicated no significant differences in corpus callosum astrogliosis between experimental groups ( $F_{(3,38)} = 1.53$ ,  $p = 0.22$ , two-way ANOVA), with all groups displaying similar measurements of GFAP % area coverage: NI ( $29.89\% \pm 2.67\%$ ), PBS-L ( $27.27\% \pm 4.38\%$ ), PBS-R ( $24.38\% \pm 2.59\%$ ), IA-L ( $26.66\% \pm 1.96\%$ ), IA-R ( $22.57\% \pm 3.62\%$ ), ET1-L ( $23.31\% \pm 3.50\%$ ) and ET1-R ( $23.61\% \pm 2.16\%$ ) (Figure 11A-C).

### *3.3.2 Insular damage does not enhance white matter microgliosis or astrogliosis in the forceps minor*

In addition to the corpus callosum, neuroinflammation was analyzed within the forceps minor. While the corpus callosum is anatomically proximal to the injured insular site, the forceps minor is a distal fibre bundle located anteriorly within the frontal lobe; allowing for the assessment of neuroinflammatory spread. Densitometry measurements of % area coverage were quantified as the total fraction of OX-6 (microglia) or GFAP (astrocytes) immunolabelled cells present within the forceps minor of one coronal tissue section. Comparisons of microgliosis or astrogliosis within the contralateral and ipsilateral forceps minor were performed to account for unilateral IC damage.

At 28 d post-insular injury, OX-6 staining for activated microglia presented no significant effect of injury for both left ( $F_{(3,38)} = 2.65$ ,  $p = 0.06$ , two-way ANOVA) and right ( $F_{(3,38)} = 1.65$ ,  $p = 0.19$ , two-way ANOVA) experimental groups. Following damage to the left

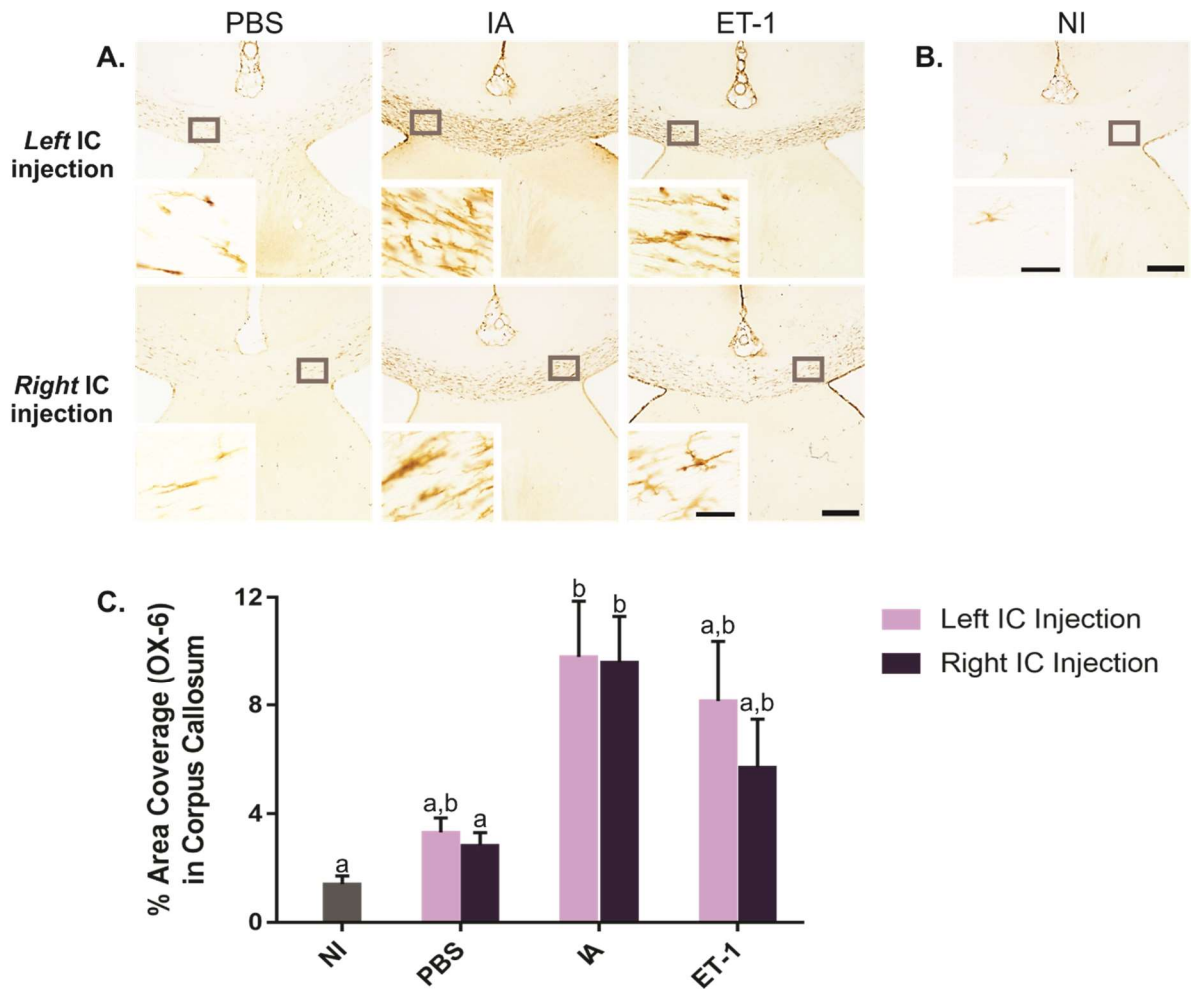


**Figure 10. Insular damage significantly increases white matter microgliosis within the corpus callosum.** Representative 2X photomicrographs of OX-6 immunohistochemical stained coronal rat brain tissue, 28 d following intracranial injection of (A) PBS, IA, ET-1 (n=6/experimental group) or (B) no injection (n=5) into the right or left insular cortex. Outlined areas represent higher-magnified regions (20X) of the corpus callosum. (C) Quantitative analysis revealed significant increases in microglia activation (% area coverage) within the corpus callosum 28 d following insular injury. Data is presented as mean  $\pm$  SEM. Non-matching letters indicate significant differences between experimental groups ( $p < 0.05$ , two-way ANOVA followed by Tukey's multiple comparison test). Scale bar = 500  $\mu$ m (2X) or 50  $\mu$ m (20X). IC = insular cortex, PBS = phosphate-buffered saline, IA = ibotenic acid, ET-1 = endothelin-1, NI = no injection



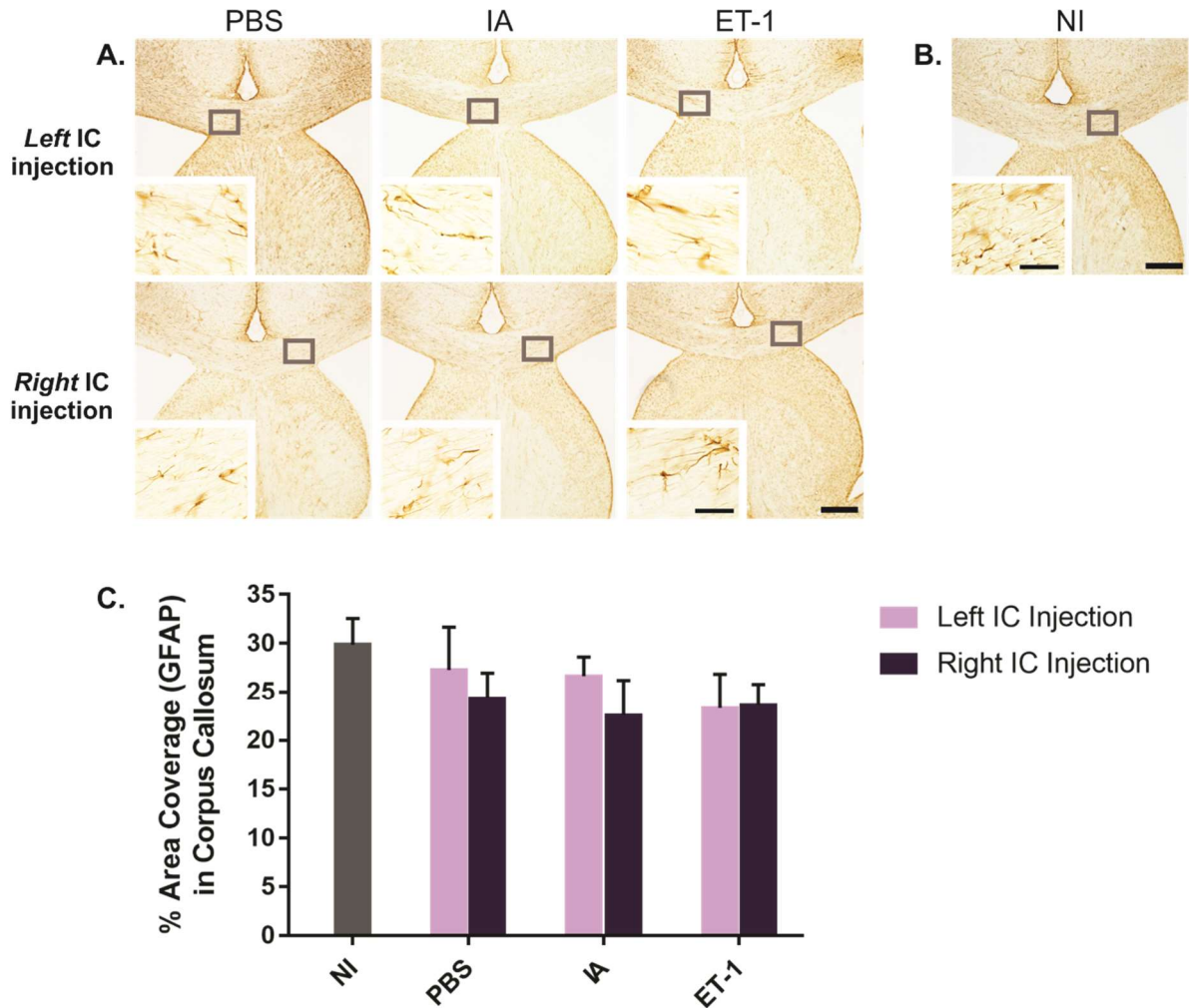


**Figure 11.** Insular damage does not enhance white matter astroglia within the corpus callosum. Representative 2X photomicrographs of GFAP immunohistochemical stained coronal rat brain tissue, 28 d following intracranial injection of (A) PBS, IA, ET-1 (n=6/experimental group) or (B) no injection (n=5) into the right or left insular cortex. Outlined areas represent higher-magnified regions (20X) of the corpus callosum. (C) Quantitative analysis revealed no significant differences in corpus callosum astroglia (% area coverage) between experimental groups. Data is presented as mean  $\pm$  SEM. Scale bar = 500  $\mu$ m (2X) or 50  $\mu$ m (20X). IC = insular cortex, PBS = phosphate-buffered saline, IA = ibotenic acid, ET-1 = endothelin-1, NI = no injection

or right IC, minimal levels of microgliosis within the ipsilateral forceps minor of IA (IA-L  $3.91\% \pm 1.33\%$ ; IA-R  $3.62\% \pm 1.51\%$ ) and ET-1 (ET1-L  $2.55\% \pm 0.79\%$ ; ET1-R  $2.50\% \pm 0.85\%$ ) groups were observed, compared to PBS (PBS-L  $2.55\% \pm 0.52\%$ ; PBS-R  $1.99\% \pm 0.50\%$ ) and NI ( $1.19\% \pm 0.32\%$ ) control animals (Figure 12A-D). Furthermore, significant differences between microglia activation within the contralateral and ipsilateral forceps minor of both left (Figure 12C;  $F_{(1,38)} = 0.01$ ,  $p = 0.92$ , two-way ANOVA) and right (Figure 12D;  $F_{(1,38)} = 0.14$ ,  $p = 0.71$ , two-way ANOVA) experimental groups were not observed.

GFAP staining for reactive astrocytes indicated no significant differences in ipsilateral forceps minor astrogliosis within left ( $F_{(3,38)} = 0.89$ ,  $p = 0.46$ , two-way ANOVA) and right ( $F_{(3,38)} = 1.06$ ,  $p = 0.38$ , two-way ANOVA) experimental groups, with all groups displaying similar measurements of GFAP % area coverage: NI ( $32.62\% \pm 7.02\%$ ), PBS-L ( $34.23\% \pm 4.42\%$ ), PBS-R ( $31.36\% \pm 4.66\%$ ), IA-L ( $28.44\% \pm 3.23\%$ ), IA-R ( $28.00\% \pm 3.43\%$ ), ET1-L ( $33.53\% \pm 3.60\%$ ) and ET1-R ( $25.52\% \pm 4.87\%$ ) (Figure 13A-D). Similar levels of reactive astrocytes were also observed within the contralateral forceps minor, revealing no significant differences in astrogliosis between the contralateral and ipsilateral forceps minor for both left (Figure 13C;  $F_{(1,38)} = 1.06$ ,  $p = 0.31$ , two-way ANOVA) and right (Figure 13D;  $F_{(1,38)} = 0.16$ ,  $p = 0.69$ , two-way ANOVA) experimental groups.

### *3.3.3 Insular damage enhances white matter microgliosis, but not astrogliosis, in the ipsilateral internal capsule*

Additional neuroinflammatory analysis was performed within the internal capsule, a subcortical fibre bundle located posteriorly to the injured IC region. Quantification of neuroinflammation within this white matter region was of particular interest, as the internal capsule comprises the corticobulbar tract; transferring information between the cortex and brainstem. With the brainstem home to numerous autonomic cardiovascular centres<sup>2,108,205</sup>, a neuroinflammatory response within the internal capsule could provide important insight into secondary neurodegeneration of autonomic brainstem structures post-insular ischemic stroke. Densitometry measurements of % area coverage were quantified as the total fraction of OX-6 (microglia) or GFAP (astrocytes) immunolabelled cells present within the internal capsule of one coronal tissue section. Comparisons of microgliosis or astrogliosis within the contralateral and ipsilateral internal capsule were performed to account for unilateral IC damage.

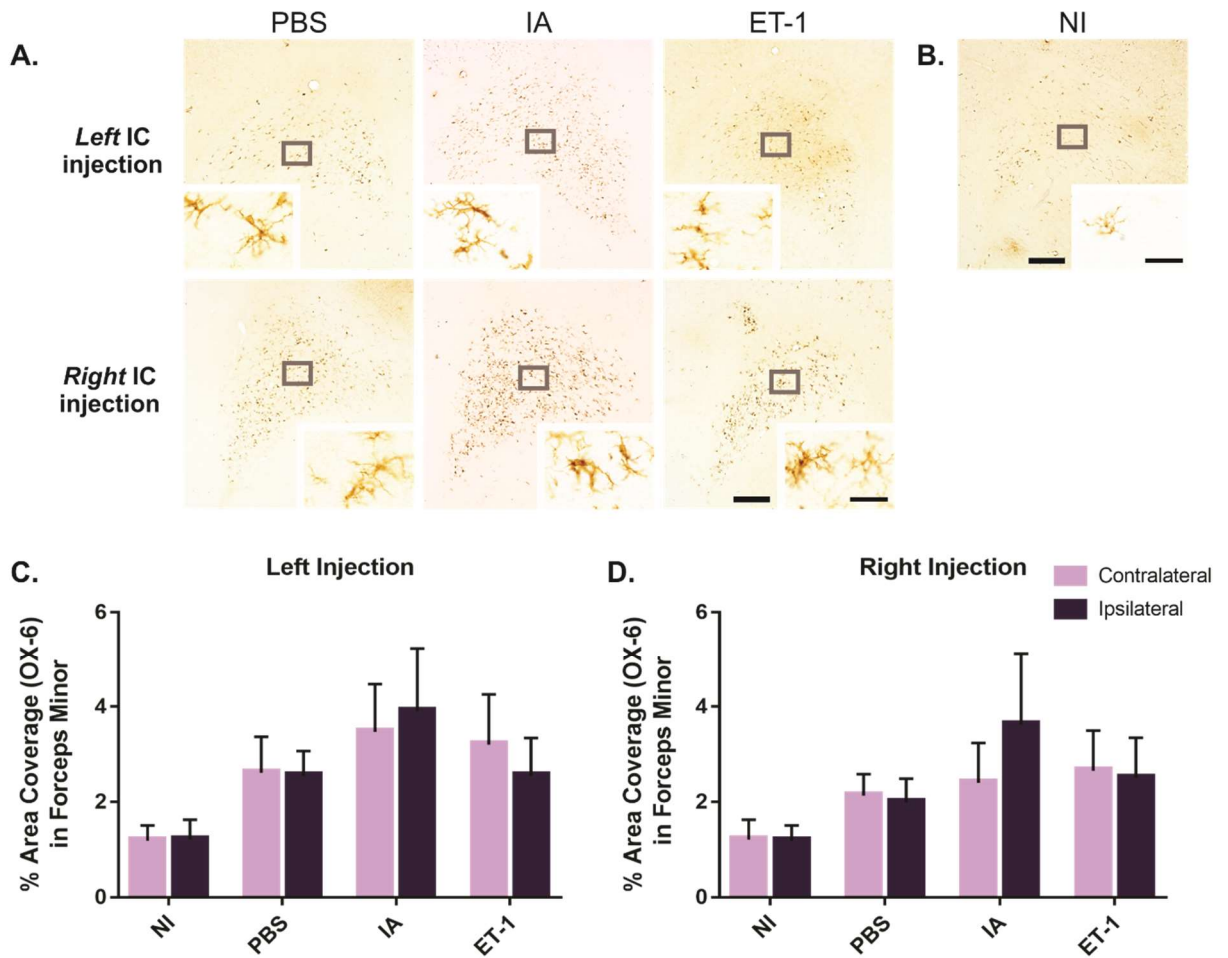


**Figure 12. Insular damage does not enhance white matter microgliosis within the forceps minor.** Representative 2X photomicrographs of OX-6 immunohistochemical stained coronal rat brain tissue, 28 d following intracranial injection of (A) PBS, IA, ET-1 (n=6/experimental group) or (B) no injection (n=5) into the right or left insular cortex. Outlined areas represent higher-magnified regions (20X) of the ipsilateral forceps minor. (C, D) Quantitative analysis revealed no significant differences in contralateral and ipsilateral forceps minor microgliosis (% area coverage) within, and between, experimental groups. Data is presented as mean  $\pm$  SEM. Scale bar = 500  $\mu\text{m}$  (2X) or 50  $\mu\text{m}$  (20X). IC = insular cortex, PBS = phosphate-buffered saline, IA = ibotenic acid, ET-1 = endothelin-1, NI = no injection

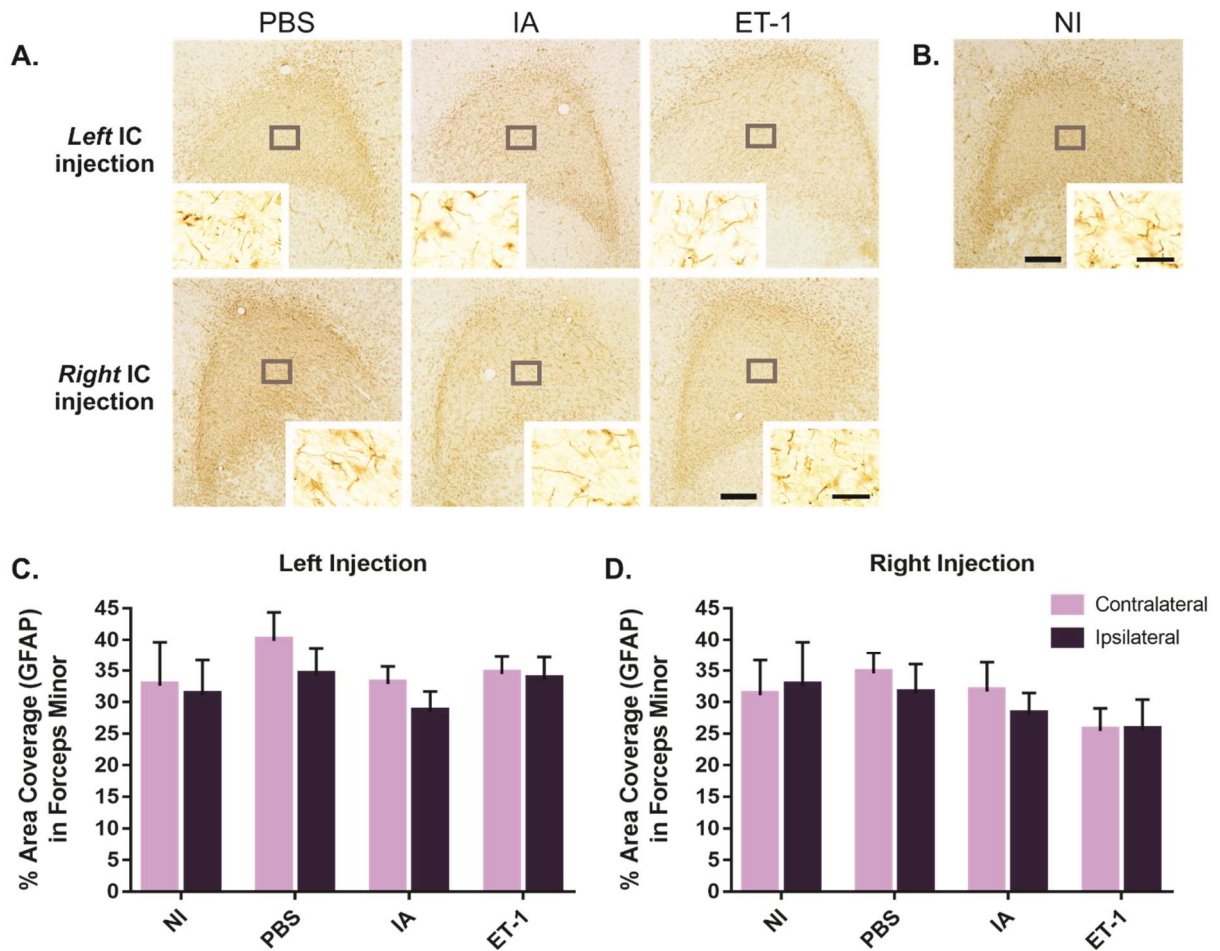


**Figure 13. Insular damage does not enhance white matter astrogliosis within the forceps minor.** Representative 2X photomicrographs of GFAP immunohistochemical stained coronal rat brain tissue, 28 d following intracranial injection of (A) PBS, IA, ET-1 (n=6/experimental group) or (B) no injection (n=5) into the right or left insular cortex. Outlined areas represent higher-magnified regions (20X) of the ipsilateral forceps minor. (C, D) Quantitative analysis revealed no significant differences in contralateral and ipsilateral forceps minor astrogliosis (% area coverage) within, and between, experimental groups. Data is presented as mean  $\pm$  SEM. Scale bar = 500  $\mu$ m (2X) or 50  $\mu$ m (20X). IC = insular cortex, PBS = phosphate-buffered saline, IA = ibotenic acid, ET-1 = endothelin-1, NI = no injection

At 28 d post-insular injury, OX-6 staining for activated microglia presented a significant effect of injury for both left ( $F_{(3,38)} = 9.32$ ,  $p < 0.01$ , two-way ANOVA) and right ( $F_{(3,38)} = 7.87$ ,  $p < 0.01$ , two-way ANOVA) experimental groups. Following damage to the left or right IC, enhanced levels of microgliosis within the ipsilateral internal capsule of IA (IA-L  $7.83\% \pm 1.61\%$ ; IA-R  $11.55\% \pm 2.45\%$ ) and ET-1 (ET1-L  $6.82\% \pm 1.06\%$ ; ET1-R  $5.66\% \pm 1.61\%$ ) groups were observed, compared to PBS (PBS-L  $3.61\% \pm 0.85\%$ ; PBS-R  $3.75\% \pm 1.06\%$ ) and NI ( $2.09\% \pm 0.46\%$ ) control animals (Figure 14A-D). Similar levels of microgliosis occurred in the ipsilateral internal capsule of both left and right experimental injury groups, indicating no significant effect of insular damage lateralization ( $F_{(1,38)} = 0.56$ ,  $p = 0.46$ , two-way ANOVA). Upon completion of Tukey's multiple comparison test, a significant difference in ipsilateral internal capsule microgliosis between NI/IA-L ( $p < 0.01$ ), NI/IA-R ( $p < 0.01$ ), NI/ET1-L ( $p = 0.01$ ), PBS-L/IA-L ( $p = 0.04$ ) and PBS-R/IA-R ( $p < 0.01$ ) groups was confirmed (Figure 14C,D). A significant difference between injured groups (IA/ET-1;  $p = 0.10$ ) or uninjured groups (NI/PBS;  $p = 0.74$ ) was not observed (Figure 14C,D). Furthermore, a significant difference between microglia activation within the ipsilateral and contralateral internal capsule was observed for both left ( $F_{(1,38)} = 9.10$ ,  $p < 0.01$ , two-way ANOVA) and right ( $F_{(1,38)} = 6.03$ ,  $p = 0.02$ , two-way ANOVA) experimental groups (Figure 14C,D). While IC damage caused enhanced internal capsule microgliosis both contralaterally and ipsilaterally, greater levels of microglia activation were observed within the ipsilateral internal capsule of IA-L (ipsilateral =  $7.83\% \pm 1.61\%$ ; contralateral =  $4.36\% \pm 1.06\%$ ), IA-R (ipsilateral =  $11.55\% \pm 2.45\%$ ; contralateral =  $4.94\% \pm 1.09\%$ ), ET1-L (ipsilateral =  $6.82\% \pm 1.06\%$ ; contralateral =  $3.92\% \pm 0.61\%$ ) and ET1-R (ipsilateral =  $5.66\% \pm 1.61\%$ ; contralateral =  $3.80\% \pm 1.16\%$ ) groups (Figure 14C,D). Upon completion of Tukey's multiple comparison test, a significant difference between microgliosis within the contralateral and ipsilateral internal capsule of the IA-R group ( $p = 0.02$ ) was confirmed (Figure 14D).

GFAP staining for reactive astrocytes indicated no significant differences in ipsilateral internal capsule astrogliosis within left ( $F_{(3,38)} = 1.37$ ,  $p = 0.27$ , two-way ANOVA) and right ( $F_{(3,38)} = 0.34$ ,  $p = 0.80$ , two-way ANOVA) experimental groups, with all groups displaying similar measurements of GFAP % area coverage: NI ( $29.76\% \pm 8.26\%$ ), PBS-L ( $29.50\% \pm 4.56\%$ ), PBS-R ( $28.59\% \pm 5.58\%$ ), IA-L ( $24.64\% \pm 2.15\%$ ), IA-R ( $25.30\% \pm 2.72\%$ ), ET1-L ( $33.53\% \pm 3.60\%$ ) and ET1-R ( $26.17\% \pm 5.63\%$ ) (Figure 15A-D). Similar levels of reactive astrocytes were also observed within the contralateral internal capsule, revealing no significant

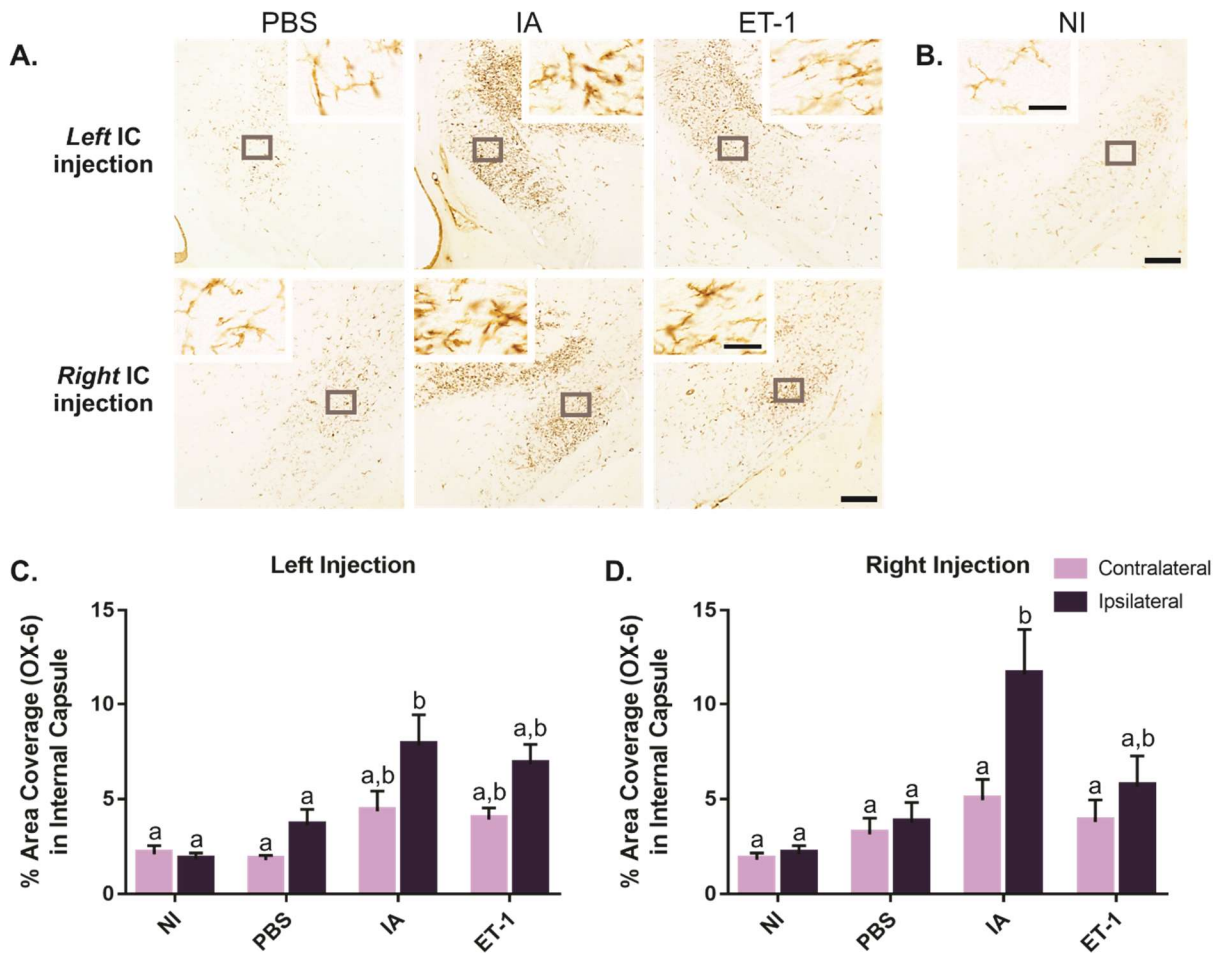


**Figure 14. Insular damage significantly increases white matter microgliosis within the ipsilateral internal capsule.** Representative 2X photomicrographs of OX-6 immunohistochemical stained coronal rat brain tissue, 28 d following intracranial injection of (A) PBS, IA, ET-1 (n=6/experimental group) or (B) no injection (n=5) into the right or left insular cortex. Outlined areas represent higher-magnified regions (20X) of the ipsilateral internal capsule. (C, D) Quantitative analysis revealed significant increases in microglia activation (% area coverage) within the ipsilateral internal capsule 28 d following insular injury. Data is presented as mean  $\pm$  SEM. Non-matching letters indicate significant differences between experimental groups ( $p < 0.05$ , two-way ANOVA followed by Tukey's multiple comparison test). Scale bar = 500  $\mu$ m (2X) or 50  $\mu$ m (20X). IC = insular cortex, PBS = phosphate-buffered saline, IA = ibotenic acid, ET-1 = endothelin-1, NI = no injection

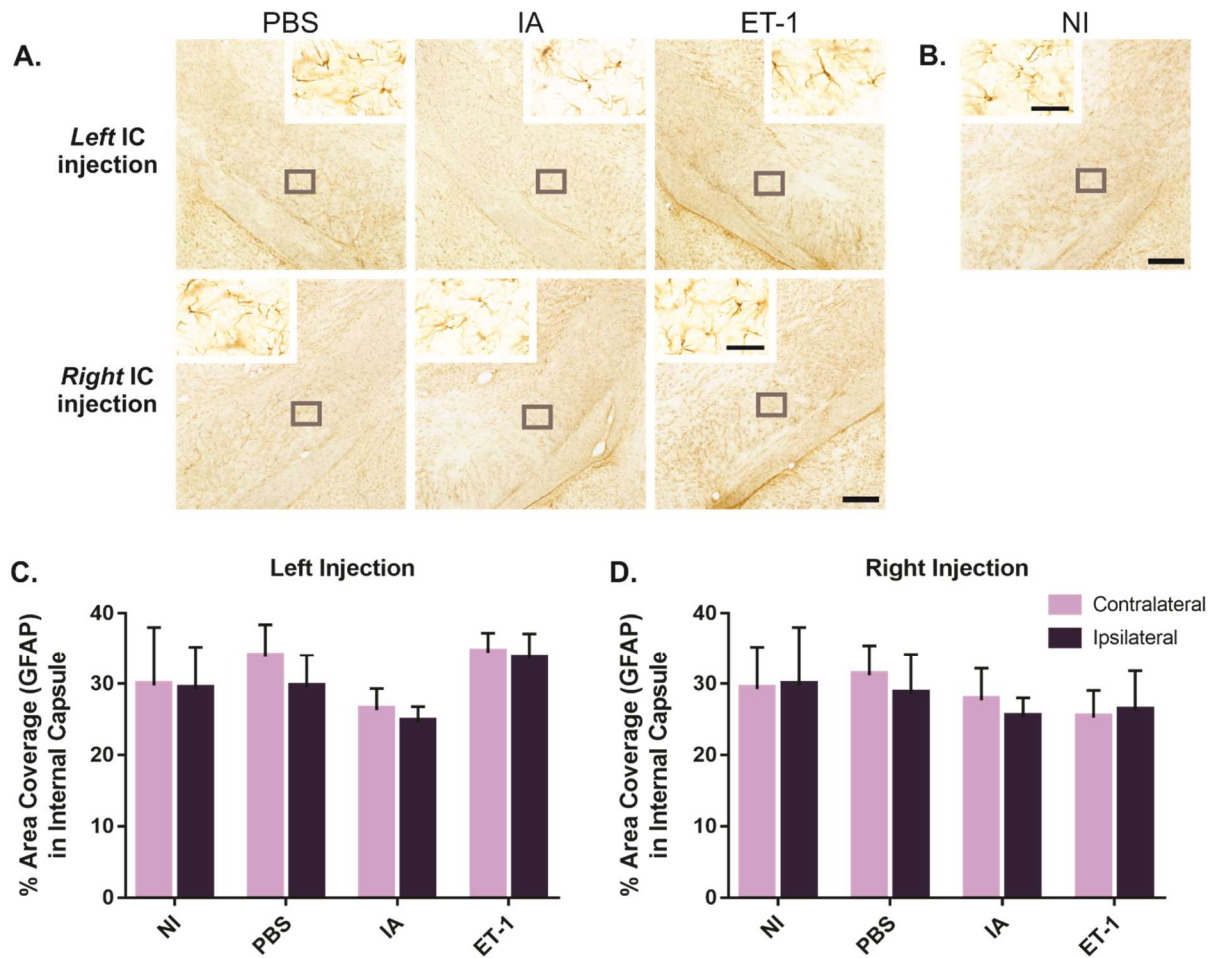


**Figure 15. Insular damage does not enhance white matter astrogliosis within the internal capsule.** Representative 2X photomicrographs of GFAP immunohistochemical stained coronal rat brain tissue, 28 d following intracranial injection of (A) PBS, IA, ET-1 (n=6/experimental group) or (B) no injection (n=5) into the right or left insular cortex. Outlined areas represent higher-magnified regions (20X) of the ipsilateral internal capsule. (C, D) Quantitative analysis revealed no significant differences in contralateral or ipsilateral internal capsule astrogliosis (% area coverage) within, and between, experimental groups. Data is presented as mean  $\pm$  SEM. Scale bar = 500  $\mu$ m (2X) or 50  $\mu$ m (20X). IC = insular cortex, PBS = phosphate-buffered saline, IA = ibotenic acid, ET-1 = endothelin-1, NI = no injection

differences in astrogliosis between the contralateral and ipsilateral internal capsule for both left (Figure 8C;  $F_{(1,38)} = 0.34$ ,  $p = \mathbf{0.56}$ , two-way ANOVA) and right (Figure 15D;  $F_{(1,38)} = 0.06$ ,  $p = \mathbf{0.81}$ , two-way ANOVA) experimental groups.

### *3.3.4 Insular damage enhances grey matter microgliosis, but not astrogliosis, in the ipsilateral ventroposterior thalamus*

In addition to the aforementioned white matter regions, secondary neuroinflammation within the grey matter was examined. Specifically, the investigation of inflammation within the VP thalamus was completed, as this region serves as an important relay centre for the transmission of cardiac autonomic information between the brainstem and IC<sup>206,207</sup>. Densitometry measurements of % area coverage were quantified as the total fraction of OX-6 (microglia) or GFAP (astrocytes) immunolabelled cells present within the VP thalamus of one coronal tissue section. Comparisons of microgliosis or astrogliosis within the contralateral and ipsilateral VP thalamus were performed to account for unilateral IC damage.

At 28 d post-insular injury, OX-6 staining for activated microglia presented a significant effect of injury for both left ( $F_{(3,38)} = 11.17$ ,  $p < \mathbf{0.01}$ , two-way ANOVA) and right ( $F_{(3,38)} = 19.41$ ,  $p < \mathbf{0.01}$ , two-way ANOVA) experimental groups. Following damage to the left or right IC, enhanced levels of microgliosis within the ipsilateral VP thalamus of IA (IA-L  $12.55\% \pm 2.25\%$ ; IA-R  $11.62\% \pm 0.70\%$ ) and ET-1 (ET1-L  $7.30\% \pm 1.57\%$ ; ET1-R  $5.40\% \pm 1.66\%$ ) groups were observed, compared to PBS (PBS-L  $2.80\% \pm 0.81\%$ ; PBS-R  $2.44\% \pm 0.61\%$ ) and NI ( $1.30\% \pm 0.44\%$ ) control animals (Figure 16A-D). Similar levels of microgliosis occurred in the ipsilateral VP thalamus of both left and right injury groups, indicating no significant effect of insular damage lateralization ( $F_{(1,38)} = 0.81$ ,  $p = \mathbf{0.38}$ , two-way ANOVA). Upon completion of Tukey's multiple comparison test, a significant difference in ipsilateral VP thalamus microgliosis between NI/IA-L ( $p < \mathbf{0.01}$ ), NI/IA-R ( $p < \mathbf{0.01}$ ), NI/ET1-L ( $p = \mathbf{0.01}$ ), NI/ET1-R ( $p = \mathbf{0.01}$ ), PBS-L/IA-L ( $p < \mathbf{0.01}$ ), PBS-R/IA-R ( $p < \mathbf{0.01}$ ), IA-L/ET1-L ( $p = \mathbf{0.03}$ ) and IA-R/ET1-R ( $p < \mathbf{0.01}$ ) groups was confirmed (Figure 16C,D). A significant difference between uninjured control groups (NI/PBS;  $p = \mathbf{0.86}$ ) was not observed (Figure 16C,D). Furthermore, a significant difference between microglia activation within the contralateral and ipsilateral VP thalamus was observed for both left ( $F_{(1,38)} = 41.47$ ,  $p < \mathbf{0.01}$ , two-way ANOVA) and right ( $F_{(1,38)} = 52.65$ ,  $p < \mathbf{0.01}$ , two-way ANOVA) experimental groups (Figure 16C,D). Damage to the left or right IC enhanced microgliosis within the ipsilateral VP



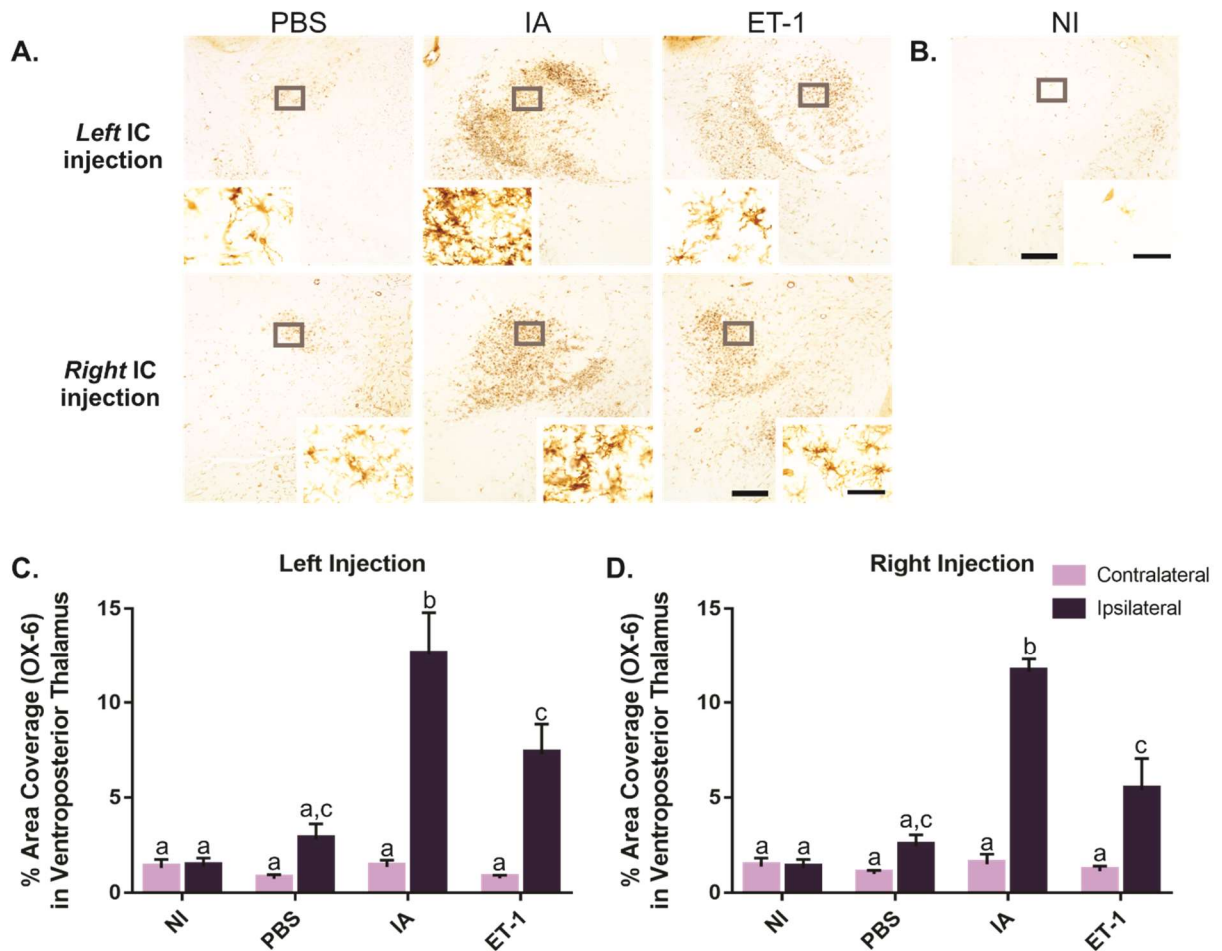


**Figure 16. Insular damage significantly increases grey matter microgliosis within the ipsilateral ventroposterior thalamus.** Representative 2X photomicrographs of OX-6 immunohistochemical stained coronal rat brain tissue, 28 d following intracranial injection of (A) PBS, IA, ET-1 (n=6/experimental group) or (B) no injection (n=5) into the right or left insular cortex. Outlined areas represent higher-magnified regions (20X) of the ipsilateral ventroposterior thalamus. (C, D) Quantitative analysis revealed significant increases in microglia activation (% area coverage) within the ipsilateral ventroposterior thalamus 28 d following insular injury. Data is presented as mean  $\pm$  SEM. Non-matching letters indicate significant differences between experimental groups ( $p < 0.05$ , two-way ANOVA followed by Tukey's multiple comparison test). Scale bar = 500  $\mu\text{m}$  (2X) or 50  $\mu\text{m}$  (20X). IC = insular cortex, PBS = phosphate-buffered saline, IA = ibotenic acid, ET-1 = endothelin-1, NI = no injection

thalamus, with minimal microglia activation occurring in the contralateral VP thalamus: IA-L (ipsilateral = 12.55% ± 2.25%; contralateral = 1.35% ± 0.35%), IA-R (ipsilateral = 11.62% ± 0.70%; contralateral = 1.50% ± 0.53%), ET1-L (ipsilateral = 7.30% ± 1.57%; contralateral = 0.75% ± 0.17%) and ET1-R (ipsilateral = 5.40% ± 1.66%; contralateral = 1.13% ± 0.26%) (Figure 16C,D). Upon completion of Tukey's multiple comparison test, a significant difference between microgliosis within the contralateral and ipsilateral VP thalamus of IA-L ( $p < 0.01$ ), IA-R ( $p < 0.01$ ), ET1-L ( $p < 0.01$ ) and ET1-R ( $p = 0.01$ ) groups was confirmed (Figure 16C,D).

GFAP staining for reactive astrocytes indicated no significant differences in ipsilateral VP thalamus astrogliosis within left ( $F_{(3,38)} = 2.20$ ,  $p = 0.10$ , two-way ANOVA) and right ( $F_{(3,38)} = 0.72$ ,  $p = 0.55$ , two-way ANOVA) experimental groups, with all groups displaying similar measurements of GFAP % area coverage: NI (10.42% ± 2.02%), PBS-L (14.79% ± 2.93%), PBS-R (13.67% ± 3.22%), IA-L (22.42% ± 3.17%), IA-R (14.39% ± 2.48%), ET1-L (18.38% ± 3.13%) and ET1-R (16.83% ± 2.12%) (Figure 17A-D). Overall, left and right IC damage enhanced astrogliosis within the ipsilateral VP thalamus, when compared to the contralateral region (Figure 17C,D). However, significant differences between contralateral and ipsilateral astrogliosis were only detected among left experimental injury groups (Figure 17C;  $F_{(1,38)} = 12.34$ ,  $p < 0.01$ , two-way ANOVA). Upon completion of Tukey's multiple comparison test, no significant differences were confirmed (Figure 17C).

### 3.3.5 Insular damage does not generate secondary neuronal loss in remote forebrain regions

As mentioned previously, chronic inflammation within remote grey and white matter regions, post-ischemic injury, has contributed to secondary neurodegeneration in brain regions anatomically-connected to the primary ischemic infarct<sup>87-91</sup>. We therefore sought to investigate the occurrence of neuronal death within the VP thalamus; an identified region in our insular ischemic model displaying significant amounts of activated microglia. Quantification of neuronal death was also completed for four additional brain regions of IC autonomic circuitry: the PFC, ACC, amygdala and hypothalamus. At 28 d post-insular injury, secondary neuroinflammation was not observed in these regions. However, neuroinflammatory timing and mechanisms can vary depending on the involved structures and their degree of axonal connectivity to the primary damaged region<sup>91</sup>. It is therefore possible that secondary neuroinflammation, and corresponding neurodegeneration, occurred prior to the sacrificed

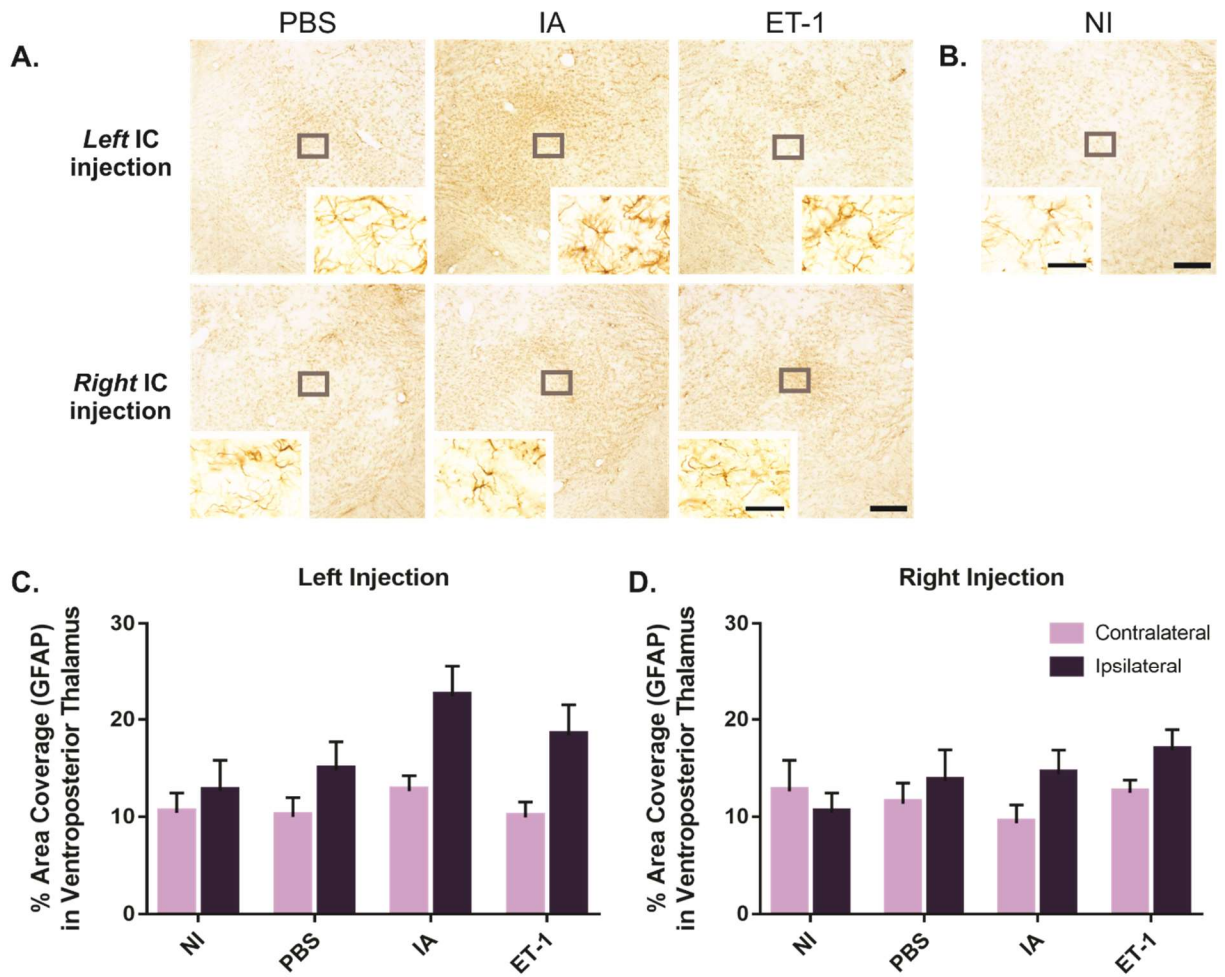


**Figure 17. Insular damage does not enhance grey matter astrogliosis within the ventroposterior thalamus.** Representative 2X photomicrographs of GFAP immunohistochemical stained coronal rat brain tissue, 28 d following intracranial injection of (A) PBS, IA, ET-1 (n=6/experimental group) or (B) no injection (n=5) into the right or left insular cortex. Outlined areas represent higher-magnified regions (20X) of the ipsilateral ventroposterior thalamus. (C, D) Quantitative analysis revealed no significant differences in contralateral and ipsilateral ventroposterior thalamus astrogliosis (% area coverage) within, and between, experimental groups. Data is presented as mean  $\pm$  SEM. Scale bar = 500  $\mu$ m (2X) or 50  $\mu$ m (20X). IC = insular cortex, PBS = phosphate-buffered saline, IA = ibotenic acid, ET-1 = endothelin-1, NI = no injection

timepoint of 28 days. Furthermore, with the observed presence of WMI in our model, IC connectivity to these regions may be impaired, providing additional justification for the analysis of secondary neurodegeneration.

To investigate the occurrence of neurodegeneration 28 d following IC injury, brain tissue was immunohistochemically stained with NeuN to identify neurons and quantify neuronal loss. Automated cell counts of NeuN immunoreactivity were performed to obtain a single measurement of NeuN+ cells for each ROI. Comparisons of neurodegeneration within the contralateral and ipsilateral area of each ROI were conducted to account for unilateral IC damage.

At 28 d post-insular injury, evidence of secondary neuronal loss in remote grey matter forebrain regions was not observed. Completion of a two-way ANOVA indicated no significant effect of left IC injury within the ipsilateral region of all ROIs: PFC (Figure 18A-C;  $F_{(3,38)} = 2.49$ ,  $p = 0.08$ ), ACC (Figure 19A-C;  $F_{(3,38)} = 0.65$ ,  $p = 0.59$ ), amygdala (Figure 20A-C;  $F_{(3,38)} = 0.19$ ,  $p = 0.90$ ), hypothalamus (Figure 21A-C;  $F_{(3,38)} = 0.18$ ,  $p = 0.91$ ) and VP thalamus (Figure 22A-C;  $F_{(3,38)} = 0.37$ ,  $p = 0.78$ ). Similar results were obtained upon completion of a two-way ANOVA for right experimental groups, with no significant differences in total neuron amounts observed within the ipsilateral PFC (Figure 18A,B,D;  $F_{(3,38)} = 0.67$ ,  $p = 0.58$ ), ACC (Figure 19A,B,D;  $F_{(3,38)} = 1.13$ ,  $p = 0.35$ ), amygdala (Figure 20A,B,D;  $F_{(3,38)} = 0.38$ ,  $p = 0.77$ ), hypothalamus (Figure 21A,B,D;  $F_{(3,38)} = 1.51$ ,  $p = 0.23$ ) and VP thalamus (Figure 22A,B,D;  $F_{(3,38)} = 2.57$ ,  $p = 0.78$ ). Additionally, similar measurements of neuronal cell counts were observed between the contralateral and ipsilateral PFC (Figure 18C,D), ACC (Figure 19C,D), amygdala (Figure 20C,D), hypothalamus (Figure 21C,D) and VP thalamus (Figure 22C,D) of all experimental groups; insinuating an absence of remote neurodegeneration.

### 3.4 Analysis of Heart Histology

#### 3.4.1. Left atrial fibrosis of the heart is observed 28 days following insular injury

While early rodent models of MCAO have mimicked the clinical appearance of cardiac lesions post-ischemic stroke<sup>55,135</sup>, specificity of IC damage in relation to SIHI has yet to be confirmed. We therefore used our novel rodent model of focal insular ischemic stroke to examine, for the first time, the downstream effect of selective IC damage on myocardial health and structural integrity.

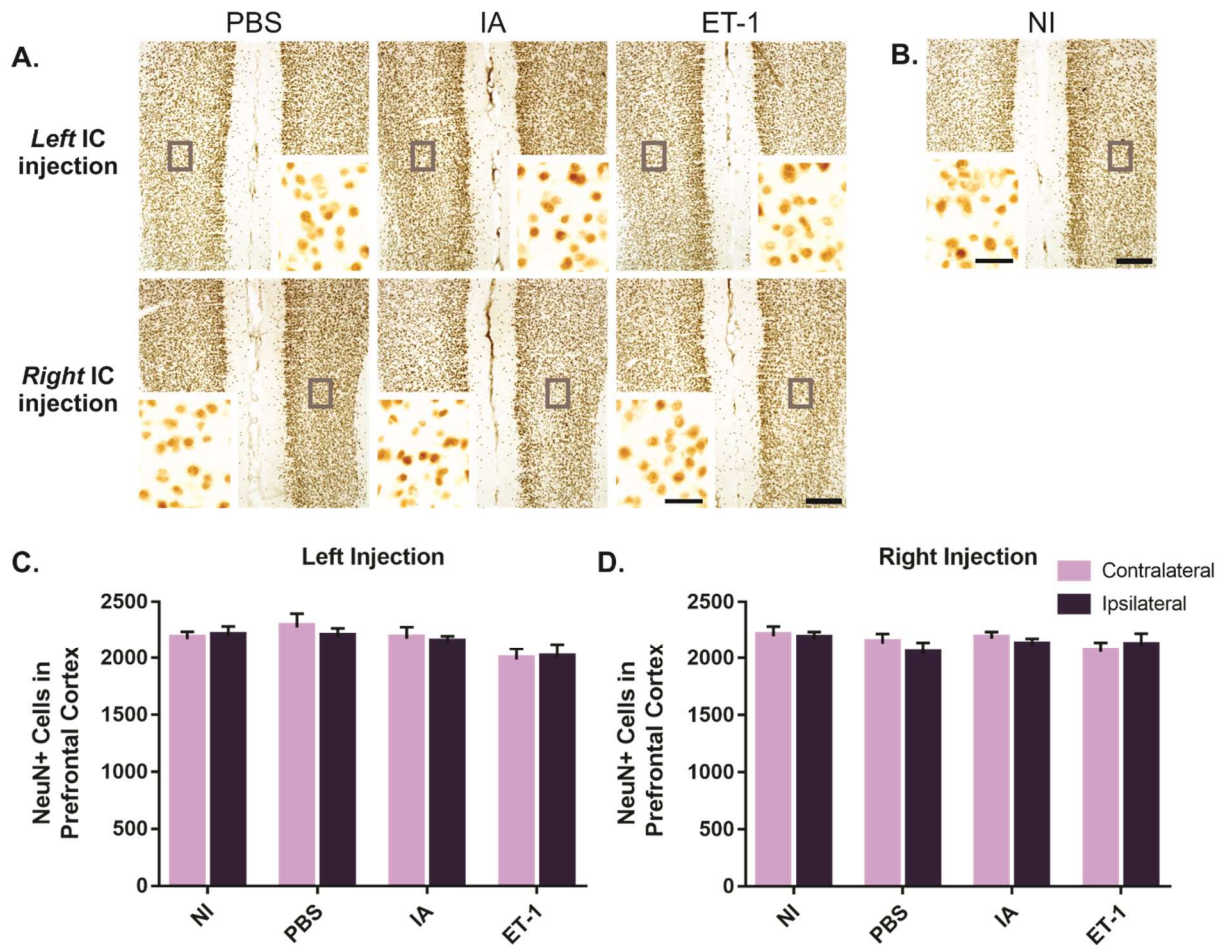


**Figure 18. Insular damage does not generate secondary neuronal loss within the prefrontal cortex.** Representative 2X photomicrographs of NeuN immunohistochemical stained coronal rat brain tissue, 28 d following intracranial injection of (A) PBS, IA, ET-1 (n=6/experimental group) or (B) no injection (n=5) into the right or left insular cortex. Outlined areas represent higher-magnified regions (20X) of the ipsilateral prefrontal cortex. (C, D) Quantitative analysis revealed no significant differences in prefrontal cortex contralateral and ipsilateral neuronal cell numbers within, and between, experimental groups. Cell counts represent the number of NeuN+ cells within a 1.50 mm<sup>2</sup> region of the prefrontal cortex. Data is presented as mean ± SEM. Scale bar = 500 μm (2X) or 50 μm (20X). IC = insular cortex, PBS = phosphate-buffered saline, IA = ibotenic acid, ET-1 = endothelin-1, NI = no injection

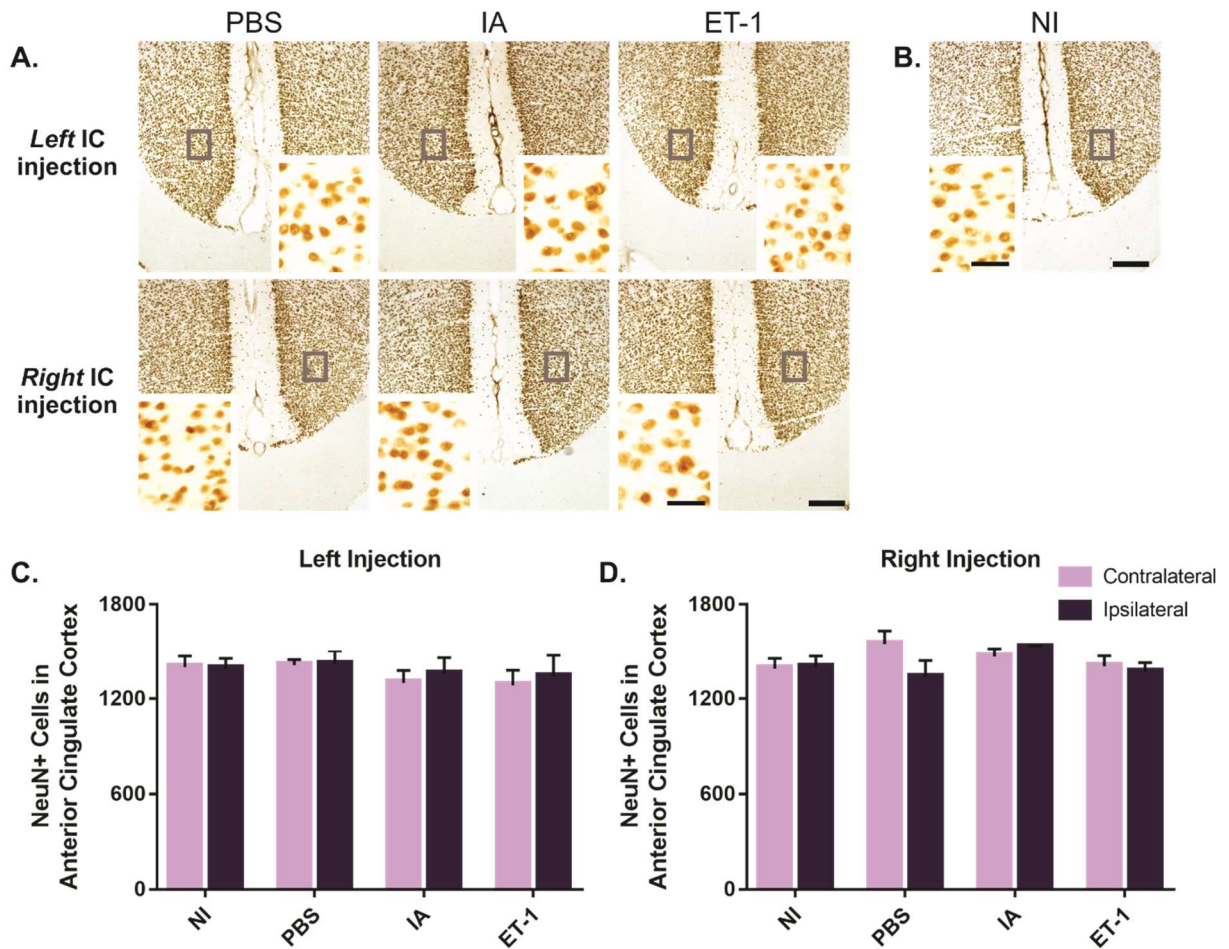


**Figure 19. Insular damage does not generate secondary neuronal loss within the anterior cingulate cortex.** Representative 2X photomicrographs of NeuN immunohistochemical stained coronal rat brain tissue, 28 d following intracranial injection of (A) PBS, IA, ET-1 (n=6/experimental group) or (B) no injection (n=5) into the right or left insular cortex. Outlined areas represent higher-magnified regions (20X) of the ipsilateral anterior cingulate cortex. (C, D) Quantitative analysis revealed no significant differences in anterior cingulate cortex contralateral and ipsilateral neuronal cell numbers within, and between, experimental groups. Cell counts represent the number of NeuN+ cells within a 1.04 mm<sup>2</sup> region of the anterior cingulate cortex. Data is presented as mean ± SEM. Scale bar = 500 μm (2X) or 50 μm (20X). IC = insular cortex, PBS = phosphate-buffered saline, IA = ibotenic acid, ET-1 = endothelin-1, NI = no injection

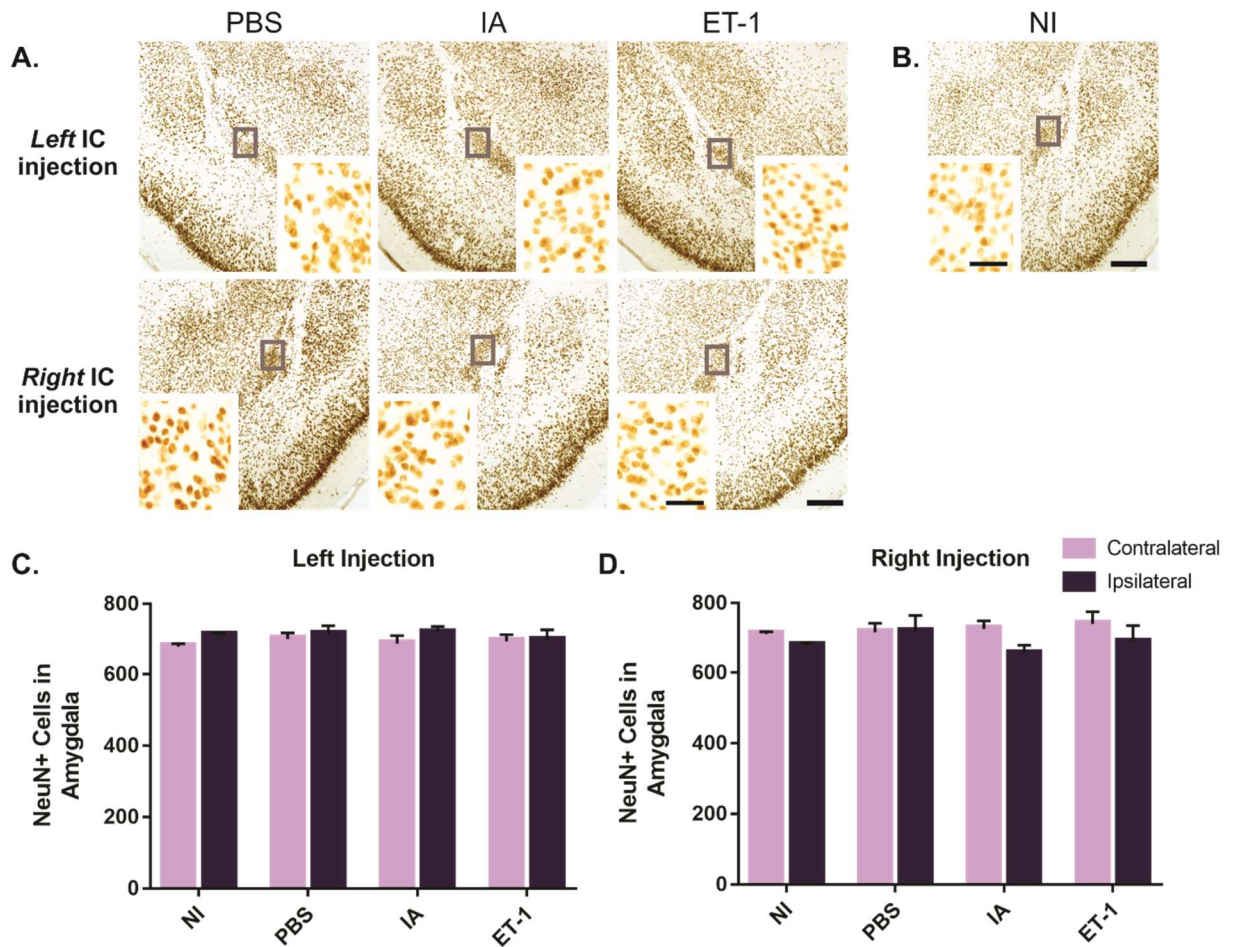


**Figure 20. Insular damage does not generate secondary neuronal loss within the amygdala.** Representative 2X photomicrographs of NeuN immunohistochemical stained coronal rat brain tissue, 28 d following intracranial injection of (A) PBS, IA, ET-1 (n=6/experimental group) or (B) no injection (n=5) into the right or left insular cortex. Outlined areas represent higher-magnified regions (20X) of the ipsilateral amygdala. (C, D) Quantitative analysis revealed no significant differences in amygdala contralateral and ipsilateral neuronal cell numbers within, and between, experimental groups. Cell counts represent the number of NeuN+ cells within a 0.58 mm<sup>2</sup> region of the amygdala. Data is presented as mean ± SEM. Scale bar = 500 μm (2X) or 50 μm (20X). IC = insular cortex, PBS = phosphate-buffered saline, IA = ibotenic acid, ET-1 = endothelin-1, NI = no injection

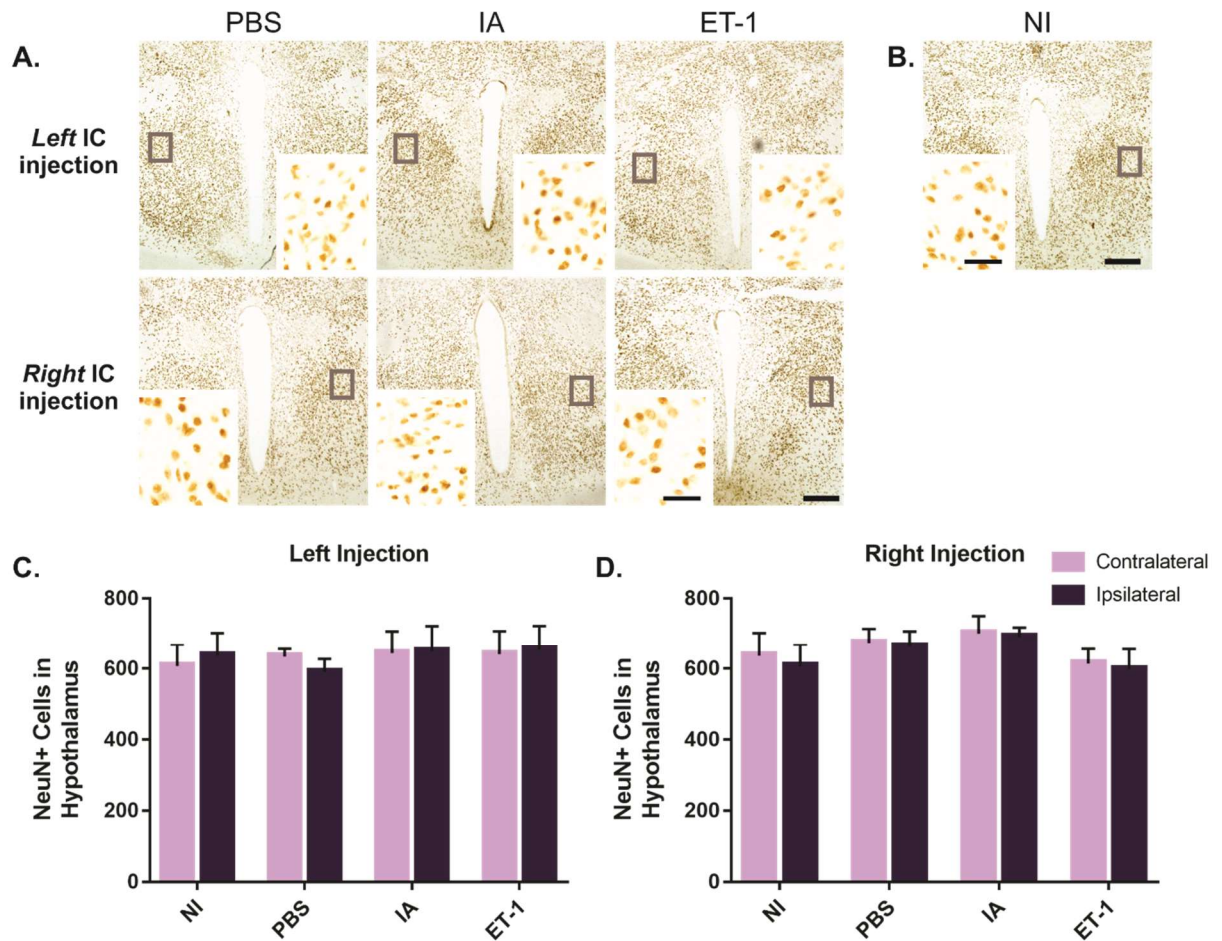


**Figure 21. Insular damage does not generate secondary neuronal loss within the hypothalamus.** Representative 2X photomicrographs of NeuN immunohistochemical stained coronal rat brain tissue, 28 d following intracranial injection of (A) PBS, IA, ET-1 (n=6/experimental group) or (B) no injection (n=5) into the right or left insular cortex. Outlined areas represent higher-magnified regions (20X) of the ipsilateral hypothalamus. (C, D) Quantitative analysis revealed no significant differences in hypothalamus contralateral and ipsilateral neuronal cell numbers within, and between, experimental groups. Cell counts represent the number of NeuN+ cells within a 0.58 mm<sup>2</sup> region of the hypothalamus. Data is presented as mean ± SEM. Scale bar = 500 μm (2X) or 50 μm (20X). IC = insular cortex, PBS = phosphate-buffered saline, IA = ibotenic acid, ET-1 = endothelin-1, NI = no injection



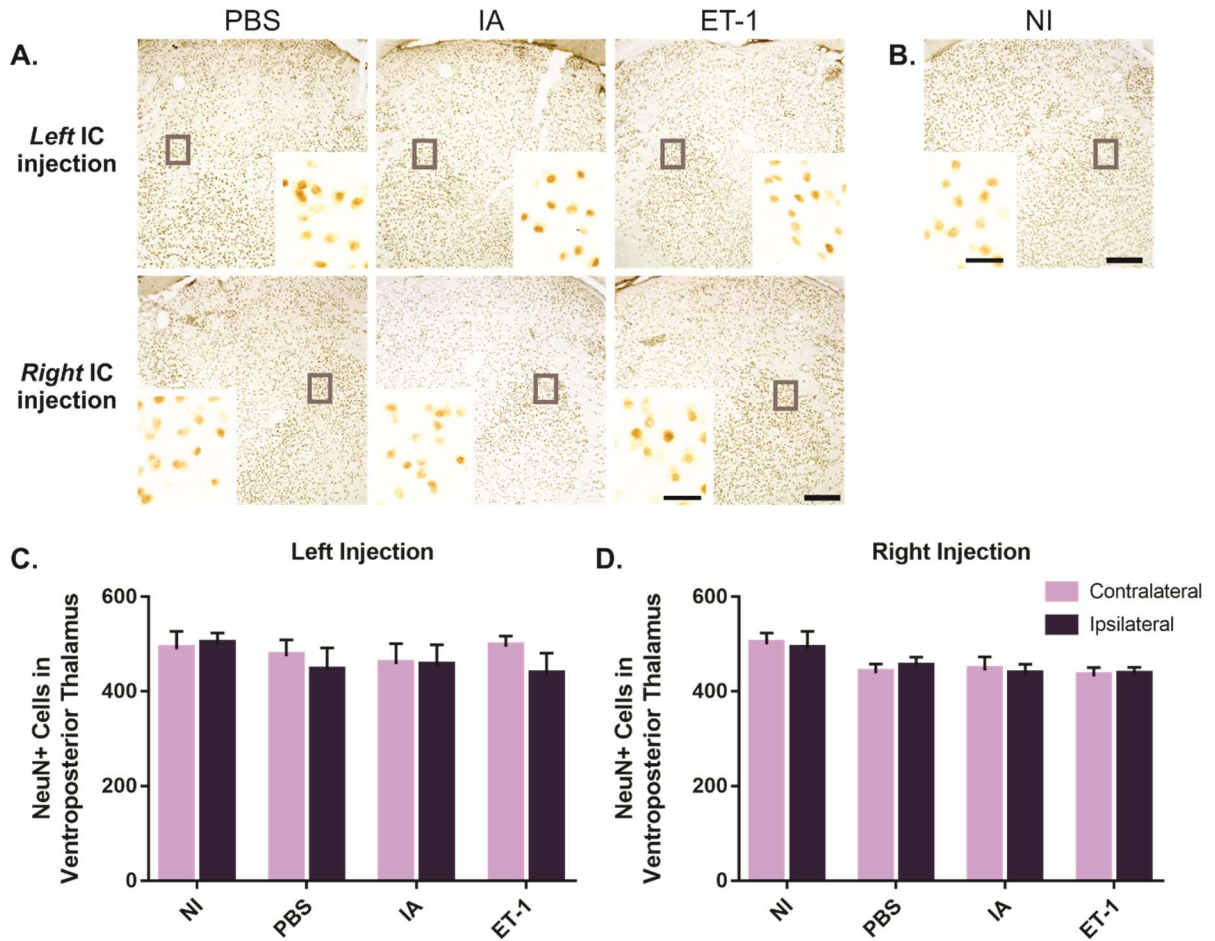


**Figure 22. Insular damage does not generate secondary neuronal loss within the ventroposterior thalamus.** Representative 2X photomicrographs of NeuN immunohistochemical stained coronal rat brain tissue, 28 d following intracranial injection of (A) PBS, IA, ET-1 (n=6/experimental group) or (B) no injection (n=5) into the right or left insular cortex. Outlined areas represent higher-magnified regions (20X) of the ipsilateral ventroposterior thalamus. (C, D) Quantitative analysis revealed no significant differences in ventroposterior thalamus contralateral and ipsilateral neuronal cell numbers within, and between, experimental groups. Cell counts represent the number of NeuN+ cells within a 0.58 mm<sup>2</sup> region of the ventroposterior thalamus. Data is presented as mean ± SEM. Scale bar = 500 μm (2X) or 50 μm (20X). IC = insular cortex, PBS = phosphate-buffered saline, IA = ibotenic acid, ET-1 = endothelin-1, NI = no injection

Specifically, cardiac tissue was histologically stained with Masson's trichrome to identify fibrotic regions. Tissue stained blue represented extensive collagen deposition, indicating the presence of interstitial fibrosis. For this thesis, fibrosis of the LA was analyzed; due to the known contribution of LA dysfunction in AF<sup>208,209</sup>, and the high clinical prevalence of AF associated with SIHI<sup>102</sup>. Percent area coverage of LA cardiac fibrosis was quantified as the averaged total fraction of blue-stained tissue present within the LA of eight randomly-selected coronal tissue sections.

At 28 d post-insular damage, a significant effect of injury was observed ( $F_{(3,38)} = 14.53$ ,  $p < 0.01$ , two-way ANOVA). Left IC damage resulted in enhanced LA fibrosis in IA ( $6.29\% \pm 1.62\%$ ) and ET-1 ( $4.49\% \pm 1.25\%$ ) injury groups, compared to PBS ( $0.79\% \pm 0.15\%$ ) and NI ( $0.53\% \pm 0.09\%$ ) control animals (Figure 23A-C). Increased LA fibrosis was also observed following injection of IA ( $3.04\% \pm 0.55\%$ ) or ET-1 ( $5.34\% \pm 0.86\%$ ) into the right IC (Figure 23A,C), indicating no significant effect of insular damage lateralization ( $F_{(1,38)} = 0.85$ ,  $p = 0.36$ , two-way ANOVA). Rats subjected to injection of PBS into the right IC displayed minimal fibrotic levels ( $0.87\% \pm 0.14\%$ ), similar to PBS-L control animals (Figure 23A,C). Upon completion of Tukey's multiple comparison test, a significant difference in LA fibrosis between NI/IA-L ( $p < 0.01$ ), NI/ET1-R ( $p = 0.01$ ), PBS-L/IA-L ( $p < 0.01$ ) and PBS-R/ET1-R ( $p = 0.01$ ) groups was confirmed (Figure 23C). A significant difference between injured groups (IA/ET-1;  $p = 0.99$ ) or uninjured groups (NI/PBS;  $p = 1.00$ ) was not observed (Figure 23C).

### 3.5 Correlative Analysis of Microglia Activation and Cardiac Fibrosis

#### 3.5.1 Increased white and grey matter microglia activation positively correlates with left atrial cardiac fibrosis

Using our novel rodent model of focal insular ischemic stroke, we have identified the presence of both (1) secondary white and grey matter microgliosis and (2) LA cardiac fibrosis, 28 d following IC injury. Interestingly, recent studies have hypothesized a causative role of inflammation in the genesis and perpetuation of myocardial fibrotic remodelling<sup>114,187,188,210,211</sup>. We therefore sought to examine the relationship between remote cerebral inflammation and cardiac fibrosis; correlating levels of activated microglia within the ipsilateral forceps minor, corpus callosum, ipsilateral internal capsule or ipsilateral VP thalamus, to LA fibrosis. Only rats subjected to ischemic injury (ET-1) and saline control

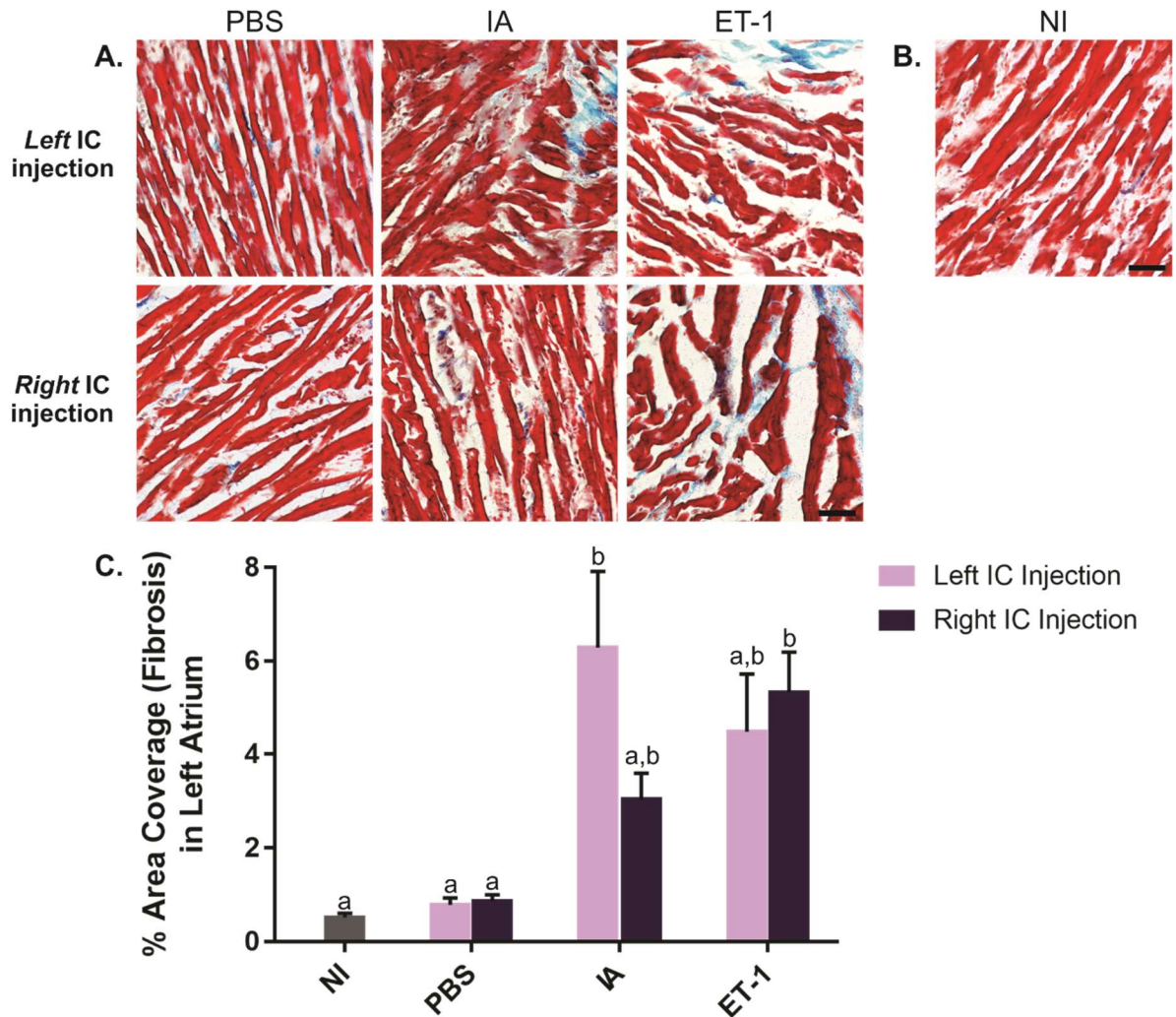


**Figure 23.** Left atrial fibrosis of the heart significantly increases following injury to the insular cortex. Representative 10X photomicrographs of Masson's trichrome stained coronal heart tissue, 28 d following intracranial injection of (A) PBS, IA, ET-1 (n=6/experimental group) or (B) no injection (n=5) into the right or left insular cortex. Tissue stained blue identifies collagen, indicating fibrosis. (C) Quantitative analysis revealed significant increases in left atrial fibrosis (% area coverage) 28 d following insular injury. Data is presented as mean  $\pm$  SEM. Non-matching letters indicate significant differences between experimental groups ( $p < 0.05$ , two-way ANOVA followed by Tukey's multiple comparison test). Scale bar = 250  $\mu$ m. IC = insular cortex, PBS = phosphate-buffered saline, IA = ibotenic acid, ET-1 = endothelin-1, NI = no injection

animals (PBS) were included in this correlative analysis.

At 28 d post-insular ischemic stroke, increased levels of activated microglia significantly correlated with enhanced LA fibrosis in the ipsilateral forceps minor (Figure 24A;  $F_{(1,18)} = 6.06$ ,  $p = 0.02$ ), corpus callosum (Figure 24B;  $F_{(1,18)} = 22.91$ ,  $p < 0.01$ ), ipsilateral internal capsule (Figure 24C;  $F_{(1,18)} = 29.38$ ,  $p < 0.01$ ) and ipsilateral VP thalamus (Figure 24D;  $F_{(1,18)} = 19.40$ ,  $p < 0.01$ ). While all four regions displayed a strong positive correlation, the strongest relationship was observed within brain regions proximal to the infarct site (corpus callosum:  $r = 0.75$ ; internal capsule:  $r = 0.79$  and VP thalamus:  $r = 0.72$ ); compared to the more distal forceps minor ( $r = 0.50$ ) (Figure 24A-D). Upon observation of this positive relationship, linear regression analysis was completed to establish regression lines for each data set (Figure 24A-D); identifying the overall influence of microglia activation (variable x) on LA fibrosis (variable y). It is important to note that although these results depict a strong linear relationship between microglia and cardiac fibrosis, the observed association remains correlative – not causative. As such, a causative implication of neuroinflammation in SIHI can not yet be discerned.

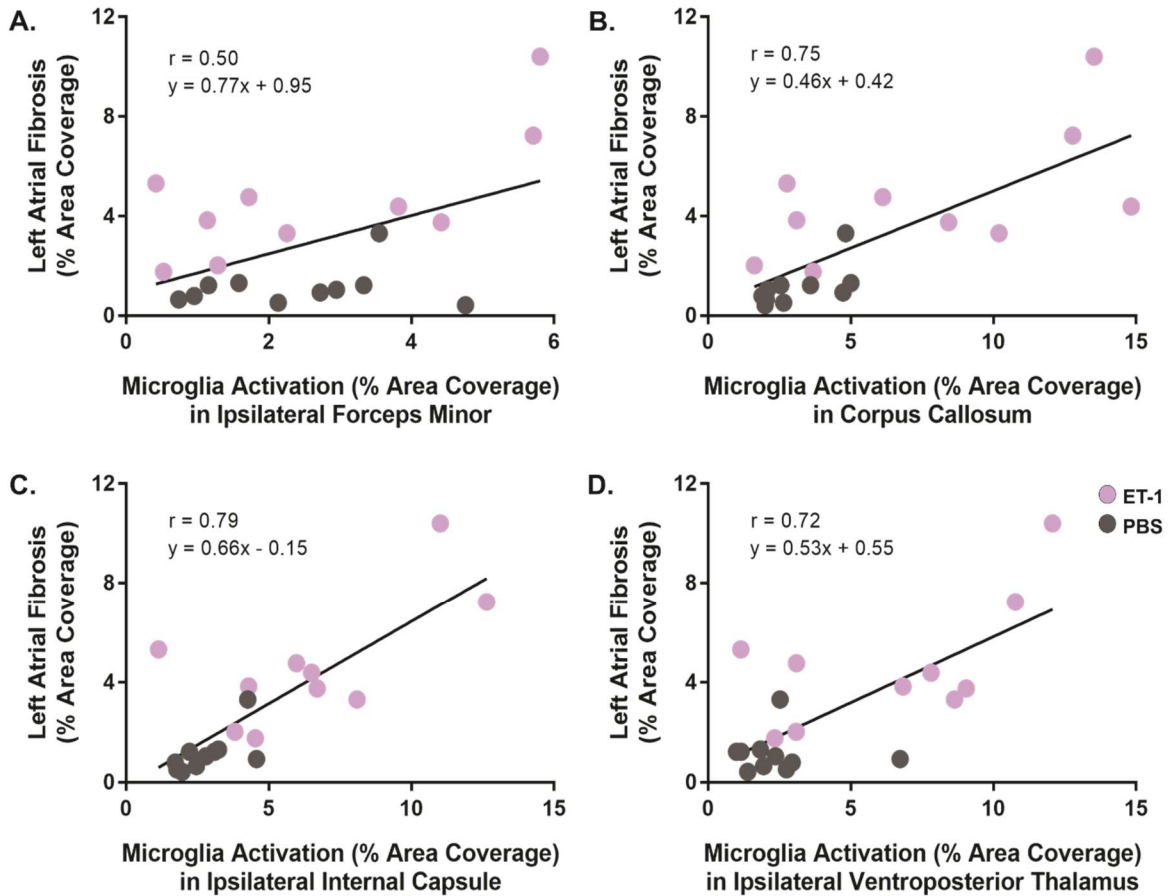


**Figure 24.** Increased white and grey matter microglia activation positively correlates with left atrial cardiac fibrosis. Correlative depiction of the significant positive association between number of activated microglia within the (A) ipsilateral forceps minor ( $p = 0.02$ ), (B) corpus callosum ( $p < 0.01$ ), (C) ipsilateral internal capsule ( $p < 0.01$ ) or (D) ipsilateral ventroposterior thalamus ( $p < 0.01$ ), and extent of left atrial cardiac fibrosis 28 d following intracranial injection of PBS (grey dots;  $n=10$ ) or ET-1 (purple dots;  $n=10$ ) into the left or right insular cortex. Significance analyzed using the simple linear regression model ( $p < 0.05$ ).

## Section 4: DISCUSSION

#### 4.1 Summary of Key Findings

Completion of this thesis was performed with the overall intent of establishing a novel experimental model of focal ischemic stroke in the rat IC, used to further elucidate the mechanistic relationship between IC ischemia and SIHI. In doing so, we confirmed, for the first time, the selective role of IC damage in generating SIHI; reaffirming clinical observations. To date, experimental studies of SIHI have exclusively involved animal models of MCAO<sup>55,135</sup>. Yet, due to the invasiveness and severity of this procedure<sup>186</sup>, observations of SIHI have been limited to acute timepoints<sup>55,135</sup>. In the present study, use of ET-1 produced a focal, and much less severe, ischemic infarct. As such, we were able to first identify the chronic display of stroke-induced cardiac fibrosis. At 28 d following IC damage, regions of secondary microgliosis were located within the corpus callosum, ipsilateral internal capsule and ipsilateral VP thalamus; a known consequence of ischemic stroke. Due to the recent implication of inflammation in the manifestation of myocardial fibrotic remodelling<sup>114,187,188,210,211</sup>, microgliosis in these remote regions was correlated to cardiac fibrosis; demonstrating, for the first time, a positive association between these two physiological variables. Lastly, development of this rodent model allowed for the implementation of a behaviour test, used to indirectly assess autonomic deficits of IC damage. Specifically, PPI of the ASR was analyzed, suggesting a lateralizing trend of left IC dominance in sensorimotor gating. Overall, with the successful development of this insular stroke model, we have begun to unravel several pathophysiological outcomes of SIHI; vitally improving current mechanistic knowledge of this complex brain-heart connection.

#### 4.2 Endothelin-1 vs. Ibotenic Acid

ET-1 is a potent vasoconstrictor, used in this study to induce insular ischemic stroke<sup>57-59,191,192</sup>. Historically, ET-1 has been recognized as a translational stroke method, best representing human ischemic conditions<sup>191</sup>. However, resulting ischemia caused by this technique will injure all structures located at the injection site; including intersecting white matter fibers<sup>190,193</sup>. Mechanistically, this makes it difficult to conclude whether reported behavioural and pathological outcomes are a direct effect of the targeted damage, or an indirect effect of non-specific white matter injury. To overcome this confounding dilemma, the neurotoxin IA was included as an additional positive control, causing selective neuronal death within the IC<sup>193,194</sup>. IA acts as a glutamate agonist, capable of binding to the NMDA glutamate

receptor, an important regulator of  $\text{Ca}^{2+}$  transport <sup>212</sup>. Upon administration of IA into the IC, neuronal membrane NMDA receptors become activated, prompting the influx of extracellular  $\text{Ca}^{2+}$  into IC neurons <sup>212,213</sup>. Similar to ischemic stroke <sup>44</sup>, the intracellular accumulation of  $\text{Ca}^{2+}$  will evoke an excitotoxic cascade, causing neuronal cell death <sup>212,213</sup>. In this study, equivalent results were obtained following the injection of IA or ET-1 into the rat IC. We can therefore conclude that the acquired behavioural and pathological findings of this thesis are a direct result of ischemic IC injury, and corresponding physiological processes – not the unspecific damage of a traversing white matter tract.

### 4.3 Behavioural Assessment: Prepulse Inhibition of the Acoustic Startle Response

In creating this rodent model of focal insular ischemic stroke, PPI of the ASR was performed as an accompanying behaviour test. Traditionally, PPI has served as a reliable measure of sensorimotor gating <sup>139,160,161</sup>; an autonomic process responsible for the filtration of unnecessary or redundant external stimuli <sup>160-162</sup>. To our knowledge, a direct relationship between the IC and PPI has not yet been reported. However, due to the known autonomic role of sensorimotor gating in the regulation of sensory input filtration <sup>160-162</sup>, we used PPI of the ASR to indirectly measure autonomic outcomes of IC injury. Physiologically, the successful implementation of this behaviour test could provide crucial insight into the lateralization of IC autonomic function; a current topic bound by contradicting results.

In 1992, Hachinski and colleagues identified an increased prevalence of severe sympathetic consequences following occlusion of the right MCA in the rat <sup>135</sup>, suggesting a parasympathetic dominance of right IC function. Corresponding with this right MCA territorial damage, was the observed elevation of plasma catecholamines (specifically NE); likely caused by sympathetic activation of the noradrenergic system <sup>135</sup>. Interestingly, Saitoh and colleagues have previously reported a noradrenergic influence on PPI, observing deficits in sensorimotor gating following blockage of this hormonal system <sup>177</sup>. We therefore expected *left* IC injury to impair PPI, reducing attenuation of the ASR. Theoretically, if the left IC truly embodies a sympathetic dominance of autonomic function, resulting damage would disrupt sympathetic control and inhibit noradrenergic activation; ultimately impeding normal sensorimotor gating.

At 28 d following IC injury, damage to the left IC caused a notable trend of reduced PPI, compared to right injury groups (IA/ET-1) and control groups (PBS/NI); supporting the potential lateralization of IC autonomic function. As part of this behaviour test, rats were



subjected to assorted prepulse trials, varying in intensity (75 dB and 85 dB) and ISI (30 ms and 100 ms). Mediation of PPI primarily occurs through a fast-acting brainstem circuit <sup>163</sup>. Although, several studies have also identified the advanced processing of prepulse stimuli at the forebrain level; capable of exerting a delayed, downstream modulatory effect on PPI <sup>139,145,214,215</sup>. For this reason, PPI is traditionally measured using two ISIs: one of short duration (30 ms) and one of long duration (100 ms), to assess experimental alterations in brainstem or forebrain circuitry <sup>184</sup>. Intriguingly, while prepulse trials of both ISIs demonstrated a trending decrease in PPI for left injury groups (IA/ET-1), observed deficits were most substantial following administration of a 75 dB prepulse with 30 ms ISI. As such, our impaired observations of PPI are likely the result of autonomic brainstem damage and/or dysfunction, caused by the downstream effects of left IC injury. However, before such conclusions can be drawn, it is important to recall that PPI of the ASR has traditionally been used to assess deficits in sensory processing <sup>160–162</sup>. Consequently, this observed trend of reduced PPI following left IC damage could very-well be attributed to the impairment of normal sensory gating processes, unrelated to autonomic dysfunction – requiring the future implementation of alternative metrics capable of *directly* evaluating autonomic changes post-insular ischemic stroke.

#### **4.4 Insular Ischemic Stroke and Secondary Neuroinflammation**

##### *4.4.1 White matter inflammation and axonal degeneration*

Following ischemic stroke, clinical imaging studies have identified chronic inflammation in major white matter tracts, persisting several months into the recovery period <sup>68–71</sup>. Recently, manifestation of this WMI has been implicated in post-stroke prognosis, contributing to worse functional outcomes <sup>68,72,73</sup>. Physiologically, white matter is essential for proper signal transduction between grey matter regions <sup>66,74</sup>. For this transmission to efficiently occur, a persistent supply of energy is required along the full axon <sup>66</sup>. Consequently, damage to one area, which may arise during ischemia, can destroy the electrophysiological properties of the entire axon; causing axonal degeneration <sup>66,71</sup>. Overtime, propagation of this axonal damage will inhibit neuronal communication, resulting in adverse functional deficits <sup>66,68,72,73</sup>. We therefore sought to identify remote areas of secondary neuroinflammation in our insular ischemic stroke rodent model. Observed damage in distal white and grey matter regions could provide valuable mechanistic insight into the neural manifestation of autonomic dysfunction, and resulting SIHI, following IC ischemia.

As anticipated, remote areas of neuroinflammation were identified 28 d following IC damage, appearing in both white and grey matter regions. In particular, enhanced microglia activation occurred in the corpus callosum, ipsilateral internal capsule and ipsilateral VP thalamus of injured groups (IA/ET-1). While minimal amounts of microgliosis were also observed within the forceps minor, a significant difference between experimental groups was not identified; likely due to the anatomical distance between its anterior location and our (more posterior) IC injection site. In this thesis, neuroinflammation was selected as a primary histological correlate, to allow for the broader observation of insular stroke-induced pathological changes.

Mechanistically, WMI does not serve as a direct correlate of axonal degeneration. However, past experimental reports have discerned microgliosis as a reputable assay for axonal health <sup>65,92,216</sup>. Recently, Wang and colleagues positively correlated axonal degeneration to M1 microglia activation, in the corpus callosum of mice subjected to traumatic brain injury <sup>65</sup>. Physiologically, this makes sense; considering the degradation of axons, or any cellular component, is naturally accompanied by an accumulation of toxic waste, stimulating activation of a neuroinflammatory response. Thus, the co-occurrence of both axonal degeneration and WMI, post-ischemic stroke, is pathologically plausible. We can therefore infer that our observations of corpus callosum and internal capsule microgliosis correspond with the chronic degeneration of local axons. This associated white matter injury can disrupt signal transduction, ultimately leading to the neurodegeneration of remote grey matter regions <sup>90,92</sup>.

Pathologically, the neurodegenerative presentation of this distal grey matter damage is anticipated to elicit a chronic, secondary cascade of remote neuroinflammation. In our current rat model, significant amounts of activated microglia were identified within the ipsilateral VP thalamus 28 d following IC damage; further supporting our mechanistic speculation of white matter axonal degeneration. Intriguingly, the VP thalamus serves as a vital relay centre for the transmission of autonomic cardiovascular information between the brainstem and IC <sup>108</sup>. As such, the downstream manifestation of neurodegeneration within this brain region, likely contributes to associated autonomic deficits of SIHI. Additional staining for histological markers specific to degeneration, such as Fluoro-Jade B <sup>91,217</sup>, should be performed to confirm this mechanistic prediction of secondary degeneration.

#### 4.4.2 Additional causes of microglia activation

In addition to the injured groups (IA/ET-1), basal levels of microgliosis were observed in our NI rats; insinuating an innate presence of microgliosis. Often, microglia are exclusively viewed as immune cells of the brain. However, these multifunctional cells participate in an array of physiological processes, regulating homeostasis and maintaining overall brain health<sup>218</sup>. During the absence of an immune response, microglia will continue to scavenge the CNS: phagocytosing aged cells, faulty synapses and/or local waste products<sup>218</sup>. Consequently, this internal cleanup of cellular debris requires the basal activation of M1 microglia; likely contributing to the observed presence of microgliosis within our NI rats.

#### 4.4.3 Pathological absence of lateralization

As discussed earlier, behavioural measurements of PPI displayed recognizable differences between left and right insular injury groups, suggesting a lateralization of IC autonomic function. Consequently, a pathological lateralization of neuroinflammation, corresponding with this behavioural observation, was anticipated. Yet, at 28 d following IC damage, similar regions (and amounts) of microgliosis were observed in all injured groups; despite hemispheric location of the insular injury. Intriguingly, Krause and colleagues recently identified a co-existence of both sympathetic and parasympathetic regions in the left and right human IC<sup>130</sup>. Although each hemisphere appears to exhibit a functional autonomic predominance (right IC = parasympathetic, left IC = sympathetic), opposing autonomic regions, in each IC, have been observed<sup>130</sup> – blurring the perceived rigidity of IC lateralization. Experimentally, similar observations of this autonomic variation have been recognized among cardiac chronotropic sites within the rat IC<sup>219</sup>. It is therefore possible that damage to the right or left IC may impact both sympathetic and parasympathetic regulatory sites, negating distinct downstream pathological effects; however, due to the autonomic predominance of each hemisphere, a lateralization of behavioural deficits was still detected.

Furthermore, the results of this thesis only assess secondary neuroinflammation within remote forebrain regions; limiting current pathological conclusions. The IC is vital to the autonomic control of cardiovascular function, transmitting this regulatory effect on the heart through several brainstem regions<sup>108-110</sup>. Neurologically, the anatomical separation of sympathetic and parasympathetic pathways involved with this autonomic process remains most apparent within the brainstem. From the IC, efferent sympathetic output predominantly

synapses at the RVLM, while parasympathetic outputs synapse at the DMV and/or NA; both located within the medulla<sup>2</sup>. As such, the pathological representation of IC lateralization may be more discernable within the brainstem medulla. Interestingly, in our current rodent model, injured rats (IA/ET-1) exhibited significant amounts of microgliosis within the ipsilateral internal capsule; a fibre bundle responsible for signal transduction between the cortex and brainstem. Consequently, chronic display of this internal capsule microgliosis likely corresponds with a downstream manifestation of brainstem damage, supporting the crucial need for additional investigation of resulting brainstem pathology.

#### *4.4.4 Insular ischemic stroke and astrogliosis*

At 28 d post-insular injury, no significant differences in astrogliosis were identified between experimental groups; corresponding with previous results obtained in our lab. Traditionally, astrocytes have been implicated as key regulators of neuroinflammation. During stroke, observations of acute astrogliosis remain constant, as astrocytes function to encapsulate the damaged region; initiating vital repair mechanisms<sup>61,62</sup>. Presently, the specific involvement of astrogliosis in chronic, stroke-induced secondary neuroinflammation, remains unknown. Pathologically, astrogliosis has been associated with several CNS diseases<sup>220-222</sup>. However, given the different origins and onsets of these injuries, the temporal and spatial changes of reactive astrocytes have been known to vary, depending on the disease<sup>221</sup>. It is therefore possible that while acute ischemic neuroinflammatory mechanisms predominately involve astrogliosis, chronic secondary neuroinflammation, particularly within the white matter, evokes alternative neuroinflammatory responses; primarily involving microglia.

### **4.5 Insular Ischemic Stroke and Remote Neurodegeneration**

In our current rodent model, increased M1 microglia activation was observed in white matter tracts 28 d following IC damage, displaying a chronic manifestation of white matter injury. As mentioned previously, past experimental studies have identified WMI as a suitable assay for axonal health; recognizing WMI as a histological correlate of axonal degeneration<sup>92</sup>. In accordance with these claims, our current observations of enhanced microglia activation (WMI) within the corpus callosum and internal capsule of injured rats (IA/ET-1), would insinuate a co-occurrence of chronic axonal damage.

Clinically, the pathological display of post-stroke white matter injury has become of increased concern, largely due to the suspected role of axonal damage in secondary neurodegeneration<sup>92</sup>; an adverse outcome of stroke involving remote brain regions distal to the infarct zone<sup>80-85</sup>. Presently, the exact mechanisms of this delayed remote pathology are unknown, and may vary depending on the affected structures<sup>91</sup>. Yet, an intriguing commonality exists between all cases of stroke-induced secondary neurodegeneration: location of the remote damage is dependent on anatomical connectivity to the primary infarct<sup>87-91</sup>, supporting the likely involvement of white matter injury<sup>92</sup>. Consequently, in observing WMI after IC damage, a chronic display of remote secondary neurodegeneration was expected in our injured rats (IA/ET-1). To affirm this anticipated outcome, total neuron counts were measured in five forebrain regions anatomically connected to the IC: the PFC, ACC, amygdala, hypothalamus and VP thalamus. Each of these areas were specifically chosen, due to their autonomic involvement with IC regulation of cardiovascular function. Neurodegeneration in any of these regions would provide valuable insight into the pathological manifestation of autonomic dysfunction, and associated SIHI.

To our surprise, neuronal loss was not observed in any of the aforementioned forebrain regions at 28 d post-insular injury, contradicting previous experimental findings. Past studies involving MCAO in the rat, have consistently reported a delayed appearance of secondary neurodegeneration in the thalamus<sup>87,88,90,92</sup>. Adding to this, in a recent study by Weishaupt and colleagues, chronic neurodegeneration and neuron cell death were observed in the retrosplenial cortex of the rat 28 d following the bilateral injection of ET-1 into the PFC<sup>91</sup>. Consistently, this data has confirmed the experimental existence of stroke-induced secondary neurodegeneration, strongly opposing the results of our study. However, when analyzing this prior data, it became evident that our study produced a substantially smaller infarct region; suggesting a mechanistic impact of stroke severity on the initiation and/or perpetuation of remote neurodegeneration. In our current model, limiting the infarct size was considered necessary to produce a well-defined IC stroke, while the creation of a unilateral lesion allowed for the evaluation of IC lateralization. Yet, it is possible that this unilateral infarct of small volume may not be severe enough to produce previously described incidents of secondary neurodegeneration, requiring a bilateral or larger site of damage.

To our knowledge, the correlative influence of stroke severity in remote neurodegeneration has yet to be investigated. However, Iizuka and colleagues have reported

an enhanced prominence of terminal degeneration, within the corticothalamic fibers of rats exhibiting a larger MCAO infarct <sup>87</sup>; supporting this proposed mechanistic interaction. Recently, Weishaupt and colleagues published comparable findings to those outlined in this thesis, discerning an absence of secondary neurodegeneration 28 d post-ischemic stroke <sup>217</sup>. Similar to our study, this experiment produced a small infarct region, injecting 1  $\mu$ L of ET-1 (10 pmol/ $\mu$ L), unilaterally, into the dorsomedial thalamus of the rat <sup>217</sup>. Interestingly, while axonal degeneration occurred within connecting thalamocortical fibres, an accompanied presence of secondary degeneration in remote grey matter regions was not observed <sup>217</sup>; reaffirming our results.

In discussing this relationship of ischemic stroke and remote neurodegeneration, it is important to note that increased M1 microglia activation was identified in the ipsilateral VP thalamus of our injured rats (IA/ET-1), without the accompanying manifestation of neuronal loss. It is therefore possible that, although the implied presence of axonal degeneration did not correspond with the anticipated secondary neurodegeneration of remote brain regions; damage to these white matter tracts parallels a chronic disruption of signal transduction. Secondary activation of M1 microglia may necessitate pruning of faulty synapses, located in remote areas like the VP thalamus, damaged as a result of this impaired axon function <sup>218</sup>.

#### **4.6 Insular Ischemic Stroke and Stroke-Induced Heart Injury**

In 1989, Cechetto and colleagues were first to experimentally investigate ischemic SIHI, recapitulating clinical observations of myocardial damage and dysfunction in a rodent model of MCAO <sup>55</sup>. Within this study, histological analysis of collected brain tissue revealed an invariable inclusion of IC damage within the MCA ischemic zone <sup>55</sup>. In seeing this, Cechetto proposed a mechanistic influence of IC damage in SIHI, based upon the known role of IC regulation in cardiovascular function. To date, various clinical and epidemiological studies have discerned an association between IC damage and SIHI <sup>7,124-127</sup>; supporting Cechetto's hypothesis. Most recently, Gonzalez Toledo and colleagues identified IC damage in 30.4% of ischemic stroke patients exhibiting atypical post-stroke ECGs; compared to a 7.3% prevalence in patients with normal post-stroke cardiac function <sup>7</sup>. As such, it was anticipated that the focal induction of IC damage would evoke structural myocardial changes in our novel rodent model of insular ischemic stroke.

At 28 d following IC injury, interstitial cardiac fibrosis was observed in the LA. To our knowledge, this is the first reported observation of stroke-induced cardiac fibrosis; as previous studies of SIHI have involved more acute timepoints <sup>55,94,95,97,98,135,136</sup>. During these prior experiments, the structural manifestation of contraction band necrosis has consistently served as a histological marker of myocardial cell death <sup>2,93,105</sup>, occurring within minutes of the hemorrhagic or ischemic stroke <sup>223,224</sup>. Intriguingly, this pathology distinctly differs from common observations of coagulative necrosis, seen after myocardial ischemia <sup>225</sup>; further supporting a mechanistic variance between traditional heart disease and SIHI. Currently, overactivation of the SNS, and accompanying NE toxicity, have been implicated as the cause of contraction band necrosis <sup>113,226,227</sup>. Physiologically, NE is required for the regulated opening of myocardial Ca<sup>2+</sup> channels, responsible for cardiac muscle contraction <sup>113</sup>. If prolonged, oversaturation of NE will stimulate cardiac muscle hypercontractility, causing irreversible cell death (contraction band necrosis) <sup>2,93</sup>. Overtime, this damaged myocardial tissue will begin to remodel, likely giving rise to our chronic observations of cardiac fibrosis.

In this thesis, fibrosis of the LA was specifically analyzed, due to the contributing role of LA dysfunction in AF <sup>208,209</sup>. AF is a form of cardiac arrhythmia known to increase the risk of stroke 5-fold <sup>15</sup>; currently recognized as the most prevalent arrhythmia of SIHI <sup>102</sup>. Clinically, these stroke-induced cases of AF have been described as brief and acute arrhythmic episodes, associated with a low recurrence of ischemic stroke <sup>228,229</sup>. However, with our recent observations of cardiac fibrosis, a chronic development of AF, capable of more drastic consequences, is certainly plausible. This local infiltration of fibrotic tissue can structurally disrupt the subendocardium, altering the cardiac conduction system; contributing to the generation of persistent AF <sup>105</sup>. Presently, it remains unknown whether the fibrotic changes observed in our study are severe enough to cause AF, having only been observed in approximately 5% of total LA area. Yet, in a clinical report by Hammermeister and Reichenbach, minor foci of myocytolysis were deemed capable of initiating ECG abnormalities <sup>230</sup>; suggesting that less obvious cardiac lesions, like those detected in this study, may be sufficient in producing detrimental changes to cardiac function. Experiments within our lab are currently ongoing to assess the temporal progression of this fibrotic remodelling.

Similar to observed brain pathology, the hemispheric localization of IC damage did not alter histological results; producing similar amounts of LA cardiac fibrosis after left or right insular injury. Anatomically, the LA is surrounded by four pulmonary veins (PV), which

together, form the PV-LA junction; a heavily innervated autonomic area, densely populated by both adrenergic (SNS) and cholinergic (PSNS) nerves<sup>231</sup>. Intriguingly, these autonomic nerves appear co-localized at both the tissue and cellular level, with a significant proportion (30%) of cardiac ganglion cells displaying dual adrenergic phenotypes<sup>231</sup>. As such, with this lack of discrete PV-LA autonomic nerve predominance, an identical pathological display would be expected; regardless the type of autonomic disturbance (sympathetic or parasympathetic).

#### 4.7 Inflammation and Stroke-Induced Heart Injury

The contribution of inflammation to the genesis and perpetuation of SIHI has gained increased interest. As mentioned previously, neuroinflammation is a natural consequence of ischemic stroke, known to disrupt the BBB<sup>37,64,66</sup>. Pathologically, this damage to the BBB enables the release of local neuroinflammatory cytokines (TNF $\alpha$ , IL-1 $\beta$ ) into the periphery; inducing a systemic inflammatory response<sup>37,66</sup>. Intriguingly, persistent systemic inflammation has been adversely linked to heart disease<sup>187,188</sup>, as observed in chronic inflammatory disease (sepsis, rheumatoid arthritis) patients<sup>232-234</sup>. We therefore sought to further explore the mechanistic influence of inflammation on SIHI, by correlating cerebral inflammation to cardiac fibrosis.

As expected, increased microglia activation (neuroinflammation) correlated with the enhanced presence of LA cardiac fibrosis; likely elicited through neuroinflammatory activation of the systemic immune response. In the heart, including other internal organs, chronic exposure to systemic inflammation can impair mitochondria function, resulting in the unnatural accumulation of ROS<sup>235,236</sup>. Inevitably, this elicits a cascade of oxidative damage, generating a local inflammatory response<sup>235,236</sup>. Interestingly, in the recent clinical study by Westermann and colleagues, increased amounts of cardiac inflammatory cells positively correlated with enhanced cardiac fibrosis and dysfunction, in heart failure patients<sup>237</sup>; validating aforementioned mechanistic predictions. Currently, ongoing studies within our lab are actively analyzing the local infiltration of immune cells (neutrophils, lymphocytes and monocytes) into cardiac tissue, following IC injury. The future correlation of these results to neuroinflammation and cardiac fibrosis, as well as the systemic measurement of proinflammatory cytokines, are crucial in elucidating the pathophysiological impact of inflammation on SIHI.



Presently, it remains unclear whether this ischemic mechanism of inflammation is independently capable of eliciting SIHI. Recently, Olshansky hypothesized a regulatory role of the ANS in myocardial cytokine production; outlining parasympathetic involvement in the attenuation of cardiac inflammation<sup>114</sup>. Furthermore, overstimulation of the SNS has been implicated in the activation of a systemic, proinflammatory response<sup>238</sup> – insinuating an autonomic influence over associated observations of inflammation post-insular injury. It is therefore possible that, following stroke, ischemic-induced systemic inflammation perturbs cardiac tissue, evoking the infiltration of inflammatory cells into the heart. Subsequently, damage to the IC decreases parasympathetic tone, hindering the suppression of unwanted inflammation. This, coupled with chronic exposure to SNS-induced systemic inflammation, further exacerbates local cardiac inflammation; contributing to the observed presence of cardiac fibrosis. In our current model, the ischemic induction of insular stroke presumably causes both systemic inflammation (a direct result of the stroke) and autonomic dysfunction (a direct result of IC damage); making it challenging to confirm an independent effect of inflammation in SIHI. As such, future studies involving an alternative stroke location should be performed, to examine whether stroke in this alternate region, not anatomically connected to the IC, can produce similar levels of cardiac fibrosis as those produced in our current model.

#### **4.8 Limitations and Future Directions**

To date, the clinical investigation of SIHI has been challenging, due to the high prevalence of shared risk factors between ischemic stroke and cardiovascular disorders<sup>2,105</sup>. As such, we sought to establish a rodent model of focal insular ischemic stroke; capable of progressing the pathophysiological understanding of SIHI, while simultaneously eliminating these clinically-inevitable confounding variables. Experimental development of this novel model has provided valuable insight into the neurological mechanisms of SIHI, confirming the isolated involvement of IC stroke in the development of structural cardiac damage. However, it is important to note that inception of this current rodent model does not exist without limitations; many of which can be resolved in future studies.

Physiologically, substantial differences exist between males and females, contributing to sex-specific alterations in the pathophysiological manifestation, progression and recovery of illness and disease<sup>239</sup>. In stroke, current epidemiological data has delineated an increased incidence in men, compared to women<sup>240-242</sup>. Yet, women frequently present with more severe

outcomes; linked to adverse mortality rates <sup>240–242</sup>. To our knowledge, sex-related differences in the underlying pathophysiology of SIHI have yet to be investigated, both clinically and experimentally. Unfortunately, current results presented in this study do not address this important, and often overlooked, phenomenon – having only used male rats. As such, future experimental studies of SIHI should incorporate the use of female rodents, to examine the likely effect of sex-specific differences involved in the mechanistic formation and perpetuation of stroke-induced cardiac dysfunction.

In the present study, behavioural and pathological observations of IC damage were restricted to the single timepoint of 28 d post-insular injury. However, it is possible that the recovery of an acute pathological response may have already occurred prior to this chronic period, resulting in the loss of key mechanistic information. Recently, Sposato and colleagues reported an acute manifestation of stroke-induced cardiac arrhythmias, of which the majority (approximately 75%) occurred within the first three days of stroke onset <sup>229</sup>. Additionally, 20–60% of ischemic stroke patients exhibit an acute elevation in serum cTnT, a known biomarker of myocardial injury <sup>104</sup>. Interestingly, in a recent study by Wrigley and colleagues, this increased presence of cTnT appeared to enhance the long-term risk for death after ischemic stroke <sup>104</sup>; implying the capable manifestation of acute SIHI into chronic, deadly outcomes. It is therefore critical to include acute timepoints in future studies, as these early pathophysiological changes may provide advanced mechanistic insight into the chronic observations of SIHI detected in our current model.

Pathologically, results from this study do not take into consideration the potential impact of infarct size on SIHI, or its underlying mechanisms. Yet, clinically, an association between infarct volume and SIHI has been identified <sup>229</sup>. In a recent study by Sposato and colleagues, 80% of patients diagnosed with stroke-induced AF displayed a large infarct volume (>15 mm), recognizing infarct size as a predictor of SIHI <sup>229</sup>. Based upon these results, Sposato hypothesized that larger infarcts are associated with more severe autonomic dysregulation, contributing to adverse outcomes of SIHI <sup>229</sup>. However, this has yet to be experimentally proven. Future comparisons of SIHI outcomes using the current rodent model, and a MCAO model, could enhance experimental understanding of this proposed mechanistic risk factor.

Lastly, in this newly developed model of focal insular ischemic stroke, a direct assessment of cardiovascular autonomic function is absent; presenting an inherent mechanistic limitation. Traditionally, HRV has served as a well-established tool used to assess cardiac

autonomic control, in both humans and animal models <sup>136,243,244</sup>. In the conscious rat, this requires the surgical implantation of a telemetric device <sup>245</sup>. Due to the high costs associated with animal telemetry, initial establishment of the present model was essential to confirm proof-of-concept. As a next step, future studies should incorporate the use of telemetry into this current insular stroke model. Analysis of HRV can verify the mechanistic role of autonomic dysfunction in SIHI, further elucidating the pathophysiological underpinnings of this complex brain-heart interaction.

In the present study, we confirmed, for the first time, the focal capability of IC ischemia to generate SIHI; pathologically represented as the chronic manifestation of LA cardiac fibrosis. At 28 d following IC injury, we identified remote microgliosis in the corpus callosum, ipsilateral internal capsule and ipsilateral VP thalamus. Traditionally, this chronic display of remote neuroinflammation has coincided with the secondary neurodegeneration of distal grey matter regions <sup>92</sup>. While the anticipated neurodegeneration of autonomic forebrain regions was not observed in this study, significant microgliosis did occur at the internal capsule; likely corresponding with the downstream manifestation of autonomic brainstem damage. Supporting this notion, behavioural assessment of PPI displayed notable deficits following left IC injury, indirectly demonstrating a possible functional impairment of autonomic activity. Physiologically, the chronic presence of secondary neuroinflammation is also known to elicit a prolonged, systemic immune response <sup>64</sup>. Based upon the recent implication of inflammation in myocardial fibrotic remodelling <sup>114,187,188,210,211</sup>, we correlated microgliosis to LA cardiac fibrosis demonstrating, for the first time, a positive association between neuroinflammation and SIHI. Taken together, these downstream observations of IC ischemia further support the hypothesized mechanistic role, of both autonomic dysfunction and inflammation, in the pathophysiological cascade of SIHI (Figure 25).

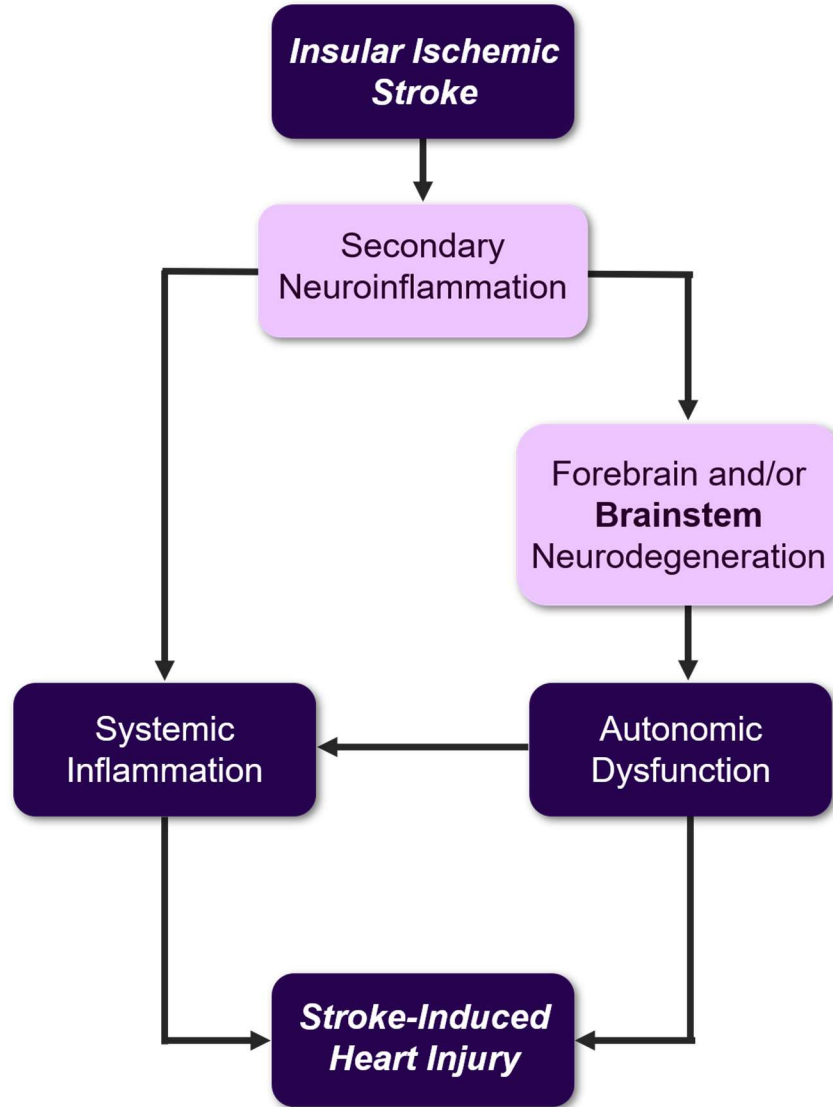


**Figure 25.** Schematic summary outlining the proposed pathophysiological cascade of stroke-induced heart injury.

## Section 5: CONCLUSION

The neurological influence of ischemic stroke in the generation of SIHI has been acknowledged for several years. Yet, despite decades of research, the underlying pathophysiology of this intricate brain-heart connection remains unknown. Clinically, it has been hypothesized that stroke involving the IC initiates SIHI, since the IC controls autonomic regulation of cardiovascular function<sup>2,108,109</sup>. However, given the high prevalence of shared risk factors between ischemic stroke and cardiovascular disorders, current conclusions from clinical studies are largely speculative<sup>105</sup>. We therefore sought to establish a novel rodent model of focal insular ischemic stroke, vitally expanding current mechanistic knowledge of SIHI.

Prior to this thesis, experimental studies of SIHI have exclusively involved animal models of MCAO<sup>55,135</sup>. However, use of this technique creates a large infarct region, extending beyond the IC<sup>55,56,120</sup>. Consequently, the isolated association of IC ischemia with SIHI has yet to be confirmed. In the present study, use of ET-1 produced a focal, and much less severe, ischemic infarct; limiting primary ischemia to the IC region. Pathologically, this confined insular injury corresponded with the structural manifestation of LA cardiac fibrosis, supporting the overarching hypothesis of focal IC involvement in SIHI development.

At 28 d following IC damage, rats subjected to left IC injury displayed an observable trend of reduced PPI, demonstrating a potential lateralization of IC autonomic function. Experimentally, this behavioural assessment of sensorimotor gating serves as a preliminary hallmark of autonomic dysfunction; indirectly supporting the mechanistic association between IC damage, autonomic impairment and SIHI. In correspondence with this behavioural phenotype, an accompanying pathology of secondary microgliosis was observed in the corpus callosum, ipsilateral internal capsule and ipsilateral VP thalamus, 28 d following IC ischemia. Traditionally, this chronic display of remote neuroinflammation has coincided with the secondary neurodegeneration of distal grey matter regions<sup>92</sup>. As such, secondary neuronal loss, within remote forebrain regions of IC autonomic circuitry, was expected. Yet, upon histological examination, this anticipated chronic display of secondary neurodegeneration was not observed. However, significant microgliosis did occur in the ipsilateral internal capsule of injured rats; likely corresponding with a downstream manifestation of autonomic brainstem damage. Consequently, future analysis of brainstem pathology, as well as the telemetric

analysis of HRV, should be performed to directly affirm the mechanistic role of autonomic cardiovascular dysfunction in SIHI.

In addition to autonomic dysfunction, inflammation has been implicated as a cause of SIHI, known to induce myocardial fibrotic remodelling<sup>114,187,188,210,211</sup>. To further examine this potential pathophysiological relationship, we correlated microgliosis of the corpus callosum, ipsilateral internal capsule and ipsilateral VP thalamus, to LA cardiac fibrosis. At 28 d following IC injury, increased microgliosis consistently associated with the enhanced presentation of LA fibrosis; demonstrating a positive correlative relationship between these two variables. Presently, it remains unclear whether this ischemic mechanism of inflammation is independently capable of eliciting SIHI. Recently, Olshansky hypothesized a regulatory role of the ANS in myocardial cytokine production, outlining a parasympathetic role of cardiac inflammation attenuation<sup>114</sup>. Furthermore, overstimulation of the SNS has been implicated in the activation of a systemic, proinflammatory response<sup>238</sup>. It is therefore possible that, following stroke, ischemic-induced systemic inflammation perturbs cardiac tissue, evoking the infiltration of inflammatory cells into the heart. Subsequently, damage to the IC decreases parasympathetic tone, hindering the suppression of unwanted inflammation. This, coupled with chronic exposure to SNS-induced systemic inflammation, further exacerbates local cardiac inflammation; contributing to the observed presence of cardiac fibrosis. As such, SIHI is likely the synergistic result of both autonomic dysfunction and inflammation, arising from the clinical occurrence of insular ischemic stroke.

To date, establishment of this insular ischemic stroke model has only just begun to scratch the complex, and compelling, mechanistic surface of SIHI. Currently, primary use of this novel model has recapitulated the clinical manifestation of SIHI after IC ischemia; creating a reliable experimental mold for the future investigation of this intricate disease. Presently, post-stroke cardiovascular complications remain a prominent cause of death<sup>105</sup>. Yet, aside from the management of associated vascular risk factors, a tailored clinical plan for the specialized treatment of SIHI does not exist<sup>105</sup>. Future use of this model will only enhance mechanistic understanding of SIHI, ultimately leading to the vital development of novel therapies capable of preventing these adverse cardiovascular outcomes of ischemic stroke.

## References

1. Cannon WB. "Voodoo" death. *Am Anthropol.* 1942; **44**:169-181.
2. Tahsili-Fahadan P, Geocadin RG. Heart-brain axis: effects of neurologic injury on cardiovascular function. *Circ Res.* 2017; **120**:559–572.
3. Mitchell JH. Electrocardiographic changes associated with a cerebrovascular accident. *Lancet.* 1964; **284**:645.
4. Dimant J, Grob D. Electrocardiographic changes and myocardial damage in patients with acute cerebrovascular accidents. *Stroke.* 1977; **8**:448–455.
5. Fentz V, Gormsen J. Electrocardiographic patterns in patients with cerebrovascular accidents. *Circulation.* 1962; **25**:22–28.
6. Daniele O, Caravaglios G, Fierro B, *et al.* Stroke and cardiac arrhythmias. *J Stroke Cerebrovasc Dis.* 2002; **11**:28–33.
7. González Toledo ME, Klein FR, Riccio PM, *et al.* Atrial fibrillation detected after acute ischemic stroke: evidence supporting the neurogenic hypothesis. *J Stroke Cerebrovasc Dis.* 2013; **22**:e486-491.
8. Lopez AD, Mathers CD, Ezzati M, *et al.* Global and regional burden of disease and risk factors, 2001: systematic analysis of population health data. *Lancet.* 2006; **367**:1747–1757.
9. Donnan GA, Fisher M, Macleod M, *et al.* Stroke. *Lancet.* 2008; **371**:1612–1623.
10. Benjamin EJ, Virani SS, Callaway CW, *et al.* Heart disease and stroke statistics - 2018 update: a report from the American Heart Association. *Circulation.* 2018; **137**:e67–492.
11. Bonita R, Duncan J, Truelsen T, *et al.* Passive smoking as well as active smoking increases the risk of acute stroke. *Tob Control.* 1999; **8**:156–160.
12. Folsom AR, Rasmussen ML, Chambless LE, *et al.* Prospective associations of fasting insulin, body fat distribution, and diabetes with risk of ischemic stroke. *Diabetes Care.* 1999; **22**:1077–1083.
13. O'Donnell MJ, Xavier D, Liu L, *et al.* Risk factors for ischaemic and intracerebral haemorrhagic stroke in 22 countries (the INTERSTROKE study): a case-control study. *Lancet.* 2010; **376**:112–123.
14. MacMahon S, Peto R, Cutler J, *et al.* Blood pressure, stroke, and coronary heart disease. Part 1, prolonged differences in blood pressure: prospective observational studies corrected for the regression dilution bias. *Lancet.* 1990; **335**:765–774.
15. Wolf PA, Abbott RD, Kannel WB. Atrial fibrillation as an independent risk factor for stroke: the Framingham Study. *Stroke.* 1991; **22**:983–988.



16. Sposato LA, Kapral MK, Fang J, *et al.* Declining incidence of stroke and dementia: coincidence or prevention opportunity? *JAMA Neurol.* 2015; **72**:1529.
17. Di Carlo A. Human and economic burden of stroke. *Age Ageing.* 2008; **38**:4–5.
18. Grysiwicz RA, Thomas K, Pandey DK. Epidemiology of ischemic and hemorrhagic stroke: incidence, prevalence, mortality, and risk factors. *Neurol Clin.* 2008; **26**:871–895.
19. Woo D, Haverbusch M, Sekar P, *et al.* Effect of untreated hypertension on hemorrhagic stroke. *Stroke.* 2004; **35**:1703–1708.
20. Kissela BM, Sauerbeck L, Woo D, *et al.* Subarachnoid hemorrhage: a preventable disease with a heritable component. *Stroke.* 2002; **33**:1321–1326.
21. Woo D, Sauerbeck LR, Kissela BM, *et al.* Genetic and environmental risk factors for intracerebral hemorrhage: preliminary results of a population-based study. *Stroke.* 2002; **33**:1190–1195.
22. Aguilar MI, Brott TG. Update in intracerebral hemorrhage. *The Neurohospitalist.* 2011; **1**:148–159.
23. Petty GW, Brown RD, Whisnant JP, *et al.* Ischemic stroke subtypes : a population-based study of functional outcome, survival, and recurrence. *Stroke.* 2000; **31**:1062–1068.
24. Béjot Y, Daubail B, Giroud M. Epidemiology of stroke and transient ischemic attacks: current knowledge and perspectives. *Rev Neurol.* 2016; **172**:59–68.
25. Kleindorfer D, Panagos P, Pancioli A, *et al.* Incidence and short-term prognosis of transient ischemic attack in a population-based study. *Stroke.* 2005; **36**:720–723
26. Kokubo Y. Epidemiology of transient ischemic attack. *Front Neurol Neurosci.* 2014; **33**:69–81.
27. Zhang L, Zhang RL, Jiang Q, *et al.* Focal embolic cerebral ischemia in the rat. *Nat Protoc.* 2015; **10**:539–547.
28. Brott T, Broderick J, Kothari R, *et al.* Tissue plasminogen activator for acute ischemic stroke. *N Engl J Med.* 1995; **333**:1581–1588.
29. Hacke W, Kaste M, Bluhmki E, *et al.* Thrombolysis with alteplase 3 to 4.5 hours after acute ischemic stroke. *N Engl J Med.* 2008; **359**:1317–1329.
30. Kleindorfer D, Kissela B, Schneider A, *et al.* Eligibility for recombinant tissue plasminogen activator in acute ischemic stroke: a population-based study. *Stroke.* 2004; **35**:e27–29.
31. Adeoye O, Hornung R, Khatri P, *et al.* Recombinant tissue-type plasminogen activator use for ischemic stroke in the United States: a doubling of treatment rates over the course of 5 years. *Stroke.* 2011; **42**:1952–1955.

32. Kleindorfer D, Lindsell CJ, Brass L, *et al.* National US estimates of recombinant tissue plasminogen activator use: ICD-9 codes substantially underestimate. *Stroke*. 2008; **39**:924–928.
33. Lipton P. Ischemic cell death in brain neurons. *Physiol Rev*. 1999; **79**:1431–1568.
34. Lo EH, Dalkara T, Moskowitz MA. Mechanisms, challenges and opportunities in stroke. *Nat Rev Neurosci*. 2003; **4**:399–414.
35. Dirnagl U, Iadecola C, Moskowitz MA. Pathobiology of ischaemic stroke: an integrated view. *Trends Neurosci*. 1999; **22**:391–397.
36. Candelario-Jalil E. Injury and repair mechanisms in ischemic stroke: considerations for the development of novel neurotherapeutics. *Curr Opin Investig Drugs*. 2009; **10**:644–654.
37. Deb P, Sharma S, Hassan KM. Pathophysiologic mechanisms of acute ischemic stroke: an overview with emphasis on therapeutic significance beyond thrombolysis. *Pathophysiology*. 2010; **17**:197–218.
38. Santos MS, Moreno AJ, Carvalho AP. Relationships between ATP depletion, membrane potential, and the release of neurotransmitters in rat nerve terminals. An in vitro study under conditions that mimic anoxia, hypoglycemia, and ischemia. *Stroke*. 1996; **27**:941–950.
39. Hodgkin AL, Huxley AF. A quantitative description of membrane current and its application to conduction and excitation in nerve. *J Physiol*. 1952; **117**:500–544.
40. Walberer M, Ritschel N, Nedelmann M, *et al.* Aggravation of infarct formation by brain swelling in a large territorial stroke: a target for neuroprotection? *J Neurosurg*. 2008; **109**:287–293.
41. Gerriets T, Walberer M, Ritschel N, *et al.* Edema formation in the hyperacute phase of ischemic stroke. *J Neurosurg*. 2009; **111**:1036–1042.
42. Kauppinen RA, McMahon HT, Nicholls DG. Ca<sup>2+</sup>-dependent and Ca<sup>2+</sup>-independent glutamate release, energy status and cytosolic free Ca<sup>2+</sup> concentration in isolated nerve terminals following metabolic inhibition: possible relevance to hypoglycaemia and anoxia. *Neuroscience*. 1988; **27**:175–182.
43. Drejer J, Benveniste H, Diemer NH, *et al.* Cellular origin of ischemia-induced glutamate release from brain tissue in vivo and in vitro. *J Neurochem*. 1985; **45**:145–151.
44. Choi DW. Excitotoxic cell death. *J Neurobiol*. 1992; **23**:1261–1276.
45. Broughton BRS, Reutens DC, Sobey CG. Apoptotic mechanisms after cerebral ischemia. *Stroke*. 2009; **40**:e331-339.
46. Siesjö BK. Pathophysiology and treatment of focal cerebral ischemia. *J Neurosurg*. 1992; **77**:337–354.

47. Fluri F, Schuhmann MK, Kleinschnitz C. Animal models of ischemic stroke and their application in clinical research. *Drug Des Devel Ther.* 2015; **9**:3445–3454.
48. Cook DJ, Tymianski M. Nonhuman primate models of stroke for translational neuroprotection research. *Neurotherapeutics.* 2012; **9**:371–379.
49. Wu D, Chen J, Wang B, *et al.* Endovascular ischemic stroke models of adult rhesus monkeys: a comparison of two endovascular methods. *Sci Rep.* 2016; **6**:31608.
50. Brint S, Jacewicz M, Kiessling M, *et al.* Focal brain ischemia in the rat: methods for reproducible neocortical infarction using tandem occlusion of the distal middle cerebral and ipsilateral common carotid arteries. *J Cereb Blood Flow Metab.* 1988; **8**:474–485.
51. Nakayama H, Dietrich WD, Watson BD, *et al.* Photothrombotic occlusion of rat middle cerebral artery: histopathological and hemodynamic sequelae of acute recanalization. *J Cereb Blood Flow Metab.* 1988; **8**:357–366.
52. Tamura A, Graham DI, McCulloch J, *et al.* Focal cerebral ischaemia in the rat: 1. description of technique and early neuropathological consequences following middle cerebral artery occlusion. *J Cereb Blood Flow Metab.* 1981; **1**:53–60.
53. Woodruff TM, Thundyil J, Tang SC, *et al.* Pathophysiology, treatment, and animal and cellular models of human ischemic stroke. *Mol Neurodegener.* 2011; **6**:11–29.
54. Carmichael ST. Rodent models of focal stroke: size, mechanism, and purpose. *NeuroRx.* 2005; **2**:396–409.
55. Cechetto DF, Wilson JX, Smith KE, *et al.* Autonomic and myocardial changes in middle cerebral artery occlusion: stroke models in the rat. *Brain Res.* 1989; **502**:296–305.
56. Longa EZ, Weinstein PR, Carlson S, *et al.* Reversible middle cerebral artery occlusion without craniectomy in rats. *Stroke.* 1989; **20**:84–91.
57. Hughes PM, Anthony DC, Ruddin M, *et al.* Focal lesions in the rat central nervous system induced by endothelin-1. *J Neuropathol Exp Neurol.* 2003; **62**:1276–1286.
58. Fuxe K, Kurosawa N, Cintra A, *et al.* Involvement of local ischemia in endothelin-1 induced lesions of the neostriatum of the anaesthetized rat. *Exp Brain Res.* 1992; **88**:131–139.
59. Agnati LF, Zoli M, Kurosawa M, *et al.* A new model of focal brain ischemia based on the intracerebral injection of endothelin-1. *Ital J Neurol Sci.* 1991; **12**:49–53.
60. Xing C, Arai K, Lo EH, *et al.* Pathophysiologic cascades in ischemic stroke. *Int J Stroke.* 2012; **7**:378–385.
61. Sofroniew MV, Vinters HV. Astrocytes: biology and pathology. *Acta Neuropathol.* 2010; **119**:7–35.

62. Moxon-Emre I, Schlichter LC. Evolution of inflammation and white matter injury in a model of transient focal ischemia. *J Neuropathol Exp Neurol*. 2010; **69**:1–15.
63. Lundgaard I, Osório MJ, Kress BT, *et al*. White matter astrocytes in health and disease. *Neuroscience*. 2014; **276**:161–173.
64. Kawabori M, Yenari MA. The role of the microglia in acute CNS injury. *Metab Brain Dis*. 2015; **30**:381–392.
65. Wang G, Zhang J, Hu X, *et al*. Microglia/macrophage polarization dynamics in white matter after traumatic brain injury. *J Cereb Blood Flow Metab*. 2013; **33**:1864–1874.
66. Wang Y, Liu G, Hong D, *et al*. White matter injury in ischemic stroke. *Prog Neurobiol*. 2016; **141**:45–60.
67. Hu X, Li P, Guo Y, *et al*. Microglia/macrophage polarization dynamics reveal novel mechanism of injury expansion after focal cerebral ischemia. *Stroke*. 2012; **43**:3063–3070.
68. Thiel A, Radlinska BA, Paquette C, *et al*. The temporal dynamics of poststroke neuroinflammation: a longitudinal diffusion tensor imaging-guided PET study with <sup>11</sup>C-PK11195 in acute subcortical stroke. *J Nucl Med*. 2010; **51**:1404–1412.
69. Radlinska BA, Ghinani SA, Lyon P, *et al*. Multimodal microglia imaging of fiber tracts in acute subcortical stroke. *Ann Neurol*. 2009; **66**:825–832.
70. Gerhard A, Schwarz J, Myers R, *et al*. Evolution of microglial activation in patients after ischemic stroke: a [<sup>11</sup>C](R)-PK11195 PET study. *Neuroimage*. 2005; **24**:591–595.
71. Uchino A, Sawada A, Takase Y, *et al*. Transient detection of early wallerian degeneration on diffusion-weighted MRI after an acute cerebrovascular accident. *Neuroradiology*. 2004; **46**:183–188.
72. Inagaki M, Koeda T, Takeshita K. Prognosis and MRI after ischemic stroke of the basal ganglia. *Pediatr Neurol*. 1992; **8**:104–108.
73. Demeurisse G, Capon A, Verhas M, *et al*. Pathogenesis of aphasia in deep-seated lesions: likely role of cortical diaschisis. *Eur Neurol*. 1990; **30**:67–74.
74. Susuki K, Rasband MN. Molecular mechanisms of node of Ranvier formation. *Curr Opin Cell Biol*. 2008; **20**:616–623.
75. Ahmad AS, Satriotomo I, Fazal J, *et al*. Considerations for the optimization of induced white matter injury preclinical models. *Front Neurol*. 2015; **6**:172.
76. Baltan S. Ischemic injury to white matter: an age-dependent process. *Neurosci*. 2009; **15**:126–133.
77. Correa F, Gauberti M, Parcq J, *et al*. Tissue plasminogen activator prevents white matter damage following stroke. *J Exp Med*. 2011; **208**:1229–1242.

78. Majid A. Neuroprotection in stroke: past, present, and future. *ISRN Neurol.* 2014; **2014**:1–17.
79. Heiss WD. The ischemic penumbra: how does tissue injury evolve? *Ann NY Acad Sci.* 2012; **1268**:26–34.
80. Jacobs AH, Tavitian B. Noninvasive molecular imaging of neuroinflammation. *J Cereb Blood Flow Metab.* 2012; **32**:1393–1415.
81. Pappata S, Levasseur M, Gunn RN, *et al.* Thalamic microglial activation in ischemic stroke detected in vivo by PET and [11C]PK1195. *Neurology.* 2000; **55**:1052–1054.
82. Yassi N, Malpas CB, Campbell BCV, *et al.* Contralesional thalamic surface atrophy and functional disconnection 3 months after ischemic stroke. *Cerebrovasc Dis.* 2015; **39**:232–241.
83. Duering M, Righart R, Csanadi E, *et al.* Incident subcortical infarcts induce focal thinning in connected cortical regions. *Neurology.* 2012; **79**:2025–2028.
84. Nakane M, Tamura A, Sasaki Y, *et al.* MRI of secondary changes in the thalamus following a cerebral infarct. *Neuroradiology.* 2002; **44**:915–920.
85. Tamura A, Tahira Y, Nagashima H, *et al.* Thalamic atrophy following cerebral infarction in the territory of the middle cerebral artery. *Stroke.* 1991; **22**:615–618.
86. Finger S, Koehler PJ, Jagella C. The Monakow concept of diaschisis. *Arch Neurol.* 2004; **61**:283.
87. Iizuka H, Sakatani K, Young W. Neural damage in the rat thalamus after cortical infarcts. *Stroke.* 1990; **21**:790–794.
88. Fujie W, Kirino T, Tomukai N, *et al.* Progressive shrinkage of the thalamus following middle cerebral artery occlusion in rats. *Stroke.* 1990; **21**:1485–1488.
89. Loos M, Dihné M, Block F. Tumor necrosis factor- $\alpha$  expression in areas of remote degeneration following middle cerebral artery occlusion of the rat. *Neuroscience.* 2003; **122**:373–380.
90. Dihné M, Grommes C, Lutzenburg M, *et al.* Different mechanisms of secondary neuronal damage in thalamic nuclei after focal cerebral ischemia in rats. *Stroke.* 2002; **33**:3006–3011.
91. Weishaupt N, Zhang A, Deziel RA, *et al.* Prefrontal ischemia in the rat leads to secondary damage and inflammation in remote gray and white matter regions. *Front Neurosci.* 2016; **10**:81.
92. Block F, Dihné M, Loos M. Inflammation in areas of remote changes following focal brain lesion. *Prog Neurobiol.* 2005; **75**:342–365.
93. Samuels MA. The brain-heart connection. *Circulation.* 2007; **116**:77–84.

94. Tung P, Kopelnik A, Banki N, *et al.* Predictors of neurocardiogenic injury after subarachnoid hemorrhage. *Stroke*. 2004; **35**:548–551.
95. Hunt D, Gore I. Myocardial lesions following experimental intracranial hemorrhage: prevention with propranolol. *Am Heart J*. 1972; **83**:232–236.
96. McNair JL, Clower BR, Sanford RA. The effect of reserpine pretreatment on myocardial damage associated with simulated intracranial hemorrhage in mice. *Eur J Pharmacol*. 1970; **9**:1–6.
97. Jacob WA, Van Bogaert A, De Groodt-Lasseel MHA. Myocardial ultrastructure and haemodynamic reactions during experimental subarachnoid haemorrhage. *J Mol Cell Cardiol*. 1972; **4**:287–298.
98. Burch GE, Sun SC, Colcolough HL, *et al.* Acute myocardial lesions; following experimentally-induced intracranial hemorrhage in mice: a histological and histochemical study. *Arch Pathol*. 1967; **84**:517–521.
99. Hawkins WE, Clower BR. Myocardial damage after head trauma and simulated intracranial haemorrhage in mice: the role of the autonomic nervous system. *Cardiovasc Res*. 1971; **5**:524–529.
100. Koskelo P, Punsar S, Sipilae W. Subendocardial haemorrhage and E.C.G. changes in intracranial bleeding. *Br Med J*. 1964; **1**:1479–1480.
101. Burch GE, Meyers R, Abildskov JA. A new electrocardiographic pattern observed in cerebrovascular accidents. *Circulation*. 1954; **9**:719–723.
102. Sposato LA, Cipriano LE, Saposnik G, *et al.* Diagnosis of atrial fibrillation after stroke and transient ischaemic attack: a systematic review and meta-analysis. *Lancet Neurol*. 2015; **14**:377–387.
103. Perez-Trepichio AD, Williams JL, Block CH, *et al.* Cardiovascular changes during focal cerebral ischemia in rats. *Stroke*. 1993; **24**:691–696.
104. Wrigley P, Khoury J, Eckerle B, *et al.* Prevalence of positive troponin and echocardiogram findings and association with mortality in acute ischemic stroke. *Stroke*. 2017; **48**:1226–1232.
105. Sposato LA, Fridman S, Whitehead SN, *et al.* Linking stroke-induced heart injury and neurogenic atrial fibrillation: a hypothesis to be proven. *J Electrocardiol*. 2018; **51**:430–432.
106. McCorry LK. Physiology of the autonomic nervous system. *Am J Pharm Educ*. 2007; **71**:78.
107. Wehrwein EA, Orer HS, Barman SM. Overview of the anatomy, physiology, and pharmacology of the autonomic nervous system. *Compr Physiol*. 2016; **6**:1239–1278.

108. Cechetto DF. Cortical control of the autonomic nervous system. *Exp Physiol.* 2014; **99**:326–331.
109. Ruiz Vargas E, Sörös P, Shoemaker JK, *et al.* Human cerebral circuitry related to cardiac control: a neuroimaging meta-analysis. *Ann Neurol.* 2016; **79**:709–716.
110. Saper CB. The central autonomic nervous system: conscious visceral perception and autonomic pattern generation. *Annu Rev Neurosci.* 2002; **25**:433–469.
111. Shivkumar K, Ajjola OA, Anand I, *et al.* Clinical neurocardiology defining the value of neuroscience-based cardiovascular therapeutics. *J Physiol.* 2016; **594**:3911–3954.
112. Gordan R, Gwathmey JK, Xie LH. Autonomic and endocrine control of cardiovascular function. *World J Cardiol.* 2015; **7**:204–214.
113. Hove-Madsen L, Méry P-F, Jurevičius J, *et al.* Regulation of myocardial calcium channels by cyclic AMP metabolism. *Basic Res Cardiol.* 1996; **91**:1–8.
114. Olshansky B. Vagus nerve modulation of inflammation: cardiovascular implications. *Trends Cardiovasc Med.* 2016; **26**:1–11.
115. Borovikova LV., Ivanova S, Zhang M, *et al.* Vagus nerve stimulation attenuates the systemic inflammatory response to endotoxin. *Nature.* 2000; **405**:458–462.
116. Jonge WJ, Ulloa L. The alpha7 nicotinic acetylcholine receptor as a pharmacological target for inflammation. *Br J Pharmacol.* 2009; **151**:915–929.
117. Wang H, Yu M, Ochani M, *et al.* Nicotinic acetylcholine receptor  $\alpha 7$  subunit is an essential regulator of inflammation. *Nature.* 2002; **421**:384–388.
118. Gogolla N. The insular cortex. *Curr Biol.* 2017; **27**:580–586.
119. Augustine JR. Circuitry and functional aspects of the insular lobe in primates including humans. *Brain Res Rev.* 1996; **22**:229–244.
120. Ibañez A, Gleichgerrcht E, Manes F. Clinical effects of insular damage in humans. *Brain Struct Funct.* 2010; **214**:397–410.
121. Singer T, Critchley HD, Preuschoff K. A common role of insula in feelings, empathy and uncertainty. *Trends Cogn Sci.* 2009; **13**:334–340.
122. Kurth F, Zilles K, Fox PT, *et al.* A link between the systems: functional differentiation and integration within the human insula revealed by meta-analysis. *Brain Struct Funct.* 2010; **214**:519–534.
123. Oppenheimer S. The insular cortex and the pathophysiology of stroke-induced cardiac changes. *Can J Neurol Sci.* 1992; **19**:208–211.

124. Scheitz JF, Erdur H, Haeusler KG, *et al.* Insular cortex lesions, cardiac troponin, and detection of previously unknown atrial fibrillation in acute ischemic stroke: insights from the troponin elevation in acute ischemic stroke study. *Stroke*. 2015; **46**:1196–1201.
125. Tokgözoğlu SL, Batur MK, Topçuoğlu MA, *et al.* Effects of stroke localization on cardiac autonomic balance and sudden death. *Stroke*. 1999; **30**:1307–1311.
126. Cereda C, Ghika J, Maeder P, *et al.* Strokes restricted to the insular cortex. *Neurology*. 2002; **59**:1950–1955.
127. Oppenheimer SM, Kedem G, Martin WM. Left-insular cortex lesions perturb cardiac autonomic tone in humans. *Clin Auton Res*. 1996; **6**:131–140.
128. Ay H, Koroshetz WJ, Benner T, *et al.* Neuroanatomic correlates of stroke-related myocardial injury. *Neurology*. 2006; **66**:1325–1329.
129. Meyer S, Strittmatter M, Fischer C, *et al.* Lateralization in autonomic dysfunction in ischemic stroke involving the insular cortex. *Neuroreport*. 2004; **15**:357–361.
130. Krause T, Werner K, Fiebach JB, *et al.* Stroke in right dorsal anterior insular cortex is related to myocardial injury. *Ann Neurol*. 2017; **81**:502–511.
131. Laowattana S, Zeger SL, Lima JAC, *et al.* Left insular stroke is associated with adverse cardiac outcome. *Neurology*. 2006; **66**:477–483.
132. Zamrini EY, Meador KJ, Loring DW, *et al.* Unilateral cerebral inactivation produces differential left/right heart rate responses. *Neurology*. 1990; **40**:1408–1411.
133. Sposato LA, Cohen G, Wardlaw JM, *et al.* Effect of right insular involvement on death and functional outcome after acute ischemic stroke in the IST-3 Trial (Third International Stroke Trial). *Stroke*. 2016; **47**:2959–2965.
134. Colivicchi F, Bassi A, Santini M, *et al.* Prognostic implications of right-sided insular damage, cardiac autonomic derangement, and arrhythmias after acute ischemic stroke. *Stroke*. 2005; **36**:1710–1715.
135. Hachinski VC, Oppenheimer SM, Wilson JX, *et al.* Asymmetry of sympathetic consequences of experimental stroke. *Arch Neurol*. 1992; **49**:697–702.
136. Butcher KS, Cechetto DF. Insular lesion evokes autonomic effects of stroke in normotensive and hypertensive rats. *Stroke*. 1995; **26**:459–465.
137. Chokroverty S, Walczak T, Hening W. Human startle reflex: technique and criteria for abnormal response. *Electroencephalogr Clin Neurophysiol*. 1992; **85**:236–242.
138. Pilz PKD, Schnitzler HU. Habituation and sensitization of the acoustic startle response in rats: amplitude, threshold, and latency measures. *Neurobiol Learn Mem*. 1996; **66**:67–79.
139. Koch M. The neurobiology of startle. *Prog Neurobiol*. 1999; **59**:107–128.



140. Landis C, Hunt WA. The startle pattern. *J Psychol.* 1936; **2**:215-219.
141. Geyer MA, Braff DL. Habituation of the blink reflex in normals and schizophrenic patients. *Psychophysiology.* 1982; **19**:1-6.
142. Graham FK. The more or less startling effects of weak prestimulation. *Psychophysiology.* 1975; **12**:238-248.
143. Yeomans JS, Frankland PW. The acoustic startle reflex: neurons and connections. *Brain Res Rev.* 1995; **21**:301-314.
144. Davis M, Parisi T, Gendelman DS, *et al.* Habituation and sensitization of startle reflexes elicited electrically from the brainstem. *Science.* 1982; **218**:688-690.
145. Koch M, Schnitzler HU. The acoustic startle response in rats--circuits mediating evocation, inhibition and potentiation. *Behav Brain Res.* 1997; **89**:35-49.
146. Lee Y, López DE, Meloni EG, *et al.* A primary acoustic startle pathway: obligatory role of cochlear root neurons and the nucleus reticularis pontis caudalis. *J Neurosci.* 1996; **16**:3775-3789.
147. Weber M, Schnitzler HU, Schmid S. Synaptic plasticity in the acoustic startle pathway: the neuronal basis for short-term habituation? *Eur J Neurosci.* 2002; **16**:1325-1332.
148. Wu MF, Suzuki SS, Siegel JM. Anatomical distribution and response patterns of reticular neurons active in relation to acoustic startle. *Brain Res.* 1988; **457**:399-406.
149. Krase W, Koch M, Schnitzler HU. Glutamate antagonists in the reticular formation reduce the acoustic startle response. *Neuroreport.* 1993; **4**:13-16.
150. Koch M, Lingenhöhl K, Pilz PK. Loss of the acoustic startle response following neurotoxic lesions of the caudal pontine reticular formation: possible role of giant neurons. *Neuroscience.* 1992; **49**:617-625.
151. Hammond GR. Lesions of pontine and medullary reticular formation and prestimulus inhibition of the acoustic startle reaction in rats. *Physiol Behav.* 1973; **10**:239-243.
152. Lingenhöhl K, Friauf E. Giant neurons in the rat reticular formation: a sensorimotor interface in the elementary acoustic startle circuit? *J Neurosci.* 1994; **14**:1176-1194.
153. Lingenhöhl K, Friauf E. Giant neurons in the caudal pontine reticular formation receive short latency acoustic input: an intracellular recording and HRP-study in the rat. *J Comp Neurol.* 1992; **325**:473-492.
154. Jordan WP, Leaton RN. Habituation of the acoustic startle response in rats after lesions in the mesencephalic reticular formation or in the inferior colliculus. *Behav Neurosci.* 1983; **97**:710-724.
155. Davis M. Effects of interstimulus interval length and variability on startle-response habituation in the rat. *J Comp Physiol Psychol.* 1970; **72**:177-192.

156. Davis M. Sensitization of the rat startle response by noise. *J Comp Physiol Psychol*. 1974; **87**:571–581.
157. Davis M. Sensitization of the acoustic startle reflex by footshock. *Behav Neurosci*. 1989; **103**:495–503.
158. Hoffman HS, Searle JL. Acoustic variables in the modification of startle reaction in the rat. *J Comp Physiol Psychol*. 1965; **60**:53–58.
159. Hoffman HS, Ison JR. Reflex modification in the domain of startle: I. Some empirical findings and their implications for how the nervous system processes sensory input. *Psychol Rev*. 1980; **87**:175–189.
160. Ellenbroek B. Pre-attentive processing and schizophrenia: animal studies. *Psychopharmacology*. 2004; **174**:65–74.
161. Braff D, Light G. Preattentive and attentional cognitive deficits as targets for treating schizophrenia. *Psychopharmacology*. 2004; **174**:75–85.
162. Takahashi H, Hashimoto R, Iwase M, *et al*. Prepulse inhibition of startle response: recent advances in human studies of psychiatric disease. *Clin Psychopharmacol Neurosci*. 2011; **9**:102–110.
163. Fendt M, Li L, Yeomans JS. Brain stem circuits mediating prepulse inhibition of the startle reflex. *Psychopharmacology*. 2001; **156**:216–224.
164. Willott JF, Carlson S, Chen H. Prepulse inhibition of the startle response in mice: relationship to hearing loss and auditory system plasticity. *Behav Neurosci*. 1994; **108**:703–713.
165. Carlson S, Willott JF. Caudal pontine reticular formation of C57BL/6J mice: responses to startle stimuli, inhibition by tones, and plasticity. *J Neurophysiol*. 1998; **79**:2603–2614.
166. Saitoh K, Tilson HA, Shaw S, *et al*. Possible role of the brainstem in the mediation of prepulse inhibition in the rat. *Neurosci Lett*. 1987; **75**:216–222.
167. Li L, Yeomans JS. Using intracranial electrical stimulation to study the timing of prepulse inhibition of the startle reflex. *Brain Res Protoc*. 2000; **5**:67–74.
168. Li L, Korngut LM, Frost BJ, *et al*. Prepulse inhibition following lesions of the inferior colliculus: prepulse intensity functions. *Physiol Behav*. 1998; **65**:133–139.
169. Leitner DS, Cohen ME. Role of the inferior colliculus in the inhibition of acoustic startle in the rat. *Physiol Behav*. 1985; **34**:65–70.
170. Meredith MA, Wallace MT, Stein BE. Visual, auditory and somatosensory convergence in output neurons of the cat superior colliculus: multisensory properties of the tecto-reticulo-spinal projection. *Exp Brain Res*. 1992; **88**:181–186.

171. Redgrave P, Mitchell IJ, Dean P. Descending projections from the superior colliculus in rat: a study using orthograde transport of wheatgerm-agglutinin conjugated horseradish peroxidase. *Exp Brain Res.* 1987; **68**:147–167.
172. Semba K, Fibiger HC. Afferent connections of the laterodorsal and the pedunculopontine tegmental nuclei in the rat: a retro- and antero-grade transport and immunohistochemical study. *J Comp Neurol.* 1992; **323**:387–410.
173. Steininger TL, Rye DB, Wainer BH. Afferent projections to the cholinergic pedunculopontine tegmental nucleus and adjacent midbrain extrapyramidal area in the albino rat: I. Retrograde tracing studies. *J Comp Neurol.* 1992; **321**:515–543.
174. Leitner DS, Powers AS, Stitt CL, *et al.* Midbrain reticular formation involvement in the inhibition of acoustic startle. *Physiol Behav.* 1981; **26**:259–268.
175. Koch M, Kungel M, Herbert H. Cholinergic neurons in the pedunculopontine tegmental nucleus are involved in the mediation of prepulse inhibition of the acoustic startle response in the rat. *Exp Brain Res.* 1993; **97**:71–82.
176. Semba K, Reiner PB, Fibiger HC. Single cholinergic mesopontine tegmental neurons project to both the pontine reticular formation and the thalamus in the rat. *Neuroscience.* 1990; **38**:643–654.
177. Saitoh K, Shaw S, Tilson HA. Noradrenergic influence on the prepulse inhibition of acoustic startle. *Toxicol Lett.* 1986; **34**:209–216.
178. Prosser CL, Hunter WS. The extinction of startle responses and spinal reflexes in the white rat. *Am J Physiol Content.* 1936; **117**:609–618.
179. Kungel M, Koch M, Friauf E. Cysteamine impairs the development of the acoustic startle response in rats: possible role of somatostatin. *Neurosci Lett.* 1996; **202**:181–184.
180. Sheets LP, Dean KF, Reiter LW. Ontogeny of the acoustic startle response and sensitization to background noise in the rat. *Behav Neurosci.* 1988; **102**:706–713.
181. Plappert CF, Pilz PK, Schnitzler HU. Acoustic startle response and habituation in freezing and nonfreezing rats. *Behav Neurosci.* 1993; **107**:981–987.
182. Glowa JR, Hansen CT. Differences in response to an acoustic startle stimulus among forty-six rat strains. *Behav Genet.* 1994; **24**:79–84.
183. Hoffman HS, Fleshler M. Startle reaction: modification by background acoustic stimulation. *Science.* 1963; **141**:928–930.
184. Valsamis B, Schmid S. Habituation and prepulse inhibition of acoustic startle in rodents. *J Vis Exp.* 2011; **55**:e3446.
185. Ison JR, Hammond GR. Modification of the startle reflex in the rat by changes in the auditory and visual environments. *J Comp Physiol Psychol.* 1971; **75**:435–452.

186. Gerriets T, Stolz E, Walberer M, *et al.* Complications and pitfalls in rat stroke models for middle cerebral artery occlusion: a comparison between the suture and the macrosphere model using magnetic resonance angiography. *Stroke*. 2004; **35**:2372–2377.
187. Fang L, Ellims AH, Beale AL, *et al.* Systemic inflammation is associated with myocardial fibrosis, diastolic dysfunction, and cardiac hypertrophy in patients with hypertrophic cardiomyopathy. *Am J Transl Res*. 2017; **9**:5063–5073.
188. Nicoletti A, Michel JB. Cardiac fibrosis and inflammation: interaction with hemodynamic and hormonal factors. *Cardiovasc Res*. 1999; **41**:532–543.
189. Cechetto DF, Chen SJ. Subcortical sites mediating sympathetic responses from insular cortex in rats. *Am J Physiol*. 1990; **258**:245–255.
190. Sozmen EG, Hinman JD, Carmichael ST. Models that matter: white matter stroke models. *Neurotherapeutics*. 2012; **9**:349–358.
191. Sharkey J, Ritchie IM, Kelly PA. Perivascular microapplication of endothelin-1: a new model of focal cerebral ischaemia in the rat. *J Cereb Blood Flow Metab*. 1993; **13**:865–871.
192. Fuxe K, Cintra A, Andbjør B, *et al.* Centrally administered endothelin-1 produces lesions in the brain of the male rat. *Acta Physiol Scand*. 1989; **137**:155–156.
193. Jarrard LE. On the use of ibotenic acid to lesion selectively different components of the hippocampal formation. *J Neurosci Methods*. 1989; **29**:251–259.
194. Schwarcz R, Hökfelt T, Fuxe K, *et al.* Ibotenic acid-induced neuronal degeneration: a morphological and neurochemical study. *Exp Brain Res*. 1979; **37**:199–216.
195. Paxinos G, Watson C. A stereotaxic atlas of the rat brain. Academic, New York. 1998.
196. Kutscher CL, Cheek M, Borski K, *et al.* Hematoxylin and thionin techniques for staining myelin and cells: variations and critical steps. *Brain Res Bull*. 1987; **19**:161–163.
197. Flaris NA, Densmore TL, Molleston MC, *et al.* Characterization of microglia and macrophages in the central nervous system of rats: definition of the differential expression of molecules using standard and novel monoclonal antibodies in normal CNS and in four models of parenchymal reaction. *Glia*. 1993; **7**:34–40.
198. Perry VH, Matyszak MK, Fearn S. Altered antigen expression of microglia in the aged rodent CNS. *Glia*. 1993; **7**:60–67.
199. Faddis BT, Vijayan AK. Application of glial fibrillary acidic protein immunohistochemistry in the quantification of astrocytes in the rat brain. *Am J Anat*. 1988; **183**:316–322.

200. Schmidt-Kastner R, Wietasch K, Weigel H, *et al.* Immunohistochemical staining for glial fibrillary acidic protein (GFAP) after deafferentation or ischemic infarction in rat visual system: features of reactive and damaged astrocytes. *Int J Dev Neurosci.* 1993; **11**:157–174.
201. Mullen RJ, Buck CR, Smith AM. NeuN, a neuronal specific nuclear protein in vertebrates. *Development.* 1992; **116**:201–211.
202. Wolf HK, Buslei R, Schmidt-Kastner R, *et al.* I. NeuN: a useful neuronal marker for diagnostic histopathology. *J Histochem Cytochem.* 1996; **44**:1167–1171.
203. Puchtler H, Isler H. The effect of phosphomolybdic acid on the stainability of connective tissues by various dyes. *J Histochem Cytochem.* 1958; **6**:265–270.
204. de Jong S, van Veen TAB, de Bakker JMT, *et al.* Monitoring cardiac fibrosis: a technical challenge. *Neth Heart J.* 2012; **20**:44–48.
205. Talman WT. Cardiovascular regulation and lesions of the central nervous system. *Ann Neurol.* 1985; **18**:1–13.
206. Yasui Y, Breder CD, Saper CB, *et al.* Autonomic responses and efferent pathways from the insular cortex in the rat. *J Comp Neurol.* 1991; **303**:355–374.
207. Cechetto DF, Saper CB. Evidence for a viscerotopic sensory representation in the cortex and thalamus in the rat. *J Comp Neurol.* 1987; **262**:27–45.
208. Naqvi TZ. The stiff left atrium is to atrial fibrillation as the stiff left ventricle is to diastolic heart failure. *Circ Arrhythm Electrophysiol.* 2016; **9**:e003952.
209. Gupta DK, Shah AM, Giugliano RP, *et al.* Left atrial structure and function in atrial fibrillation: ENGAGE AF-TIMI 48. *Eur Heart J.* 2014; **35**: 1457-1465.
210. Passino C, Barison A, Vergaro G, *et al.* Markers of fibrosis, inflammation, and remodeling pathways in heart failure. *Clin Chim Acta.* 2015; **443**:29–38.
211. Lu L, Guo J, Hua Y, *et al.* Cardiac fibrosis in the ageing heart: contributors and mechanisms. *Clin Exp Pharmacol Physiol.* 2017; **44**:55–63.
212. Johnston GAR, Curtis DR, de Groat WC, *et al.* Central actions of ibotenic acid and muscimol. *Biochem Pharmacol.* 1968; **17**:2488–2489.
213. Schwarcz R, Hökfelt T, Fuxe K, *et al.* Ibotenic acid-induced neuronal degeneration: a morphological and neurochemical study. *Exp Brain Res.* 1979; **37**:199–216.
214. Swerdlow NR, Caine SB, Braff DL, *et al.* The neural substrates of sensorimotor gating of the startle reflex: a review of recent findings and their implications. *J Psychopharmacol.* 1992; **6**:176–190.

215. Swerdlow NR, Geyer MA. Using an animal model of deficient sensorimotor gating to study the pathophysiology and new treatments of schizophrenia. *Schizophr Bull.* 1998; **24**:285–301.
216. Sloane JA, Hollander W, Moss MB, *et al.* Increased microglial activation and protein nitration in white matter of the aging monkey. *Neurobiol Aging.* 1999; **20**:395–405.
217. Weishaupt N, Riccio P, Dobbs T, *et al.* Characterization of behaviour and remote degeneration following thalamic stroke in the rat. *Int J Mol Sci.* 2015; **16**:13921–13936.
218. Aloisi F. Immune function of microglia. *Glia.* 2001; **36**:165–179.
219. Oppenheimer SM, Cechetto DF. Cardiac chronotropic organization of the rat insular cortex. *Brain Res.* 1990; **533**:66–72.
220. Colombo E, Farina C. Astrocytes: key regulators of neuroinflammation. *Trends Immunol.* 2016; **37**:608–620.
221. Choudhury GR, Ding S. Reactive astrocytes and therapeutic potential in focal ischemic stroke. *Neurobiol Dis.* 2016; **85**:234–244.
222. Sofroniew MV. Astrocyte barriers to neurotoxic inflammation. *Nat Rev Neurosci.* 2015; **16**:249–263.
223. Oppenheimer SM, Hachinski VC. The cardiac consequences of stroke. *Neurol Clin.* 1992; **10**:167–176.
224. van der Bilt IAC, Vendeville J-P, van de Hoef TP, *et al.* Myocarditis in patients with subarachnoid hemorrhage: a histopathologic study. *J Crit Care.* 2016; **32**:196–200.
225. Rona G. Catecholamine cardiotoxicity. *J Mol Cell Cardiol.* 1985; **17**:291–306.
226. Zimmerman AN, Hülsmann WC. Paradoxical influence of calcium ions on the permeability of the cell membranes of the isolated rat heart. *Nature.* 1966; **211**:646–647.
227. Hearse DJ, Humphrey SM, Bullock GR. The oxygen paradox and the calcium paradox: two facets of the same problem? *J Mol Cell Cardiol.* 1978; **10**:641–668.
228. Sposato LA, Cerasuolo JO, Cipriano LE, *et al.* Atrial fibrillation detected after stroke is related to a low risk of ischemic stroke recurrence. *Neurology.* 2018; **90**:e924–e931.
229. Sposato LA, Klein FR, Jáuregui A, *et al.* Newly diagnosed atrial fibrillation after acute ischemic stroke and transient ischemic attack: importance of immediate and prolonged continuous cardiac monitoring. *J Stroke Cerebrovasc Dis.* 2012; **21**:210–216.
230. Hammermeister KE, Reichenbach DD. QRS changes, pulmonary edema, and myocardial necrosis associated with subarachnoid hemorrhage. *Am Heart J.* 1969; **78**:94–100.

231. Tan AY, Li H, Wachsmann-Hogiu S, *et al.* Autonomic innervation and segmental muscular disconnections at the human pulmonary vein-atrial junction. *J Am Coll Cardiol.* 2006; **48**:132–143.
232. Khalid U, Egeberg A, Ahlehoff O, *et al.* Incident heart failure in patients with rheumatoid arthritis: a nationwide cohort study. *J Am Heart Assoc.* 2018; **7**:e007227.
233. Kakihana Y, Ito T, Nakahara M, *et al.* Sepsis-induced myocardial dysfunction: pathophysiology and management. *J Intensive Care.* 2016; **4**:22.
234. van Leuven SI, Franssen R, Kastelein JJ, *et al.* Systemic inflammation as a risk factor for atherothrombosis. *Rheumatology.* 2008; **47**:3–7.
235. Burks TN, Marx R, Powell L, *et al.* Combined effects of aging and inflammation on renin-angiotensin system mediate mitochondrial dysfunction and phenotypic changes in cardiomyopathies. *Oncotarget.* 2015; **6**:11979–11993.
236. Lopez-Candales A, Hernández Burgos PM, Hernandez-Suarez DF, *et al.* Linking chronic inflammation with cardiovascular disease: from normal aging to the metabolic syndrome. *J Nat Sci.* 2017; **3**:e341.
237. Westermann D, Lindner D, Kasner M, *et al.* Cardiac inflammation contributes to changes in the extracellular matrix in patients with heart failure and normal ejection fraction. *Circ Hear Fail.* 2011; **4**:44–52.
238. Pongratz G, Straub RH. The sympathetic nervous response in inflammation. *Arthritis Res Ther.* 2014; **16**:504.
239. Arnold AP. Promoting the understanding of sex differences to enhance equity and excellence in biomedical science. *Biol Sex Differ.* 2010; **1**:1.
240. Yu C, An Z, Zhao W, *et al.* Sex differences in stroke subtypes, severity, risk factors, and outcomes among elderly patients with acute ischemic stroke. *Front Aging Neurosci.* 2015; **7**:174.
241. Reeves MJ, Bushnell CD, Howard G, *et al.* Sex differences in stroke: epidemiology, clinical presentation, medical care, and outcomes. *Lancet Neurol.* 2008; **7**:915–926.
242. Appelros P, Stegmayr B, Terént A. Sex differences in stroke epidemiology: a systematic review. *Stroke.* 2009; **40**:1082–1090.
243. Akselrod S, Gordon D, Ubel FA, *et al.* Power spectrum analysis of heart rate fluctuation: a quantitative probe of beat-to-beat cardiovascular control. *Science* . 1981; **213**:220–222.
244. Camm AJ, Malik M, Bigger JT, *et al.* Heart rate variability: standards of measurement, physiological interpretation and clinical use. *Circulation.* 1996; **93**:1043–1065.

245. Brockway BP, Mills PA, Azar SH. A new method for continuous chronic measurement and recording of blood pressure, heart rate and activity in the rat via radio-telemetry. *Clin Exp Hyperten*. 1991; **13**:885–895.



## Appendix



**AUP Number:** 2016-027

**PI Name:** Whitehead, Shawn N

**AUP Title:** Mechanisms Of Vascular Cognitive Impairment And Prevention Of Stroke And Its Consequences

**Approval Date:** 09/09/2016

**Official Notice of Animal Use Subcommittee (AUS) Approval:** Your new Animal Use Protocol (AUP) entitled "Mechanisms Of Vascular Cognitive Impairment And Prevention Of Stroke And Its Consequences" has been APPROVED by the Animal Use Subcommittee of the University Council on Animal Care. This approval, although valid for four years, and is subject to annual Protocol Renewal.2016-027::1

1. This AUP number must be indicated when ordering animals for this project.
2. Animals for other projects may not be ordered under this AUP number.
3. Purchases of animals other than through this system must be cleared through the ACVS office. Health certificates will be required.

The holder of this Animal Use Protocol is responsible to ensure that all associated safety components (biosafety, radiation safety, general laboratory safety) comply with institutional safety standards and have received all necessary approvals. Please consult directly with your institutional safety officers.

Submitted by: Copeman, Laura  
on behalf of the Animal Use Subcommittee  
University Council on Animal Care

Curriculum Vitae  
**VICTORIA THORBURN**

Education:

- **Master of Science | SEPT 2016 – AUG 2018**
  - Department of Anatomy and Cell Biology, Western University (London, ON)
  - Supervisors: Dr. Shawn Whitehead and Dr. Luciano Sposato
- **Bachelor of Medical Science (Honors) | SEPT 2011 – APR 2015**
  - Honors specialization in Basic Medical Sciences, minor in French Studies
  - Western University (London, ON)

Awards & Scholarships:

- London Health Research Day Platform Presentation Award (\$650) | MAY 2018
- Anatomy and Cell Biology Travel Award (\$500) | APR 2018
- Lawson Internal Research Fund Scholarship (\$15,000) | JAN 2017 – DEC 2017
- Western Graduate Research Scholarship (\$4,500) | SEPT 2016, SEPT 2017
- Undergraduate Dean's Honour List | 2013 – 2015
- Western Scholarship of Excellence (\$2000) | SEPT 2011
- CLAC Union Scholarship (\$1000) | SEPT 2011

Graduate Teaching Assistantships:

- **Neuroscience for Rehabilitation Sciences (ACB 9531A) | SEPT 2017 – DEC 2017**
  - Department of Anatomy and Cell Biology, Western University (London, ON)
  - Course Coordinator: Dr. Shawn Whitehead

Relevant Volunteer Activities:

- Anatomy and Cell Biology Social Committee Member | SEPT 2017 – AUG 2018
- University Mentor for London Central Secondary School Co-operative Education Program | SEPT 2017 – MAY 2018

Publications & Presentations:

Balint B, Jaremek V, **Thorburn V**, et al. Cardiac inflammation and fibrosis following selective insular cortical stroke in the rat. *Stroke*. Submitted July 2018 [under review].

Paquet M, Cerasuolo JO, **Thorburn V**, et al. Pathophysiology and risk of atrial fibrillation detected after ischemic stroke (PARADISE): a translational, integrated and transdisciplinary approach. *J Stroke Cerebrovasc Dis*. 2018; **27**: 606-619.

**Thorburn V**, Balint B, Paquet M, Sposato LA and Whitehead SN. Development of an insular ischemic stroke animal model to study the pathophysiology of atrial fibrillation detected after stroke (AFDAS). **Canadian Association for Neuroscience, May 2018** (Vancouver, BC, CAN) *Poster presentation by Victoria Thorburn*

**Thorburn V**, Balint B, Paquet M, Sposato LA and Whitehead SN. Development of an insular ischemic stroke animal model to study the pathophysiology of atrial fibrillation detected after stroke (AFDAS). **London Health Research Day, May 2018** (London, ON, CAN) *Oral presentation by Victoria Thorburn*

**Thorburn V**, Balint B, Jaremek V, Paquet M, Sposato LA and Whitehead SN. Development of an ischemic insular stroke animal model to study the pathophysiology of atrial fibrillation detected after stroke. **Clinical Neurological Sciences Research Day, April 2018** (London, ON, CAN) *Poster presentation by Victoria Thorburn*

**Thorburn V**, Balint B, Jaremek V, Paquet M, Whitehead SN and Sposato LA. Characterizing the neuroinflammatory response of focal ischemic stroke in the rat insular cortex. **American Academy of Neurology, April 2018** (Los Angeles, CA, USA) *Poster presentation by Dr. Shawn Whitehead*

Balint B, **Thorburn V**, Jaremek V, Paquet M, Whitehead SN and Sposato LA. Left atrial endothelial dysfunction, inflammation and fibrosis induced by selective insular cortex ischemic stroke in rats. **American Academy of Neurology, April 2018** (Los Angeles, CA, USA) *Oral presentation by Dr. Shawn Whitehead*

**Thorburn V**, Balint B, Jaremek V, Paquet M, Sposato LA and Whitehead SN. Development of an ischemic insular stroke animal model to study the pathophysiology of atrial fibrillation detected after stroke. **Anatomy and Cell Biology Research Day, October 2017** (London, ON, CAN) *Poster presentation by Victoria Thorburn*

**Thorburn V**, Balint B, Paquet M, Whitehead SN and Sposato LA. Development of a selective insular ischemic stroke animal model to study the pathophysiology of atrial fibrillation detected after stroke. Results from the experimental arm of PARADISE study. **Clinical Neurological Sciences Research Day, April 2017** (London, ON, CAN) *Oral presentation by Victoria Thorburn*